UNIVERSITÀ DEGLI STUDI DI ROMA "TOR VERGATA"

DOTTORATO DI RICERCA IN SCIENZE CHIMICHE
XVII CICLO

"Mechanism of membrane perturbation by the antibiotic peptide trichogin GA IV: *a physico-chemical study on fluorescent analogs*"

Presented by Claudia Mazzuca

Supervisor: dr. Lorenzo Stella

Ph.D. School coordinator: prof. Bruno Crociani

ACADEMIC YEAR 2003-2004

1

"It's 106 miles to Chicago, we've got a tank full of gas
half a pack of cigarettes, it's dark
and we're wearing sunglasses."
"Hit it!"
Dan Aykroyd and John Belushi – The Blues Brothers

Introduction

1.1 Antimicrobial resistance

Since their discovery, antimicrobial agents (antibiotics and related medicinal drugs) have substantially reduced the threat posed by infectious diseases. By helping to bring many serious infectious diseases under control, these drugs have also contributed to the major extension in life expectancy experienced during the final part of last century.

These advantages are now seriously jeopardized by the recent emergence and spread of microbes that are resistant to these drugs. Some important examples include penicillin-resistant *Streptococcus pneumoniae*, vancomycin-resistant *enterococci*, methicillin-resistant *Staphylococcus aureus*, multi-resistant *salmonellae*, and multi-resistant *Mycobacterium tubercolosys*. The development of resistance to drugs commonly used to treat malaria is of particular concern, as is the emerging resistance to anti-HIV drugs.

Resistance to antimicrobials is a natural biological phenomenon that can be amplified or accelerated by a variety of factors, including human practices. The use of an antimicrobial for any infection, real or feared, in any dose or over any time period, is a selective pressure which forces microbes to either adapt or die.

Bacteria are particularly efficient at enhancing the effects of resistance, not only because of their ability to multiply very rapidly, but also because they can pass on their resistance genes to other related bacteria through "conjugation", whereby plasmids carrying the genes jump from one organism to another, leading to the emergence of "multidrug resistant strain" (W.H.O., 2002)

An example, regarding the spread of the multi-drug resistant strains of *Salmonella typhi* (W.H.O., 2004) is shown in Figure 1.1.

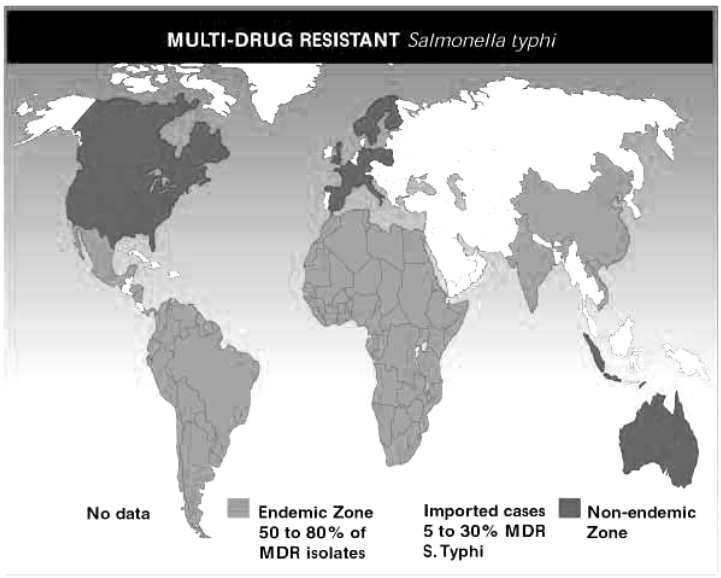

Source: World Health Organization/VRD

Figure 1.1 World-wide diffusion of antimicrobial resistance

1.2 Antimicrobial peptides

The antibiotic resistance problem has spurred an active research for new antimicrobial compounds. One of the possibilities presently pursued are antimicrobial peptides. These compounds are produced by all living organism as part of the innate immunity system, a non specific defense system that complements the highly specific cell-mediated immune response. Antimicrobial peptides are evolutionary ancient weapons, as suggested by their widespread distribution throughout all phylogenetic kingdoms (Zasloff, 2002). In higher organisms, including humans, they are produced at low metabolic cost on epithelial surfaces and in phagocytic cells, where they are easily stored in large amounts, and readily available after an infection to rapidly neutralize a broad range of microbes, including bacteria, fungi and protozoa (Bulet *et al.,* 2004).

Their potential to overcome bacterial resistance is based on the fact that their mechanism of action is different from that of traditional antibiotics. These act by penetrating into the microorganisms and by interacting with specific targets, leading to inhibition to cell wall, DNA or protein biosynthesis in growing cells. Most antimicrobial peptides, on the other hand, simply bind aspecifically to phospholipid bilayers. Their insertion into the cell membranes alters their permeability, leading to cell death by collapse of transmembrane electrochemical gradients and osmolysis (Sitaram and Nagaraj, 1999). The lack of any specific association in the mechanism of action of antimicrobial peptides is supported by studies showing that enantiomers of lytic peptides, composed solely of D-amino acids, possess a biological activity which is indistinguishable from that of the parent molecules (Blondelle *et al.,* 1999; Juvvadi *et al.,* 1996 Papo and Shai, 2003).

Although this mode of action does not involve any specific binding, some antimicrobial peptides are able to selectively target the membranes of microbes instead of those of mammals. This selectivity is probably due to the different lipid composition of the membranes involved. While the outer leaflet of mammalian cell walls are mainly constituted of neutral and zwitterionic phospholipids, that of bacterial cells contains phosphatidylglycerol or in general

anionic lipids. Furthermore, these membranes differ also in their cholesterol content (Zasloff, 2002; Epand and Vogel 1999a; Matsuzaki, 1998).

Due to their mechanism of action, the emergence of resistance to antimicrobial peptides is less probable than for conventional antibiotics. This has led several research groups to develop antimicrobial peptides, both natural and synthetic, into therapeutically useful agents (Zasloff, 2002) as well as to initiate many studies aimed to understand their mode of action.

In recent years hundreds of antimicrobial peptides have been isolated and several have been *de novo* designed and synthetically produced (see Table 1.1) (Andrès and Dimarq, 2004).

Table 1.1 Update of clinical development of cationic antimicrobial peptides

Compound	Structural characteristics	Species	Topical or parenteral use	Indications – phase of clinical trials
Pexiganan (MSI-78)	α-helices	Skin of xenop	Cream	Impetigo and diabetic foot ulcer infections – phase III trial
Iseganan (IB-367)	Peptides that contain disulfide bridges	Leucocytes of pig	Oral solution	Anticancer therapies, induced oral mucosistis – phase III trial
			Aerosol	Long infections in cystic fibrosis patients and ventilator-associated pneumonia – phase I trial
Peptides MBI (MBI-226)	α-helices	Not communicated	Cream	Catheter-related bloodstream infections – phase III trial; acute acne and nasal carriage of *S. aureus* – phase I trial
Histatine variants	α-helices	Human	Oral solution	Gengivitis and mouth infections – phase II trial; oral candidiasis and *Pseudomonas aeruginosa* long infections – phase I trial
Heliomocin variants (ETD151)	Peptides that contain disulfide bridges	Insect: lepidopteran *Heliothis virescens*	Parenteral use	Systemic deep and invasive fungal infections. Immunocompromised patients – preclinical development
Insect defensins variants				Systemic multiresistant Gram-positive bacterial infections – preclinical development
Neuprex (RBPI 21)	α-helices	Human	Parenteral use	Pediatrics meningococcæmia – phase III trial (Orphan drug status from FDA)
Mycoprex (XMP366)	α-helices	Human	Parenteral use	Systemic fungal infections

This large repertoire of antimicrobial peptides displays a wide diversity in chain length (with sizes between 9 and 100 amino acids), secondary and tertiary structures (α-helices, β-sheets or cyclic), and number of disulfide bonds. Nevertheless, most of them share common properties: although they can be differently charged, they have at least 50% hydrophobic aminoacid residues (Hanckock and Chapple, 1999). Most importantly, they share an amphipathic structure with a polar face and a hydrophobic face. As it will be explained later, amphipathicity seems to be a fundamental prerequisite for their activity.

The spectrum of activity of antimicrobial peptides varies significantly: some of them are toxic only against Gram-positive bacteria (e. g. cecropins), others against both Gram-positive and Gram-negative bacteria (e.g. magainins and dermaseptins); some peptides can be active solely on fungi or toward both bacteria and fungi (e. g. cathelicidins). Finally, some peptides are toxic both to microorganisms and mammalian cells, like mellitin and pardaxin (Shai, 2002).

The mechanism by which antimicrobial peptides act is still debated, and the details of the actual membrane permeation process are still not clear (Shai, 2002; Epand and Vogel 1999a). However, the understanding of how the peptides act is of fundamental importance to fully exploit the use of these peptides as antimicrobial agents.

In recent years, several models has been proposed to tentatively explain the mode of action of these peptides (Shai, 2002; Matsuzaki, 2001; Yang *et al.,* 2001; Huang, 2000; Pouny and Shai,1992). They are graphically summarized in Figure 1.2.

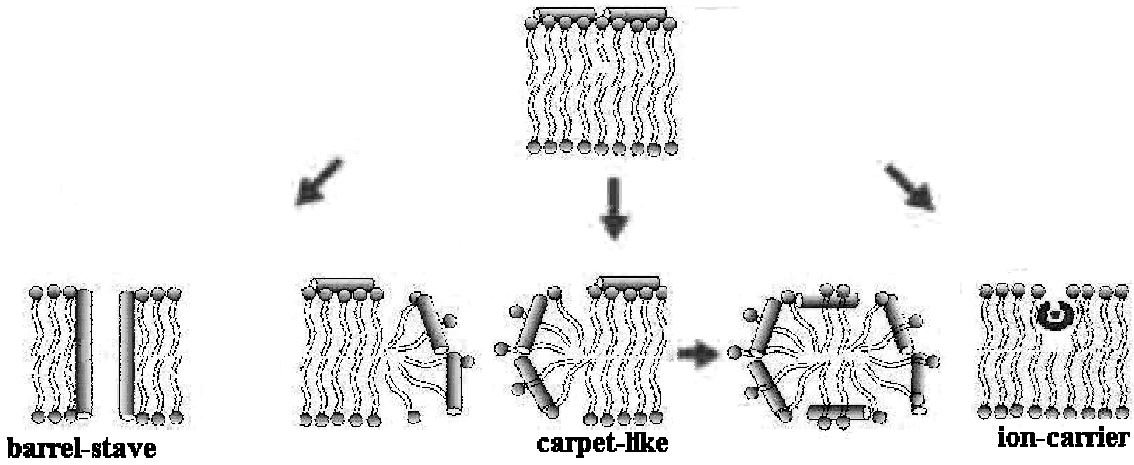

Figure 1.2 Possible mechanisms of action for antimicrobial peptides

The "barrel stave" mechanism describes the formation of transmembrane pores/channels by bundles of amphipatic α-helices, which aggregate like the staves of a barrel, so that their hydrophobic surfaces interact with the lipid core of the membrane and their hydrophilic surfaces point towards the interior of the pore, which is filled with water. Since this model requires peptide insertion into the hydrophobic core of the lipid bilayer, it is reasonable to assume that in this case peptide association with the target membrane is driven predominantly by hydrophobic interactions. The best studied peptide for which this model seems to hold is alamethicin, a peptide belonging to the peptaibol family (Chugh J. K., and Wallace, 2001; Ludtke and Huang, 1996; Spach *et al.,* 1989; Schwarz *et al.,* 1987).

In the "carpet-like" model, peptides are in contact with the phospholipid head groups throughout the entire process of membrane permeation and do not penetrate into the lipid hydrophobic core neither do aggregate, in contrast to the barrel-stave mechanism. Peptides lay parallel to the membrane surface (with the hydrophobic face pointing towards the lipid core, and the hydrophilic face to water). Membrane permeation occurs only if there is a high local concentration of membrane-bound peptides (so that they form a "carpet"). In this case, the surface tension caused by peptide insertion in the headgroup region is released by the formation of transient membrane spanning pores, made up of dynamic peptide-lipid supramolecular complexes (Gazit *et al.,* 1995; Matsuzaki, 2001). In these holes, the lipid bilayer bends back onto itself

forming a toroidal structure ("toroidal model"). As a consequence, a fraction of peptide molecules translocates into the inner leaflet of the membrane, significantly reducing the peptide density in the outer layer, and leading to the closing of the pore. Furthermore, at higher concentrations, the peptide causes the disintegration of the membrane and the formation of micelles (micellization). In this mechanism, as the peptide interacts strongly with the phospholipid head groups, electrostatic interactions presumably play a crucial role. Magainin 2 is one of the most studied peptides thought to act according to this mode of action (Matsuzaki, 1998; Matsuzaki *et al.,* 1997).

In the third model, the so-called "ion carrier" mechanism, peptides bind the ions or the molecules to be transferred across the membrane. This complex can have a 1:1 stoichiometry, or the molecules can be included inside a supramolecular peptide aggregate. In these complexes the peptides expose their hydrophobic face to the outside, facilitating the translocation of hydrophilic molecules across the lipid bilayer. One example of an ion-carrier peptide is valynomicin (Roeske and Kennedy, 1983; Boheim *et al.,* 1980).

Despite extensive studies on the mechanism of action of antibiotic peptides, it is not clear which of these models better describes the real situation in each specific case. A detailed understanding of the activity and selectivity of these peptides is a necessary starting point for the design of novel antimicrobial agents with improved properties.

1.3 The Peptaibols

Peptaibols are a unique group of antibiotic peptides isolated from soil fungi, mainly of the genus *Trichoderma*. They are 11-20 aminoacids in length, and their name derives from their chemical composition: "Pept" is the abbreviation of peptide, "Aib" indicates a high content of the unusual $C^{\alpha,\alpha}$-disubstituted aminoacid Aib (aminoisobutiryc acid), and "ol" is due to the presence of a C-terminal 1,2-amino alcohol; they also contain an N-terminal acetyl group. (Chugh J. K., *et al.,* 2001).

Aib is a well-known helix-inducing amino acid, since the presence of the second methyl group on the C^{α} atom imposes strong stereochemical restrictions on the peptide backbone (Karle and Balaram, 1990; Pispisa *et al.,* 2000a and 2000b), that is constrained to adopt a 3_{10} or a α-helical conformation. Indeed all peptaibol structures determined so far are helical (Rebuffat *et al.,* 1999). A schematic representation of the two kinds of helices is reported in Figure 1.3.

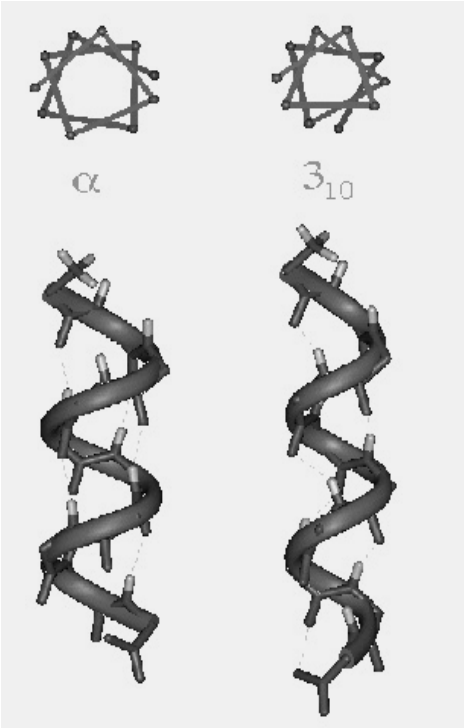

Figure 1.3 Schematic representation of α and 3_{10} helices.

These peptides can contain also other kinds of $C^{\alpha,\alpha}$-disubstituted amino acids like Iva (isovaline or C^{α}-methyl-C^{α}-ethylglycine), or Etn (α-ethylnorvaline or C^{α}-ethyl-C^{α}-*n* –propylglycine), and many have a number of imino acids (either proline or hydroxyproline), that tend to promote bends or kinks in the structures. The presence of modified aminoacids in the sequence is due to the fact that peptaboils are not biosynthesized through the classical ribosomial pathway, but by means of the multienzymatic complex "peptide synthetases". This leads to microheterogeneus mixtures of closely related analogs (Kleinkauf and von Dören 1990), which, in most cases, differ for just a single aminoacid. The principal member of this family is alamethicin, a 20 amino acids long peptide, which, as reported in Section 1.2, is thought to act according to the barrel stave model (Rebuffat *et al.,* 1999; Ludtke and Huang,1996).

Lipopetaibols are a novel sub-class of peptaibols, which at present consists of six members. They are characterized by a N-terminal fatty acyl moiety (from 8 to 15 carbon atoms long) and a very short sequence (7-11 aminoacid) (Rebuffat *et al.,* 1999; Toniolo *et al.,* 2001).

Interest in this peptide family arises from the fact that they exhibit a strong antibiotic activity (Toniolo *et al.,* 2001), making them suitable candidates for pharmaceutical applications (see Table 1.2); however their mechanism of action is still unsettled.

Table 1.2 Survey of the biological activity of lipopeptaibols

Lipopeptaibols	**Description of biological activities**
Trichopolyns	Immunosuppressants, with a mode of action different from that of cyclosporin A (in particular, they do not affect the production of interleukin 4). IC_{50} (nM) for proliferation of lymphocytes in mouse allogeneic MLR: trichopolyn I 5.2, trichopolyn II 10.7 (for comparison cyclosporin A 7.5).
Trichogin GA IV	Antibacterial activity against *Staphylococcus aureus*; inhibition diameter: 13 mm at 3 μg/pit, 9 mm at 1.5 μg/pit.
Trikoningins	Antibacterial activity against *Staphylococcus aureus* (strain 209P); inhibition diameter: 11 mm at 6 μg/pit. Inactive against *Escherichia coli.*
LP 237s	Cytotoxicity (antitumor activity) against mouse leukemia cells ($IC_{50} \approx 0.5$ μg/mL) and a number of carcinoma cell lines (lung, ovarian, colon, breast) (IC_{50} =0.2-0.5 μg/mL).
Helioferins	Hemolysis at >100 μg/mL. Cytostatic activity (IC_{50} =0.01-0.04 μg/mL) against leukemia and mouse fibroblast cell lines. Protonophoric activity (moderate) causing uncoupling of oxidative phosphorylation in mitochondria. Strong antibacterial activity against Gram-positive bacteria and mycobacteria, and strong antifungal activity.

1.4 Trichogin GA IV

Trichogin GA IV is the main component of the lipopeptaibol family and was first isolated in 1992, by Bodo and coworkers (Auvin-Guette *et al.,* 1992) from the soil fungus *Trichoderma longibrachiatum.* It has the following sequence:

Oct-Aib[1]-Gly[2]-Leu[3]-Aib[4]-Gly[5]-Gly[6]-Leu[7]-Aib[8]-Gly[9]-Ile[10]-Lol

where Oct is *n*-octanoyl, and Lol is leucinol.

The great interest towards this peptide is due to the fact that it is very active against Gram-positive bacteria even if it is it only 11 aminoacids long, and therefore too short to span the membrane (Toniolo *et al.,* 1994; 2001). The presence of a long fatty acyl chain at the N-terminus is thought to play an essential role in its activity (Toniolo *et al.,* 1996; 2001; Locardi *et al.,*1998) as trichogin analogs acetylated with a chain shorter than four carbon atoms, or with an Aib residue replacing the fatty acyl moiety at the N-terminus, are not active.

Trichogin aminoacid composition displays two contrasting features, from a structural standpoint: it contains both a high proportion of the helix inducing residue Aib, and four glycines, that favor flexibility. Furthermore two glycines are adjacent and in the middle of the sequence: this feature can lead to a certain degree of flexibility and probably to the formation of a bend in the structure (Gatto *et al.,* unpublished results).

The structure of trichogin was analyzed in methanol solution using CD, EPR and NMR data (NOE temperature coefficient of NH and CO groups and ^{13}C relaxation measurements), while the crystal structure of the peptide was determined using a centrosymmetric space group obtained by co-crystallization of racemic crystals (Auvin-Guette *et al.,* 1992; Locardi *et al.,* 1998; Monaco *et al.,* 1998; Toniolo *et al.,* 1994, 1996, 2001).

All of these studies suggest that the peptide adopts a flexible, right-handed, mixed $3_{10}/\alpha$ helical structure, about 2 nm long. More in detail, at the N-terminus the peptide forms an incipient, distorted 3_{10} helix, while the C-terminus forms a

longer segment of α–helix. The Gly^5-Gly^6- stretch forms a hinge point between the two helical regions. More importantly, the crystallographic data, suggest the structure of trichogin to be amphiphilic, with all of the hydrophobic groups (*n*-octanoyl and Leu, Ile and Lol aliphatic side chains) on one helix face and the four glycine residues comprising the hydrophilic face. Aligned on the border between these two helical faces are the Aib methyl groups (Figure 1.4).

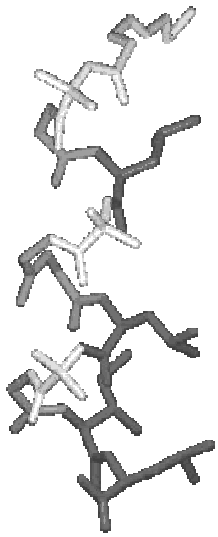

Figure 1.4 3D representation of the secondary structure of GA IV. Light grey, dark grey and black residues are Aib, Gly and Leu amino acids, respectively.

Studies in different solvents like $CDCl_3$ (FTIR), DMSO (NMR), TFE (CD), and SDS (CD, NMR, FTIR) show that the main structural features found in methanol for this peptide are preserved in all other solvents. Furthermore, an increase in ordered secondary structure is found in a membrane mimicking environment like SDS (Toniolo *et al.,* 2001, Monaco *et al.,* 1998; Locardi *et al.,* 1998).

Synthetic analogs, like [Leu^{11}-OMe] trichogin (called Tric-OMe), with a leucine methyl ester at the C-terminus replacing Lol, or [$TOAC^{4,8}$ Leu^{11}-OMe], with a TOAC residue replacing Aib in position 4 or 8, display the same structural features and activity of trichogin GA IV. (Toniolo *et al.,*1996, 2001; Monaco V. *et al.,* 1999; Anderson *et al.,* 1999).

Trichogin was found to be very active against Gram positive bacteria, like *Staphylococcus aureus,* but also against erytrocytes (Toniolo *et al.,* 1996, Epand

et al., 2001). Several experiments have been performed in order to relate the structural features of this peptide to its activity (Toniolo *et al.,* 1996, Peggion *et al.,* 2003).

A preliminary investigation of membrane activities of the two trichogin enantiomers suggested that their interaction with the lipid environment is comparable (Peggion *et al.,* 2003). Furthermore, the loss of amphipaticity obtained substituting the Leu(3) and Leu(7) residues with the less hydrophobic valines, led to a significant decrease in activity. An increase in peptide-induced membrane perturbation is gained introducing more polar residues as serines instead of glycines. Finally, it has been shown that a significant modulation of trichogin ability to make membranes permeable can be reached by varying the number of carbon atoms of the aliphatic N-terminal chain.

The molecular details of the mode of action of this peptide are still unsettled. Several different mechanism have been proposed including bilayer destabilization (Epand *et al*, 1999b; Monaco *et al.,* 1999), ion carrier (Milov *et al.,* 2003) or channel formation (Scrimin *et al.*, 2002). In particular, Epand and collaborators and Monaco and coworkers have employed modified analogs in which one Aib residue at a time was substituted with a TOAC amino acid to perform fluorescence quenching experiments using liposomes containing fluorescent labeled lipids and ESR measurements. Both approaches led them to suggest that the long helix axis of trichogin is oriented in the plane of the bilayer with the hydrophobic face oriented toward the membrane, and the polar face facing water. Milov and coworkers, using pulsed electron-electron double resonance (PELDOR) technique on similar nitroxide labeled trichogin analogs have found significant evidences in favor of peptide self-assembly, suggesting an ion-carrier mechanism. Finally, experiments performed with a tripodal peptide composed of trichogin units, indicated channel formation as the principal mechanism of action (Scrimin *et al.*, 2002).

1.5 Aim of the work.

All the observations reported in the previous Section concur to determine the importance of a detailed study of the mode of action of this peptide.

To this end, the interaction of trichogin GA IV with model membranes has been investigated using several spectroscopic techniques (like steady-state and time-resolved fluorescence, circular dichroism, UV-Vis and Infrared absorption). Our purpose was to analyze at the molecular level all the phenomena involved in the membrane perturbing activity, such as water-membrane partition, aggregation, trichogin orientation with respect to the bilayer, etc.

To this end, two fluorescent analogs of Tric-OMe (henceforth called A3 and F10), were designed for our spectroscopic studies and synthesized in the laboratory of Prof. Toniolo at the University of Padua (Didonè, 2001).

The fluorescent labels azulene and fluorene have been introduced in position 3 and 10, respectively:

Oct-Aib-Gly-Aal-Aib-Gly-Gly-Leu-Aib-Gly-Ile-Leu-OMe (A3)

Oct-Aib-Gly-Leu-Aib-Gly-Gly-Leu-Aib-Gly-Dab(Fmc)-Leu-OMe (F10)

Here azulene was inserted in the peptide chain as β-(1-azulenyl)-L-alanine (Aal or azulenylalanine), kindly provided by prof. L. Moroder (Max-Planck-Institut für Biochemie, Martinsrield, Germany), who recently synthesized it for the first time (Loidl *et al.*, 2000). Fmc is fluorenyl-9-methylcarbonyl, linked to the side chain of 2,4-diaminobutyric acid (Dab) (Figure 1.5).

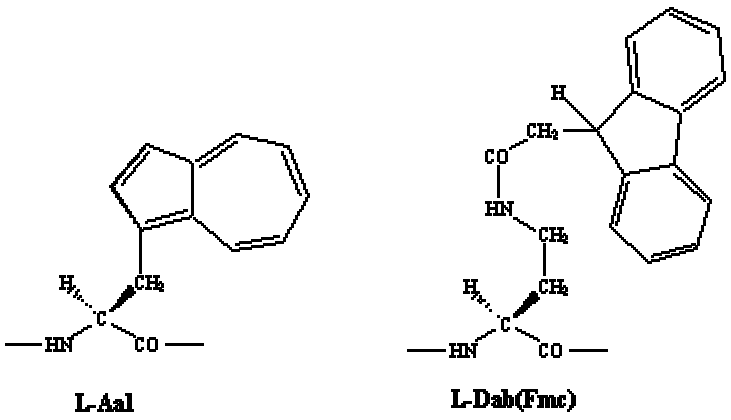

Figure 1.5 Structure of the two fluorescent amino acids.

Labeling occurred by substitution of the two hydrophobic leucine residues, in order to minimize perturbation to the peptide structure. The two fluorescent probes were located at the two end of the peptide chain, so that information on the two different peptide domains could be obtained. Finally, these two fluorophores were chosen because they can act as a Förster resonance energy transfer donor-acceptor pair, as already reported by our laboratory (Venanzi *et al.,* 2004; Pispisa *et al.,* 2000c).

This research was carried out in three successive steps, each analyzing a different fundamental aspect of the interaction between trichogin and the lipid membranes:

1) characterization of the different peptide equilibria in a water-membrane system;
2) investigation of the peptide topology in the membrane;
3) study of peptide activity and definition of its mode of action.

2

“Though this be madness, yet there’s method in ‘t”
William Shakespeare – Hamlet, act II, scene 2

Materials, methods & techniques

2.1 Liposomes

2.1.1 Introduction

Liposomes are the model membranes most commonly used in studies of peptide interaction with lipid bilayers (Epand and Epand, 2000). They are closed membranes of spherical shape, separating a water compartment from the bulk water. The value of liposomes as model membrane systems derives from the fact that the liposome membrane forms a bilayer structure which is in principle identical to the lipid portion of natural cell membranes (New, 1990). In this thesis work, only unilamellar vesicles have been used, i.e. liposomes consituted by a single phospholipid bilayer. These liposomes can be classified on the basis of their dimension: they are called small unilamellar vesicles (SUVs) , large unilamellar vesicles (LUVs) and giant unilamellar vesicles (GUVs) if their diameters are approximately in the range 15-50 nm, 100-400 nm and 1 -200 μm, respectively.

As far as the composition is concerned, phospholipids (some representative examples of which are reported in Table 2.1) are the major structural components of biological membranes, and therefore they are used also for liposomes. The most common phospholipids are phosphatidylcholine molecules (PC), amphipatic molecules in which a glycerol bridge links two hydrophobic acyl hydrocarbon chains to an hydrophilic polar headgroup, phosphocholine (New, 1990). It should be noted that phosphatidylcholine, also known as "lecithin", can be derived from natural sources such as egg yolk (ePC) or synthesized. The phosphatidylcholine extracted from natural sources is, actually, a mixture of phosphatidylcholines, with chains of different lengths and varying degrees of saturation.

Another important phospholipid found in nature (which has also been employed in this work) is phosphatidylethanolamine (PE), characterized by having a primary, instead of quaternary, ammonium headgroup and, consequently, a pH-dependent charge state.

Table 2.1 Chemical structure of some common phospholipids.

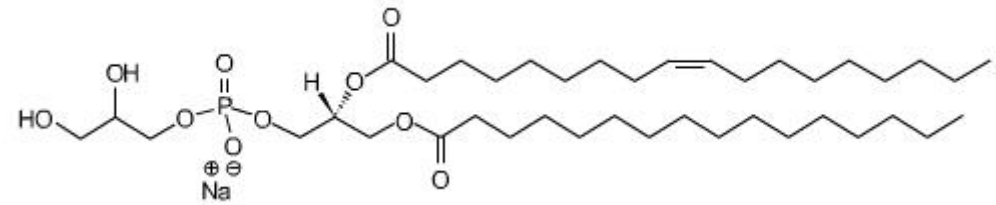

POPG: 1-Palmitoyl-2-Oleoyl-*sn*-Glycero-3-Phosphoglycerol

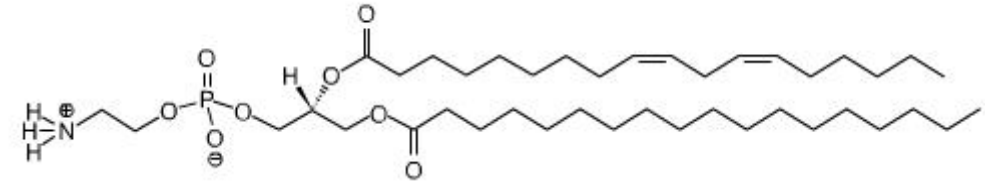

SOPE: 1-Stearoyl-2-Oleoyl-*sn*-Glycero-3-Phosphoethanolamine

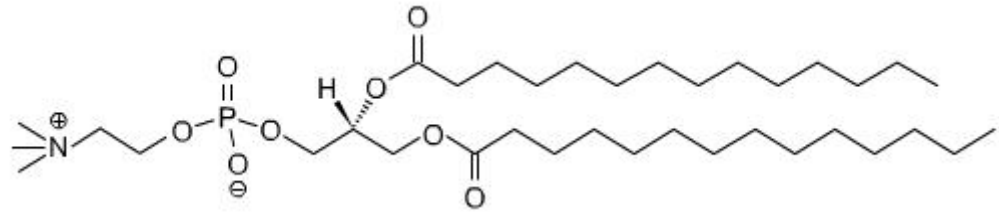

DMPC: 1,2-Dimyristoyl-*sn*-Glycero-3-Phosphocholine

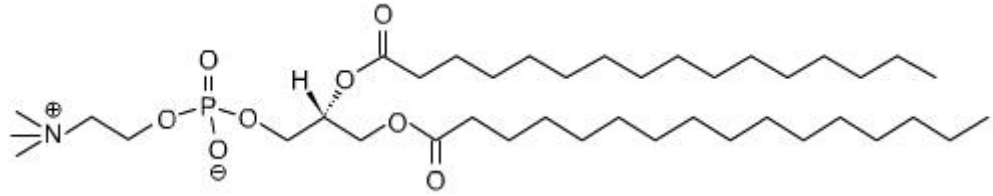

DPPC: 1,2-Dipalmitoyl-*sn*-Glycero-3-Phosphocholine

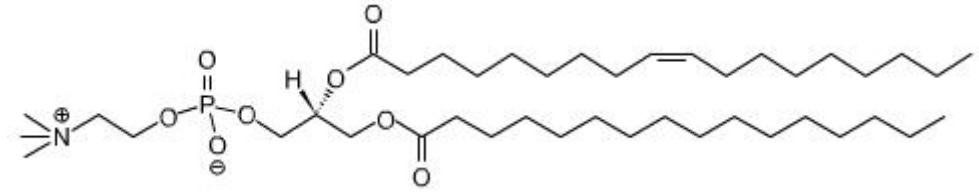

POPC: 1-Palmitoyl-2-Oleoyl-*sn*-Glycero-3-Phosphocholine

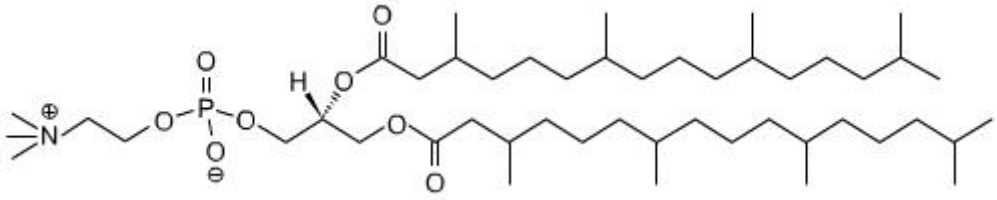

DPhPC: 1,2-Diphytanoyl-*sn*-Glycero-3-Phosphocholine

Table 2.2 Chemical structure of the labeled phospholipids used in this research

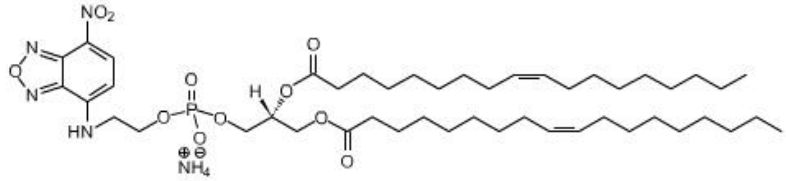 **N-NBD-PE:** 1,2-Dioleoyl-*sn*-Glycero-3-Phosphoethanolamine-N-(7-nitro-2-1,3-benzoxadiazol-4-yl)
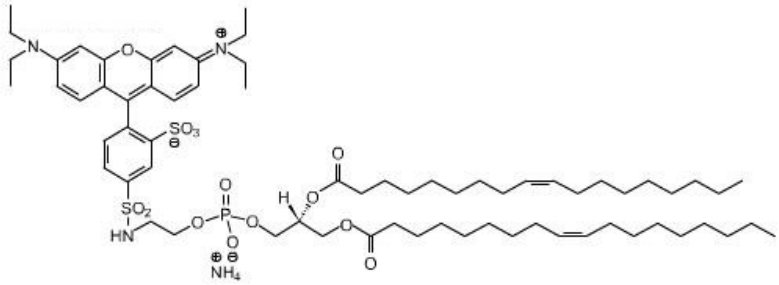 **Rho-PE:** 1,2-Dioleoyl-*sn*-Glycero-3-Phosphoethanolamine-N-(Lissamine Rhodamine B Sulfonyl)
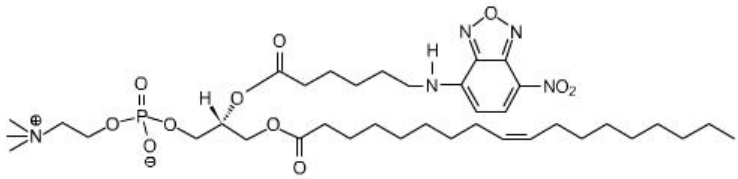 **C6-NBD-PC:** 1-Oleoyl-2-[6-[(7-nitro-2-1,3-benzoxadiazol-4-yl)amino]hexanoyl]-*sn*-Glycero-3-Phosphocholine
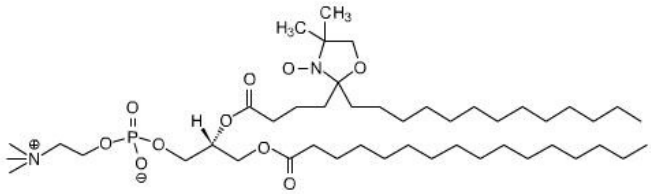 **5-DOXYL-PC:** 1-Palmitoyl-2-Stearoyl-(5-DOXYL)-*sn*-Glycero-3-Phosphocholine
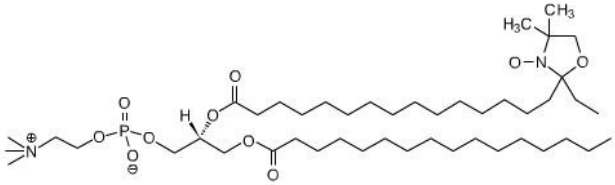 **16-DOXYL-PC:** 1-Palmitoyl-2-Stearoyl-(16-DOXYL)-*sn*-Glycero-3-Phosphocholine
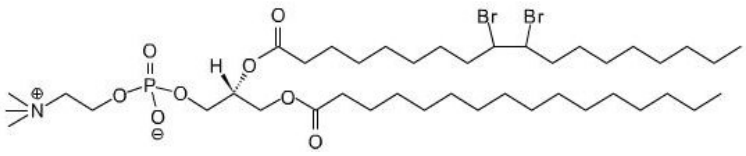 **9,10-diBr-PC:** 1-Palmitoyl-2-Stearoyl-(9,10-dibromo)-*sn*-Glycero-3-Phosphocholine

Moreover, sterols, and in particular cholesterol (henceforth abbreviated as Cho), are other important components of most natural membranes. Due to the rigidity of their structure, their incorporation in the lipid bilayer can bring about major changes in the properties of the membranes, such as a reduction in the freedom of motion of the fatty acyl chain carbon atoms. Being an amphipatic molecule, cholesterol inserts into the membranes with its hydroxyl groups oriented towards the aqueous surface and the aliphatic chain aligned parallel to the acyl chains in the center of the bilayer (New, 1990).

During this thesis work, unless where explicitly stated otherwise, we performed experiments using large unilamellar vesicles made up of ePC:Cho 1:1, prepared as described in Section 2.1.3. When necessary, liposomes labeled with substituted lipids have been used; their structures and abbreviations are reported in Table 2.2.

2.1.2 Phase transitions of phospholipid membranes.

Depending on temperature, lecithin membranes can exist in a fluid phase and a gel phase. The phase behavior of a liposome membrane determines such properties as permeability, fusion, aggregation and protein binding (Seddon and Templer, 1995).

In the gel phase, the hydrocarbon chains are essentially in the all-*trans* conformation, aligned with the glycerol backbone approximately perpendicular to the plane of the membrane, and the phosphocholine headgroup in a straight line roughly parallel to the membrane surface. Therefore, the rotations of the fatty acid chains about the carboxyl bond are strongly hindered, as well as lipid lateral diffusion. As the temperature increases, reaching the gel $\rightarrow$ fluid transition temperature (called also "melting transition temperature"), the fatty acyl chains experience a considerable increase in their conformational freedom and in the area occupied by each lipid molecule.

The melting transition temperature is strongly affected by the lipid chain length. For example, T_m=25° C for DMPC, and 41°C for DPPC, the latter having two more methylene groups per chain. It is also dependent on the degree (and

positions) of lipid insaturations: for example, the T_m for 1-palmitoyl-2-steroyl phosphatidylcholine and 1-palmitoyl-2-oleyl-phosphatydilcholine, which differ for 1 double bond only, are 44° C and –2°C, respectively (Szoka and Papahadjiopoulos, 1980; Sackman,1995). Moreover, in the presence of more than 33% (mol:mol) cholesterol there is no more evidence of the membrane phase transition, as this sterol is able to alter the membrane fluidity both below and above the transition temperature (Miao *et al.,* 2002; New,1990).

2.1.3 Large and small unilamellar vesicle preparation.

Large unilamellar vesicles (LUVs) were prepared by dissolving the desired amount of lipids in a chloroform/methanol solution (2:1 v/v). The solvents were evaporated under an argon atmosphere, to avoid lipid oxidation, until a thin film was formed. Complete evaporation was ensured by applying a rotary vacuum pump for at least 2 hours. The film was hydrated with a 20 mM Tris buffer (pH 7.0), containing 140 mM NaCl and 1 mM EDTA, while for release experiments a 30 mM carboxyfluorescein solution (pH 7.0), or a 0.1 mM solution of Texas Red labeled dextran were used. At this stage, the sample contains large, multilamellar vesicles (LMV), analogous in structure to an onion, with each lipid bilayer separated by a water layer. After vigorous stirring and 10 freeze and thaw cycles, to achieve a better separation between lipid bilayers in LMVs, the lipid suspension was extruded for 31 times through two stacked polycarbonate membranes with 100 nm pores (Avestin, Inc., Ottawa, ON, Canada). All these processes must be performed at a temperature above the melting temperature of the lipid used, i.e. at room temperature in the case of ePC/Cho 1:1 or POPC liposomes, and at 45°C for DMPC vesicles. Small unilamellar vesicles (SUVs) were prepared by sonication (Auvin-Guette et al., 1992). In particular, the MLV solution was left at rest for about 15 hours and then sonicated for at least 45 minutes (Branson sonicator mod. 250) at 0°C. Successively, the solution was filtered with a PRO-X hydrophilic LIDA filter of 0.45 μm.

The unencapsulated fluorescent tracer was separated from the liposomes by gel filtration on a Sephadex G-50 medium column, in the case of carboxyfluorescein, or a Sephacryl S-300 column for dextran. Final phospholipid concentration was determined by the Stewart method, presented in Section 2.1.5 (Stewart, 1980).

2.1.4 Giant Unilamellar Vesicles

Giant unilamellar vesicles are characterized by a diameter varying from 1 to 200 μm, very similar to those of cells. Due to their size, they can be directly visualized under an optical microscope. This property gives rise to multiple applications of GUVs. For instance, it is possible to isolate a specific vesicle under the microscope, and/or to perfuse a membrane-active agent in the proximity of that liposome in order to visualize its effects. Furthermore, reagents can also be injected into the vesicles interior (Menger and Angelova, 1998).

GUVs can be prepared by several methods, such as electroformation (Angelova and Dimitrov 1986) or the so-called "gentle hydratation" method (Akashi *et al.,* 1996 and 1998).

We performed release experiments using GUVs prepared by electroformation (see Section 3.9.1)

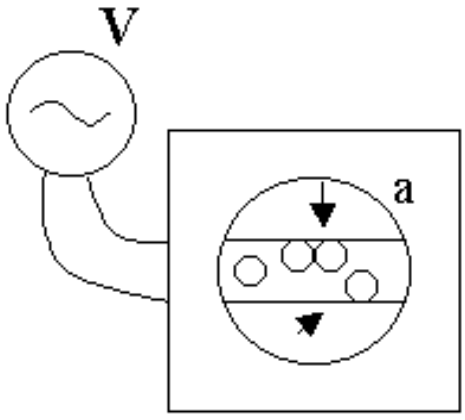

Figure 2.1 Schematic representation of the Teflon cell (denoted as a) in which liposomes (empty circles) are formed. Arrows indicate the platinum wires.

To this end we have designed a Teflon cell with a quartz window on the bottom (to allow microscopic measurements in the UV region) containing two 0.5 mm diameter platinum wires spaced 0.5 cm apart (Figure 2.1). The upper part of the cell is open to facilitate the addition of reagents. A 1μL droplet of a lipid solution (1 mM in $CHCl_3$/MeOH 1:1) is deposited on the center of each wire under a stream of Argon. The solvent is evaporated using a rotary vacuum pump for at least two hours. Successively, the cell is filled with an aqueous solution of the dye that has to be entrapped into liposomes (3 μM CF or 18 μM Texas Red dextran, see Section 2.1.6 and 3.9.1). An initial voltage of 0.2 V (that is slowly increased to 1 V) is then applied at an alternated frequency of 10 Hz for almost an hour, at a temperature above the melting temperature of lipids. GUVs are then formed. They remain attached to the wires, do not evolve once voltage is terminated and are stable for several hours. A further increase in the voltage up to 4 V would cause the detachment of liposomes from wires.

The mechanism of GUV electroformation in an alternated field is not well understood. Probably, since the growing vesicles were observed to vibrate at the same frequency as the applied voltage, the electric field may serve to create a gentle mechanical agitation that assists in the formation, fusion and detachment of the vesicles (Menger and Angelova, 1998).

After liposome formation, the aqueous layer outside vesicles is partially removed (leaving the wires always immersed in the solution) and substituted with pure deionized water. This process is repeated for several times, until the signal of the fluorescent marker entrapped in GUVs is distinguishable from the background.

This method is very simple, and the fact that vesicles are partially attached to the platinum wires allows a fast change of the external solution. For this reason, it is particularly suited to release experiments. On the other hand, during this thesis work we have also attempted to use GUVs for conductance measurements, with the voltage-clamp technique (see Section 3.9.3). In this case, the presence of a relatively high salt concentration in solution is needed, but this is not possible with the electroformation method. For this reason, we

have used a different approach to GUV preparation, namely the "gentle hydration" method of Akashi (Akashi *et al.*, 1996;1998).

In this case, lipids were dissolved in a chloroform/methanol solution (1:2 v/v) in a 5mL glass tube, at a final volume of 400μL. The solvent was evaporated at 45° C (or 60 °C for DPPC containing liposomes) in a rotary evaporator under argon atmosphere, and a thin lipid film was formed on the whole glass tube. Complete evaporation was ensured by applying a rotary vacuum pump overnight. The completely dried lipids were then prehydrated at 47°C (65 °C for DPPC containing liposomes) with water-saturated N_2, until the film became transparent (about 45 minutes). Five milliliters of buffer, N_2 purged, were added to the tube. The tube was then filled with Argon and incubated for three hours at 37°C (45°C for DPPC containing liposomes), and gently rocked every hour to disperse the lipid film uniformly in the solution. After further incubation overnight at room temperature, we found a bulky cloud floating in the middle of the solution, which contained giant liposomes. They remain stable for more than two weeks, if stored at 4°C, and some days at room temperature.

2.1.5 Phospholipid assay

Phospholipid concentration was determined according to Stewart's method (Stewart, 1980), which consists in measuring the absorbance of the association complex between ammonium ferrothiocyanate and the phosphatidyl head group (λ_{max} = 488 nm).

More in detail, 1.5 mL of a 0.1 M ammonium ferrothiocyanate aqueous solution was added to 1.5 mL of chloroform solution, containing the lipid to be determined, and the test tube was vigorously shaken for 60 s to favor the formation of the complex. Complex formation between ferrothiocyanate and phospholipids brings an aliquot of the water-soluble ammonium ferrothiocyanate, proportional to the lipid concentration, in the chloroform phase. After centrifugation (3 min at 3800 rpm) to rapidly separate the two solvent phases, and removal of the upper aqueous phase, the chloroform

solution was transferred in a quartz cuvette and its absorbance at λ_{max} measured. The phospholipid concentration was determined by comparison with a calibration curve, obtained by using solutions of known title. A linear behavior was observed at least up to 0.04 μmol of phospholipid present in the chloroform solution. Calibration curves determined for ePC, DMPC and 6,7-DiBr-PC are reported in Figure 2.2. The slopes of the curves are 4.5±0.2 $\mu moles^{-1}$, 4.9±0.1 $\mu moles^{-1}$ and 4.8±0.2 $\mu moles^{-1}$ respectively; R= 0.998 in all cases. All the experiments were performed in triplicate.

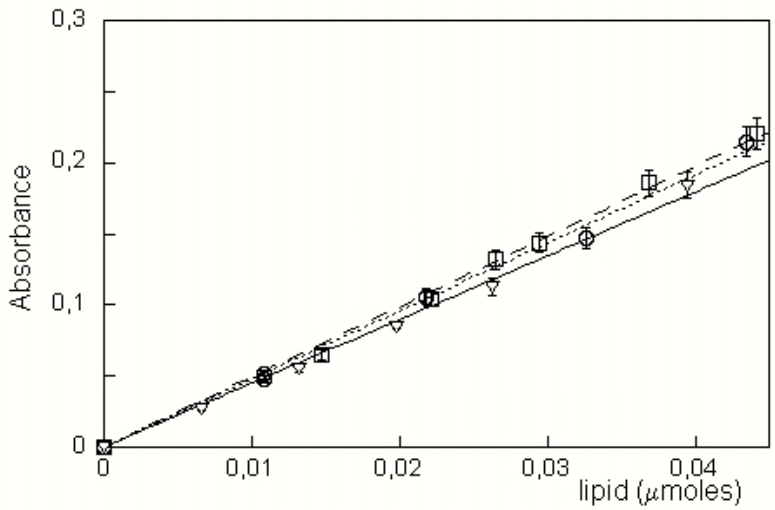

Figure 2.2 Calibration curves obtained using standard solutions of ePC (triangles and continuous line), DMPC (squares and dashed line)and 6,7-DiBr-PC (circles and dotted line). Points represent experimental data, while lines the fits.

Cholesterol content was estimated based on its ratio to the phospholipid concentration.

Finally, we verified that the presence of labeled phospholipids like NBD-PE, Rho-PE at few percent of the total lipid concentration, does not affect the accuracy of the phospholipid assay.

2.1.6 Liposome leakage

2.1.6.1 Release experiments from LUVs

Perturbation of membrane permeability was determined by measuring the fractional release of a fluorophore entrapped inside liposomes. In the case of carboxyfluorescein (CF, 30 mM concentration), this quantity can be measured directly by the increase in fluorescence intensity (excitation 490 nm, emission 520 nm) caused by the reduction in self-quenching (Chen and Knutson, 1988). When the entrapped molecule was Texas-red (TR) labeled dextran (0.1 mM concentration), leakage was measured by adding to the outside solution anti-TR antibodies to a 10 μg/mL final concentration (according to what reported on the operating procedures provided by the manufacturer, Molecular Probes. Inc).

Antibody binding to the fluorophore causes a change in its fluorescence intensity (Sharpe and London, 1999), measured with $\lambda_{exc.}$ = 592 nm and $\lambda_{em.}$ = 604 nm. In both cases, fractional release (R) was determined by the following formula:

$$R = \frac{F - F_{0\%}}{F_{100\%} - F_{0\%}} \qquad (2.1)$$

where $F_{0\%}$ is the fluorescence intensity before peptide addition, and $F_{100\%}$ is the intensity corresponding to 100 % leakage, determined after vesicles were completely disrupted by adding Triton X-100. The release kinetics was recorded with a 0.2 s timestep.

2.1.6.2 Release experiments from GUVs

Release of dye entrapped in GUVs prepared by electroformation (Section 2.1.4) was followed using a Nikon TE200 inverted microscope (Nikon, Tokio, Japan) equipped with two excitation/emission filter sets: the "blue" excitation filter set (B-2E/C,λ_{exc}=465-495 nm, λ_{em}= 515-555 nm), and the "green" excitation filter set or G-2E/C:λ_{exc}=528-553 nm, λ_{em}= 590-650 nm). The use of these two filters allows the concomitant visualization of two different dyes, one entrapped inside the vesicle and the other included in their phospholipid bilayer.

Other details are reported in Section 3.9.1.

2.2 Techniques

2.2.1 Fluorescence Spectroscopy

2.2.1.1 Introduction

Fluorescence spectroscopy is a particularly important experimental technique to investigate chemical and biochemical systems, since it is non destructive, extremely sensitive and its time-scale (0.1-100 ns) is comparable to that of many biological processes (protein rotations, conformational fluctuations, etc.).

The phenomenon of fluorescence consists in the radiative decay of a molecular (or atomic) system, following the absorption of a photon from a luminous source. More in detail, when light of an opportune wavelength is absorbed by a molecule, resulting in a spectroscopic transition to a less stable, higher energy state, the dissipation of this excess energy can follow different competitive pathways: non-radiative (excited state reactions, collisions with the solvent or with other molecules, energy transfer) or radiative (fluorescence or phosphorescence). In the radiative decay, the relaxation to the ground state occurs through the emission of a photon (red-shifted with respect to the excitation wavelength, because of vibrational, and solvent relaxation in the excited state) (Lakowicz, 1983).

A fluorescence spectrum consists in registering the emission intensity of the sample at different wavelengths with a constant excitation radiation of opportune energy. Conversely, the excitation spectrum records the dependence of emission intensity at a single wavelength as a function of the excitation wavelengths.

A quantitative way to characterize the relative importance of the radiative relaxation pathway is the so-called quantum yield (q), which is defined as the ratio between emitted photons (n_f) and absorbed photons (n_a):

$$q = \frac{n_f}{n_a} = \frac{k_R}{k_R + k_{NR}} \tag{2.2}$$

where k_R and k_{NR} are the rate constants for the radiative (fluorescence emission) and non radiative decay, respectively. Therefore, this quantity represents the probability that an excited system returns to the ground state by emitting a photon.

Experimentally, the quantum yield (q) is proportional to the ratio of the steady-state fluorescence intensity (F) emitted by the probe to its absorbance (A):

$$q \propto \frac{F}{A} \tag{2.3}$$

Therefore, q is determined by using a fluorescent standard whose quantum yield is known and whose emission spectral properties closely match those of the material under investigation (IUPAC, 1988). The quantum yield of the sample is then operationally defined as:

$$q_{sample} = \frac{F_{sample}}{A_{sample}} \frac{A_{st} n_{sample}^2 q_{st}}{F_{st} n_{st}^2} \tag{2.4}$$

where q is the quantum yield, A is the absorbance at the excitation wavelength, F is the integrated emission area across the band, n the refractive index of the solvent and the subscripts $sample$ and st refer to the sample and to the standard, respectively.

Another important parameter is the fluorescence lifetime of the probe. When a population of identical fluorophores is excited by a short light pulse, the time evolution of the emitted intensity can be represented by a single exponential function:

$$F(t) = F_o e^{-(k_R + k_{NR})t} = F_o e^{-t/\tau} \tag{2.5}$$

where F_0 and $F(t)$ are the fluorescence intensities measured just after the pulse (at t=0 s) and a given time t, respectively. The fluorescence lifetime τ is the

average time that molecules spend in their excited state before returning to ground state; therefore, by definition, it is the reciprocal of the sum of the rate constants of all decay processes:

$$\tau = \frac{1}{k_R + k_{NR}} \tag{2.6}$$

In the absence of non radiative decay, the fluorophore lifetime is called intrinsic lifetime and is given by:

$$\tau_0 = \frac{1}{k_R} = \frac{1}{A_{Em}} \tag{2.7}$$

where A_{Em} is the Einstein's coefficient for spontaneous emission. By combining equations (2.6) and (2.7) it can be shown that the quantum yield is related to the lifetime:

$$q = \frac{k_R}{k_R + k_{NR}} = \frac{\tau}{\tau_0} \tag{2.8}$$

2.2.1.2 Förster resonance energy transfer (FRET)

Among all the possible non radiative pathways, one is particularly important to study biological systems at a molecular level, namely Förster energy transfer. This process consists in the transfer of excitation energy from a fluorophore in the excited state (donor) to a chromophore in its ground state (acceptor) without any emission or absorption of photons: it is caused by a resonance phenomenon due to the dipolar interaction between the donor and acceptor molecules. In order for this resonance to occur, it is necessary that the emission spectrum of the donor overlaps (at least partially) to the absorption spectrum of the acceptor. Being a stochastic process with a probability depending on the distance and mutual orientation between the two chromophores, energy transfer provides structural information on the sample under investigation (Lakowicz, 1983).

The energy transfer efficiency E_{FRET}, defined as the probability that an excited donor relaxes to the ground state by non radiative energy transfer, can be expressed as:

$$E_{FRET} = \frac{k_{ET}}{k_{ET} + k_D^0} \tag{2.9}$$

where k_{ET} is the rate constant for energy transfer while k_D^0 is the rate constant for all the other decay pathways, which take place also in the absence of acceptor molecules.

According to Förster theory (Förster, 1948), the dependence of the energy transfer efficiency on the structural parameters can be expressed as:

$$E_{FRET} = \left[1 + \frac{2}{3\kappa^2} \left(\frac{r}{R_0} \right)^6 \right]^{-1} \tag{2.10}$$

r being the distance between the donor and the acceptor and κ^2 a parameter depending on their mutual orientation, which, in the case of fast rotation of the probes, averages to 2/3; R_0, called Förster radius, is the characteristic distance corresponding to 50% energy transfer efficiency (for κ^2=2/3). It is defined as:

$$R_0 = \left(\frac{2}{3} \alpha \cdot n^{-4} \cdot q_D^0 \cdot J \right)^{\frac{1}{6}} \tag{2.10}$$

where α is a constant (8.8 10^{-25} M cm^3), n is the refractive index of the medium, q_D^0 is the quantum yield of the donor when no acceptor is present and J is the superposition integral between the fluorescence spectrum of the donor (F_D) and the absorption spectrum of the acceptor (ε_A = molar extinction coefficient), weighted by λ^4 (λ being the wavelength of the radiation):

$$J = \frac{\int_0^\infty F_D(\lambda)\varepsilon_A(\lambda)\lambda^4 d\lambda}{\int_0^\infty F_D(\lambda)d\lambda} \tag{2.11}$$

Experimentally, energy transfer efficiency can be measured both by steady-state and time-resolved fluorescence. Förster efficiency can be expressed as:

$$E_{FRET} = 1 - \frac{q_D^A}{q_D^0} = 1 - \frac{\tau_D^A}{\tau_D^0} \tag{2.12}$$

q_D^A (τ_D^A) and q_D^0 (τ_D^0) being the donor quantum yields (lifetimes) measured in the presence and in the absence of the acceptor, respectively. If the energy transfer acceptor is a fluorophore, steady-state FRET efficiency can also be experimentally determined by measuring the increase of its emission signal after interaction with the donor. In particular, when donor molecules are absent, the acceptor fluorescence intensity (at the excitation wavelength used in FRET experiments) is:

$$F_A^0 \propto q_A A_A \tag{2.13}$$

where q_A and A_A are the quantum yield and the absorbance of the acceptor respectively, and the superscript refers to the absence of donor.

In the presence of donor molecules, this quantity increases, due to energy transfer according to:

$$F_A^D \propto q_A A_A + E_{FRET} q_A A_D \tag{2.14}$$

Here F_A^D is the fluorescence intensity of acceptor in the presence of donor molecules and A_D is the absorbance of the donor at the excitation wavelength.

Combining equations 2.13 and 2.14, one can easily obtain the relative increase in the acceptor fluorescence as a function of transfer efficiency:

$$\frac{F_A^D}{F_A^0} = \frac{q_A A_A + E_{FRET} q_A A_D}{q_A A_A} = 1 + \frac{A_D}{A_A} E_{FRET} \qquad (2.15)$$

2.2.1.3 Anisotropy measurements

In this technique the sample is excited by linearly polarized light: the probability of excitation of a given molecule is proportional to $\cos^2\theta$ (where θ is the angle between the excitation transition dipole of the probe and the polarization direction). Consequently, a "photoselection" is performed, and the excited molecules have their transition dipoles oriented preferentially in the direction of the excitation radiation. The emission photons have a polarization direction that is again distributed with a $\cos^2\theta$ law with respect to the emission transition dipole orientation. Therefore, in the absence of diffusional motions, the emitted light is anisotropic: the fluorescence polarized parallel ($I_{//}$) with respect to the excitation polarization direction is more intense than the perpendicular one ($I_{\perp}$) (Stella, 2000).

To characterize on a quantitative basis this phenomenon, an experimental observable called fluorescence anisotropy (r) is introduced:

$$r = \frac{I_{//} - I_{\perp}}{I_{//} + 2I_{\perp}} \qquad (2.16)$$

For a completely polarized fluorescence $I_{\perp} = 0$ and therefore r = 1, while for depolarized fluorescence $I_{//} = I_{\perp}$ and hence r = 0.

Actually, the maximum observable anisotropy (called fundamental or limiting anisotropy and observable by performing measurements on a diluted sample in glycerol at –20 °C) is <1, and in particular is defined as:

$$r_0 = \frac{\left(3\cos^2 \vartheta - 1\right)}{5} \qquad (2.17)$$

ϑ being the angle between the absorption and emission transition dipoles of the fluorescent probe: in the case of parallel transition dipoles (ϑ=0) a limiting value of 0.4 is obtained.

The emission can be depolarized by several phenomena, like diffusive motions during the lifetime of the fluorophore excited state, so that the observed anisotropy is generally lower than its limiting value. As the extent of the diffusive motions depends on the viscosity of the solvent and the size and shape of the diffusing species, the measurement of anisotropy provides an estimate of the dimensions of the fluorophore or of the molecule the probe is linked to.

In particular, in the simplest case in which a molecule is assumed to be a rigid sphere with a mono-exponential intensity decay, anisotropy is given by the Perrin equation:

$$r = \frac{r_0}{1 + \frac{\tau}{\varphi_r}} \tag{2.18}$$

where τ is the fluorophore lifetime and φ_r is the rotational correlation time, which can be computed from the Stokes-Einstein equation:

$$\varphi_r = \frac{V\eta}{kT} \tag{2.19}$$

Here, V is the volume of the solvated molecule and η the viscosity of the solution.

2.2.1.4 Instrumental apparatus

Excitation and emission spectra, and anisotropy values were obtained by steady-state fluorescence experiments on a thermostatted Spex Fluoromax spectrofluorimeter (Edison, NJ, USA) operating in a single photon counting mode. Anisotropy experiments were performed by equipping the spectrofluorimeter with Glan-Thomson polarizer prisms.

Time dependent fluorescence decays were recorded on a thermostatted CD900 time-correlated single photon counting (TCSPC) apparatus (Edimburgh instruments). This technique is a statistical sampling method based on the stochastic nature of fluorescence emission, which requires that a single photon be detected after each excitation pulse.

A schematic illustration of the instrument is reported in Figure 2.3.

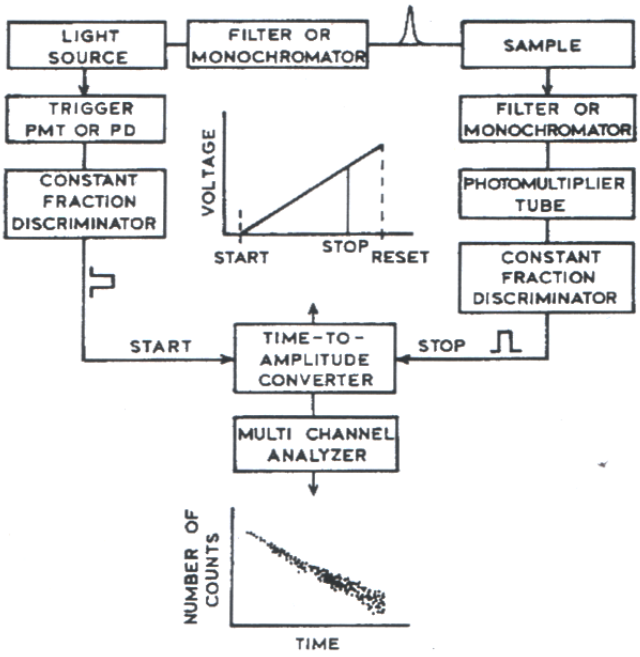

Figure 2. 3 Schematic illustration of the time-correlated single photon counting apparatus.

The sample is repetitively excited using a pulsed light source (a flash-lamp filled with ultrapure hydrogen 0.3 bar, 30KHz repetition rate, full width at half maximum: 1.2 ns). Each pulse is optically monitored by a high speed photomultiplier (PMT) to produce a start signal, which is used to trigger the voltage ramp of the time-to-amplitude converter (TAC). The voltage ramp is stopped when the first fluorescence photon from the sample is detected. It must be stressed that, to avoid pulse pile-up effects which would distort the signal, biasing the decay to shorter times, only one or two photons every hundred exciting pulses should be detected. The TAC provides an output pulse whose voltage is proportional to the time between the start and the stop signal. A multichannel analyser (MCA) converts this voltage to a time channel using an

analog to digital converter. Summing over many pulses the MCA builds up a probability histogram of counts versus time channels.

In order for the probability distributions to be statistically significant, the experiment is continued until one has collected at least 10^4 counts in the peak channel. Under this conditions, the histogram of photon arrival times represents the intensity decay of the sample. However, due to the light pulse having a finite width, the observed decay (here called $R(t)$) is the convolution of the "true" intensity decay of the sample ($I(t)$) and the instrument response function (the "Lamp" profile, $L(t)$):

$$R(t) = \int_0^t L(t-t')I(t')dt' \tag{2.20}$$

In the common practice, the a posteriori analysis of the results of a time-dependent experiment (to obtain the number of different species, their lifetimes and relative populations) is carried out by performing the so-called *iterative reconvolution*. This technique relies on choosing a suitable test function with adjustable parameters (I_c) and iteratively varying the values of the parameters until a minimum of the function χ^2 is reached. χ^2 is defined as:

$$\chi^2 = \frac{1}{n-m-1}\sum_{t=0}^{n}\frac{\left[R(t)-\widetilde{R}(t)\right]^2}{R(t)} \tag{2.21}$$

where $\widetilde{R}(t)$ is the reconstructed decay profile obtained after convolving the test function $I_c(t)$ with the lamp profile, m is the number of fitting parameters and the summation is performed over the n collected data points. In particular, the fluorescence decay of many heterogeneous samples (see Section 3.2.2) can be expressed as a sum of exponential functions, so that $I_c(t)$ is given by:

$$I_c(t) = I_0 \sum_{i}^{n=1,2,3,\ldots} \alpha_i e^{-\frac{t}{\tau_i}} \tag{2.22}$$

where τ_i are the fluorescence lifetimes of the individual emitting species.

However, it has been demonstrated that, for the accurate recovery of complex time-resolved experiments, it is advantageous to combine more than one fluorescence decay curve into a single analysis. The simultaneous analysis of multiple decay experiments is referred to as "global analysis" (Knutson *et al.*, 1983; Beechem *et al.*, 1991). Global analysis procedures are of significant advantage when some unknown parameters of interest are linked between two or more fluorescence decay experiments performed under different conditions (e.g. temperature, excitation/emission wavelengths, etc.). These parameters, which are invariant in all data sets, are called global parameters. The decay parameters α_i and τ_i are then obtained minimizing global χ^2, defined as:

$$\chi^2 = \frac{1}{N-m-1}\sum_{i=1}^{N_{exp}}\sum_{t=0}^{n}\frac{\left[R_i(t)-\widetilde{R}_i(t)\right]^2}{R_i(t)} \qquad (2.23)$$

Here $R(t)$ and $\widetilde{R}_i(t)$ are the observed and reconstructed decay profile for the i^{th} experiment, m is the number of fitting parameters and N is the total number of data points.

Global analysis results in a much steeper χ^2 surface with respect to individual decay analysis and, as a consequence, in a higher probability of recovery of the correct fitting parameters.

Analysis of experimental data has been performed with the software provided by Edimburgh Instruments.

2.2.1.5 Experimental details

Peptide adsorption on cell walls (see Section 3.2.1). Quartz and poly(methylmethacrylate) cuvettes were treated with a 5% (weight/weight) solution of poly(vinylalcohol), poly(ethyleneimine) or poly(ethyleneglycole), overnight. Before use, cuvettes were then thoroughly rinsed with deionized water. Peptide adsorption was quantified by the decrease in emission intensity with time, after the fluorescent analog F10 was dissolved in water from a concentrated methanolic solution (final concentration1 μM). λ_{exc} = 265 nm, λ_{em} = 302 nm; timestep = 1 s.

Lipid flip-flop (see Section 3.7.3). Peptide-induced lipid flip-flop was determined by adding bovine serum albumin (BSA; final concentration = 0.2 mM) to a solution of C6-NBD-PC labeled liposomes (1% molar ratio; total lipid concentration = 0.2 mM). This caused the extraction of C6-NBD-PC molecules located in the outer layer, resulting in a quenching of the NBD fluorescence intensity. After equilibration, a given peptide concentration was added. If this caused lipid flip-flop, C6-NBD-PC becoming exposed to the outer layer could be extracted by BSA, and a further decrease in fluorescence intensity would be observed.

NBD fluorescence was excited at 467 nm, and BSA binding was monitored by measuring NBD fluorescence at 522 nm.

Iodide quenching experiments (see Section 3.8.1). Iodide quenching experiments were performed by titrating a liposome solution 2 mM in lipid, containing 1.0 μM of F10 or A3, with small aliquots of a concentrated iodide solution ([KI] = 4M) prepared on the same day, containing also Na_2SO_3 1 mM, which prevents iodide oxidation to iodine.

Samples were excited at 280 nm, and emission was measured at 304 nm for fluorene and 382 nm for azulene.

Depth dependent quenching experiments (see Section 3.8.2). Quenching experiments using dibromide derivatives were performed with liposomes entirely composed of ePC phospholipids marked with bromine atoms. The relative amount of dibrominated lipids was the same for all three products, as demonstrated by HPLC-MS experiments performed in the manufacturer's laboratory (Avanti Polar Lipids, Alabaster, AL, U.S.A).

Doxyl-containing liposomes were formed by ePC:Cho 1:1 molar ratio with a 7% of labeled lipids (the doxyl moiety is a much more effective quencher of our fluorophore than bromine). The spin label content was determined by double integration of EPR spectra (Chattopadhyay and London, 1987) performed both on the stock solutions of labeled lipids, and directly on an aliquot of the final

liposome solutions (~ 5mM, total lipid concentration), diluted 1:10 with isopropanol. All vesicle preparation contained the same amount of spin labels, within a 10% error.

All depth-dependent quenching experiments (both using dibromide- and doxyl-derivatives) were performed by adding peptide analogs to the different labeled liposomes and to a reference unlabeled liposome solution. The fluorescent analogs were excited at 290 nm (cut-off filter at 295 nm) and, after a 20 minutes equilibration period, the emission spectra were collected between 300 nm and 400 nm (F10) or between 350 nm and 450 nm (A3).

2.2.2 UV-Vis Absorption

UV-Vis Absorption spectra were recorded on a thermostatted J7850 Jasco apparatus (Tokio, Japan).

The concentration of fluorescent peptide analogs was determined by measuring the absorbance of the chromophores linked to the peptide chain (λ=301 nm for Fmc and λ=343 nm for Aal) and comparing it to the corresponding calibration curves (Fmc: ε(301 nm) = (6.3$\pm$0.1) 10^4 $M^{-1}cm^{-1}$; Aal: ε(343 nm)= (4.3$\pm$0.1) 10^4 $M^{-1}cm^{-1}$)

2.2.3 Circular Dichroism (CD)

Circular dichroism is probably the most used spectroscopic technique for the investigation of the secondary structure of peptides and proteins. It consists in measuring the differential absorption of right- and left-circularly polarized UV (or visible) light by dissymmetric molecules. In particular, the main structural information for peptides are obtained in the far UV region (180-250 nm), where the $n\rightarrow\pi^*$ and $\pi\rightarrow\pi^*$ transitions of the amidic bond occur. This signal is strongly dependent on the backbone conformation (Cantor and Schimmel,1980).

When aromatic compounds or other chromophores are linked to the peptide chain, further structural information can be obtained by examining their CD (λ>240 nm): even if these groups are intrinsically not chiral, they can show an induced dichroism due to electronic interactions with the dissymmetric environment.

Based on these considerations, CD was used to determine trichogin secondary structure both in solutions and in the membrane phase. Experimentally, we performed our measurements a thermostatted Jasco J600 apparatus (Tokio, Japan) using quartz cuvettes of 1 mm path length in the far UV region, and 1cm path length for measurements in the aromatic region. 8 scans were recorded during the acquisition of each spectrum, in order to maximize the signal to noise ratio, and an *a posteriori* correction for the background signal was performed, by subtracting the spectrum of a blank solution. Additionally, measurements on large unilamellar vescles (see Section 3.5.1) were carried out at a 1 mM lipid concentration, where the effect of light scattering by liposomes is negligible, as confirmed by recording the spectrum of liposomes alone and by the independence of the signal on the distance between the sample-holder and the detector (Mao and Wallace, 1984).

2.2.4 ATR-FTIR

Attenuated total reflection Fourier transform infrared (ATR FTIR) is one of the most powerful methods for recording IR spectra of biological materials like membranes. It requires few micrograms of sample, and provides information about the conformation and orientation of proteins and peptides in a lipid environment. Because of the long IR wavelength, light scattering problems are virtually non-existent, and highly aggregated molecules or large membrane fragments can be investigated (Tamm, 2002).

In an ATR-FTIR experiment, an internal reflection prism (in our case made of germanium) is covered with single or multiple lipid layer(s) containing the proteins or the peptides, and the infrared beam is focused into the plate (Figure 2.4).

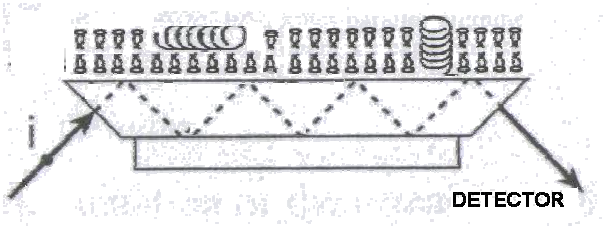

Figure 2.4 Schematic representation of an ATR-FTIR experiment on supported lipid bilayers containing peptides. The incident (i) IR beam propagates via multiple internal reflections within the trapezoidal ATR germanium plate.

The light is propagated into the crystal by multiple internal reflections until it exits to the detector. Wherever the light is reflected, it creates an evanescent field outside the plate, which decays exponentially within a distance comparable to the wavelength used. Absorption of the energy of the evanescent field by the supported membrane (and peptide) provides spectra, which in general are very similar to those obtained with a transmission geometry.

Infrared spectra of proteins and polypeptides exhibit a number of so-called amide bands, which represent different vibrations of the peptide moieties. The amide I normal vibrational mode is the most widely used to study the peptide secondary structure. It originates from the C=O stretching vibration of the amide group (coupled to the in-phase bending of the N-H bond and the stretching of the C-N bond) and gives rise to infrared band(s) in the region between approximately 1600 and 1700 cm^{-1}. The location of the amide I maximum depends on the pattern of hydrogen bonding and on the orientation and distance of interacting dipoles and thus it provides information about the geometrical arrangement of peptide groups in a polypeptide chain. The relationship between the position of the amide I and the type of secondary structure has been recognized by analyzing IR spectra of peptides that fold into well-defined structures (Haris and Chapman 1995). Typical absorption frequencies for α-helices and 3_{10} helices are 1650-1660 cm^{-1} and 1660-1670 cm^{-1}, respectively (Jackson and Mantsch, 1992; Gazit, 1996). In the presence of water or water vapor, the random coil signal falls at the same frequency of the α-helix, hindering an univocal identification of the secondary structure. Substitution of water with D_2O causes the substitution of amide protons with

deuterons in the peptide in random coil conformation, shifting their amide I absorption to lower frequencies (~1640 cm^{-1}).

Experimentally, all the spectra have been recorded on a Nicolet FT-IR (Thermo Electron Co., Madison, WI, U.S.A.) equipped with an ATR germanium cell (12 total reflections on the film side at an incidence angle of 45°C). The ATR element was modified, placing over the plate a homemade gas-tight cover, containing a holder for D_2O, in order to saturate the compartment with D_2O vapors and allow the exchange with water.

In particular, a 200μL droplet containing 13.16 mM POPC and 0.05:1 peptide in CH_3Cl/MeOH 1:1 (v/v) was deposited onto the surface of the germanium crystal (preventively treated with a basic detergent in order to increase its hydrophylicity), taking care to make the film as uniform as possible. The solvent was then evaporated using a gentle argon flow. While evaporating, capillary forces flatten the membranes which spontaneously form oriented bilayers.

512 interferograms were accumulated at a resolution of 2 cm^{-1} and the resulting spectrum was background-corrected by subtracting the signal of the empty cell.

2.2.5 Stopped flow

Stopped-flow allows the kinetics of a reaction to be followed continuously in the millisecond to second time scale, after rapid mixing of the reactants.

A schematic representation of the instrument is shown in Figure 2.5.

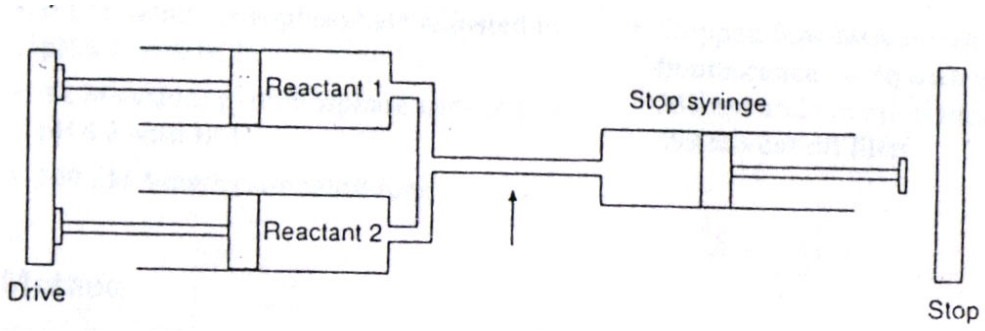

Figure 2.5 Diagrammatic representation of the stopped-flow method. The arrow represents the point of observation.

Two solutions are rapidly mixed together and pass down the observation chamber; by the use of a back syringe, the flow of mixed reactants is suddenly stopped in the cell and the reaction is followed in real time with a suitable detection system (Eccleston *et al.,* 2000).

Our measurements were performed in the laboratory of Prof. G. Coletta in our University, using a SX.18 MV apparatus (Applied Photophysics Limited, Leatherhead, U.K.) with a fluorescence detector and a nominal mixing time of 1 ms. Mixing of asymmetric volumes (1:10 alcoholic peptide solution/liposome system) was employed, to avoid peptide aggregation in water or liposome leakage due to the presence of a large amount of methanol.

2.2.6 Black lipid membranes (BLMs)

Planar lipid bilayer membranes, also called black lipid membranes (BLMs), allow the determination of the ion current that can flow through a pore made up of antibiotic peptides in a membrane (Menestrina *et al.,* 1986).

Figure 2.6 shows the experimental setup used for experiments with planar membranes.

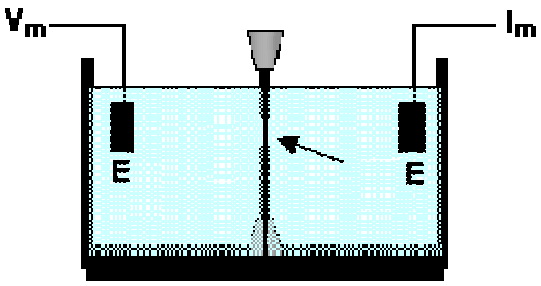

Figure 2.6 Schematic representation of a chamber for the BLM setup. It is divided in two compartments, named cis and trans. The arrow indicates the hole where the bilayer is placed, "E" are the electrodes (Ag/AgCl), V_m indicates the external applied voltage, and I_m the current that flows across the bilayer in the presence of toxins (see text for details).

In this apparatus, the Teflon chamber is divided in two compartments, defined as cis and trans, depending on the side where the membrane-active compound is added. They are separated by a thin Teflon film, characterized by

an hole (0.2 mm wide), where the bilayer is formed (in Figure 2.6, the lipid membrane is indicated by an arrow). Each compartment is provided with a stirrer.

In these experiments, the membrane voltage is externally controlled (V_m) and the transmembrane current required to maintain that voltage (I_m) is measured.

In the absence of peptide, the current is substantially zero, while the introduction of perturbing agents that spontaneously incorporate into the bilayer generates measurable currents. Even the ionic current through a single channel can be readily observed.

BLMs experiments were performed in the laboratory of Dr. Giancarlo Menestrina at the I.T.C. in Povo (Trento, Italy), using membranes formed by 1,2-diphytanoyl-*sn*-glycerophosphocoline (see Table 2.2). Both cell compartments were filled with a solution containing 10 mM Tris (pH 7.00) and 100 mM KCl, and two Ag/AgCl electrodes were used, whose 3M KCl internal solution was separated from the bulk by a 1.5% agarose bridge in order to avoid electrode polarization.

2.2.7 Voltage clamp experiments

Voltage clamp measurements were performed by L/M-EPC7 patch-clamp amplifier (HEKA, Lambrecth, Germany) and data were acquired by a TL-1 Labmaster interface, while simultaneous microscopic visualization was carried out by a Nikon TE300 inverted microscope (Nikon Instruments Corporation, Tokyo, Japan). Other experimental details are reported in Section 3.9.3.2.

2.3 Materials

2.3.1 Peptide synthesis

Synthesis of TricO-Me, F10 and A3 was performed in the laboratory of Professor C. Toniolo at the University of Padua.

It was carried out in solution, using the fragment condensation approach, starting from the C-terminal Leu-OMe group. The benzyloxycarbonyl moiety was used as N-protecting group, and the peptide coupling reactions were performing according by either the 1-(3-dimethylaminopropyl)-3-ethylcarbodiimide (EDC)/HOBt (1-hydroxy-1,2,3-benzotriazole) (König and Geiger, 1970) or by the EDC/HOAt (7-aza-1-hydroxy-1,2,3-benzotriazole) method (Carpino, 1993). The Fmc group was introduced into the Dab side chain using EDC/HOAt. Aal was kindly provided by L. Moroder (Loidl *et al.,* 2000). The purity of the compounds synthesized was checked by Mass-spectrometry (ESI-TOFF), melting point determination, TLC in four elution mixtures and analytical HPLC. Other details were reported by Didonè (2001).

2.3.2 Reagents

All lipids were purchased from Avanti Polar Lipids (Alabaster, AL, U.S.A.) while doxyl-labeled stearic acids from Sigma (St. Louis, MO, U.S.A). Carboxyfluorescein and Texas-red labeled dextran (average molecular weight 10000, neutral form) were obtained from Molecular Probes, Inc. (Eugene, OR, U.S.A.). Spectroscopic grade solvents (Carlo Erba, Milano, Italy) were used. Polyvinyl alcohol (PVA), average M.W. 22000, 88% hydrolyzed and Triton X-100 were purchased from Acros (Geel, Belgium), while Sephacryl S-300, Sephadex G-50 and bovine serum albumin (VI fraction) from Sigma (St. Louis, MO, U.S.A). Fluoren-9-acetic acid, and azulene are Aldrich (St. Louis, MO, U.S.A.)

products, while Laurdan and naphtalene are from Fluka (Buchs, Switzerland). Inorganic salts were purchased from Carlo Erba (Milano, Italy).

3

"An expert is a man who has made all the mistakes,
which can be made, in a very narrow field"
Niels Bohr

Results

3.1. Influence of the fluorophores on peptide properties

As a preliminary step in our investigation, we verified whether both the secondary structure and the membrane perturbing activity of trichogin are affected by covalently attached fluorophores. In addition, we also investigated whether the spectroscopic properties of these fluorophores are perturbed as compared to the isolated molecules. To this end, we performed UV-Vis absorption, circular dichroism, steady-state and time-resolved fluorescence experiments in methanol, where the peptides are very soluble.

3.1.1 UV-Vis Absorption in methanol.

The UV-Vis absorption spectra of analogs F10 and A3 are presented in Figure 3.1.

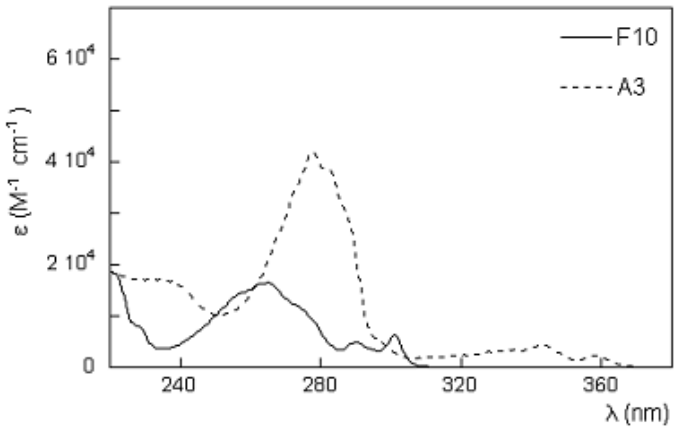

Figure 3.1 Absorption spectra of the peptides investigated, in methanol (25°C).

The absorption spectrum of F10 exhibits the characteristic fluorene absorption bands (Pispisa *et al.*,2002b; Bree and Zwarich, 1969), with maxima at 265 nm [$\varepsilon = (1.6 \pm 0.1)\ 10^4\ M^{-1}\ cm^{-1}$], 290 nm [$\varepsilon = (4.8 \pm 0.1)\ 10^3\ M^{-1}\ cm^{-1}$] and 301 nm [$\varepsilon = (6.3 \pm 0.1)\ 10^3\ M^{-1}\ cm^{-1}$]. Analog A3 exhibits three broad bands, with maxima at 277 nm [$\varepsilon = (4.2 \pm 0.1)\ 10^4\ M^{-1}\ cm^{-1}$], 343 nm [$\varepsilon = (4.3 \pm 0.1)\ 10^3$

M^{-1} cm^{-1}], and 358 nm [ε = (2.2 $\pm$ 0.1) 10^3 M^{-1} cm^{-1}]. This spectrum is very similar to that of Aal, and slightly different from that of azulene (Figure 3.2). The derivatization of the fluorophore with the alanine side chain weakly perturbs the electronic states of azulene, resulting in a small shift of the $S_0 \rightarrow S_2$ and $S_0 \rightarrow S_3$ transitions from 338 and 272 nm, respectively, for azulene to 343 and 277 nm for both A3 and the isolated Aal aminoacid (Foggi *et al.,* 2003; Venanzi *et al.*, 2004).

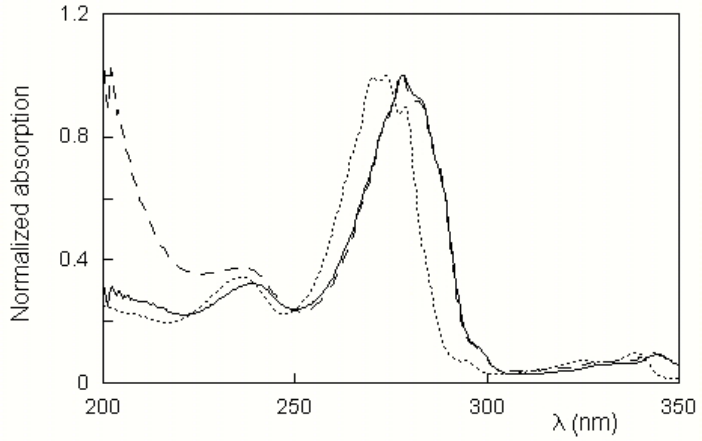

Figure 3.2 Normalized absorption spectra of of A3 (solid line), Aal (dashed line) and azulene (dotted line) in methanol.

3.1.2. Circular dichroism in methanol

The far-UV circular dichroism spectra of the fluorescent analogs and of Tric-OMe in methanol are shown in Figure 3.3.

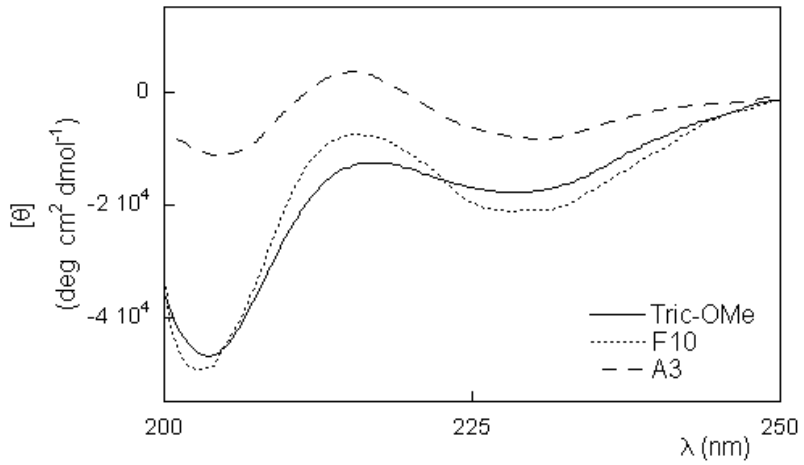

Figure 3.3 Far-UV CD spectra of F10, A3 and Tric-OMe in methanol solution; peptide concentration: 0.1 mM, T=25 °C. Molar ellipticity is based on peptide concentration.

The F10 spectrum is similar to that of Tric-OMe, and displays a negative, rather strong band at about 204 nm (corresponding to the electrically allowed $\pi \rightarrow \pi^*$ transition of the peptide bond) and a weak band at about 227 nm (corresponding to the $n \rightarrow \pi^*$ transition of the peptide bond). These spectral features are typical of right handed helices (Polese *et al.,* 1996; Manning and Woody, 1991), and, in the case of trichogin, they were assigned to a mixed $\alpha/3_{10}$ helical secondary structure (Toniolo *et al.,* 1996).

The similarity between the spectra of F10 and Tric-OMe suggests that no significant structural perturbation is caused by the introduction of the fluorescent label. Interestingly, the lack of an induced dichroic contribution by the fluorene moiety, which is strongly absorbing in this spectral region, indicates that the intrinsically achiral fluorophore is not significantly perturbed by the dissymmetric peptide chain. This probably because of the peripheral position of the chromophore.

The CD spectrum of A3 is significantly different from those of the other analogs. This finding may be ascribed either to a perturbed secondary structure or to an extrinsic dichroic contribution from azulene, this chromophore being separated from the trichogin backbone by only two achiral bonds, as compared to the six bonds in the Fmc group.

To verify the latter hypothesis, we subtracted the spectrum of the unlabeled Tric-OMe from that of the A3 analog (Figure 3.4, left). The difference spectrum shows two positive CD bands, centered at around 203 and 225 nm, corresponding to two azulenylalanine absorption bands (Figure 3.4, right).

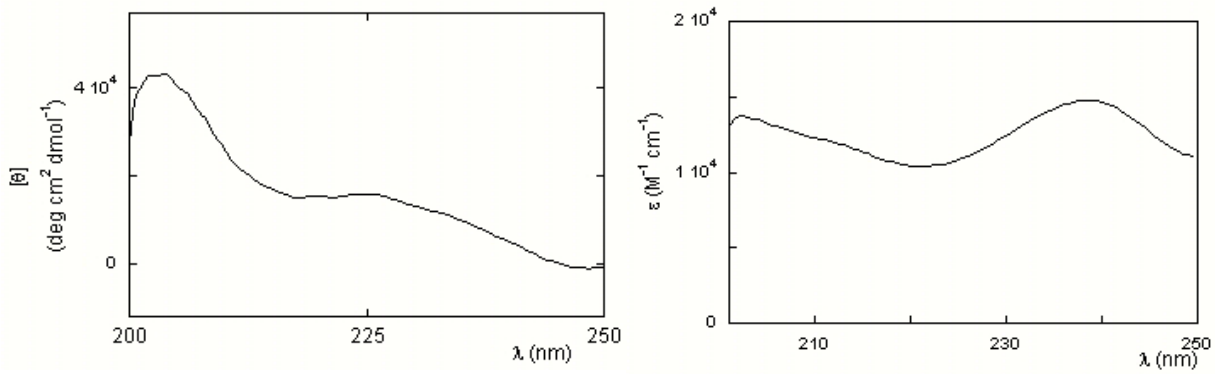

Figure 3.4 Left panel: difference CD spectrum between A3 and Tric-OMe in methanol. Right panel: absorption spectrum of azulenylalanine within the same region (25°C).

Strong induced dichroism bands of azulene are observed in the near-UV region too, where this is the only chromophore that absorbs (Figure 3.5).

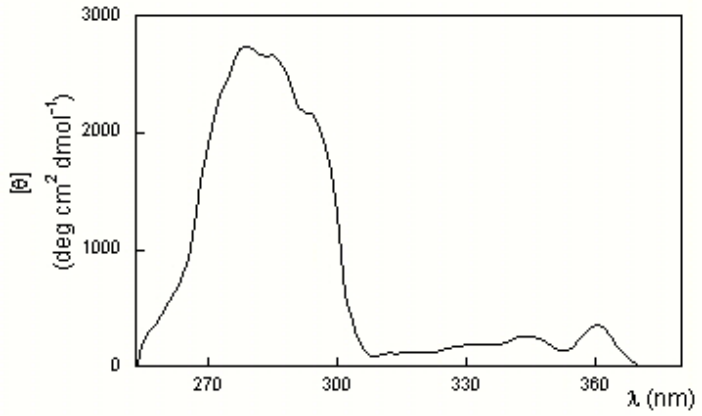

Figure 3.5 Circular dichroism spectrum of A3 in the aromatic absorption region.

The foregoing data show that a significant extrinsic dichroism characterizes both the far and the near UV spectrum of A3. This severely complicates the use of CD spectra for determining the peptide secondary structure (Pispisa *et al.*, 2000a). However, the differences observed in the CD spectra of A3 and Tric-OMe might be due to the induced dichroism contribution of azulene, in which

case the observed CD spectrum would be compatible with a substantially unperturbed secondary structure.

3.1.3 Fluorescence studies in methanol

Steady-state fluorescence spectra of the two analogs are reported in Figure 3.6.

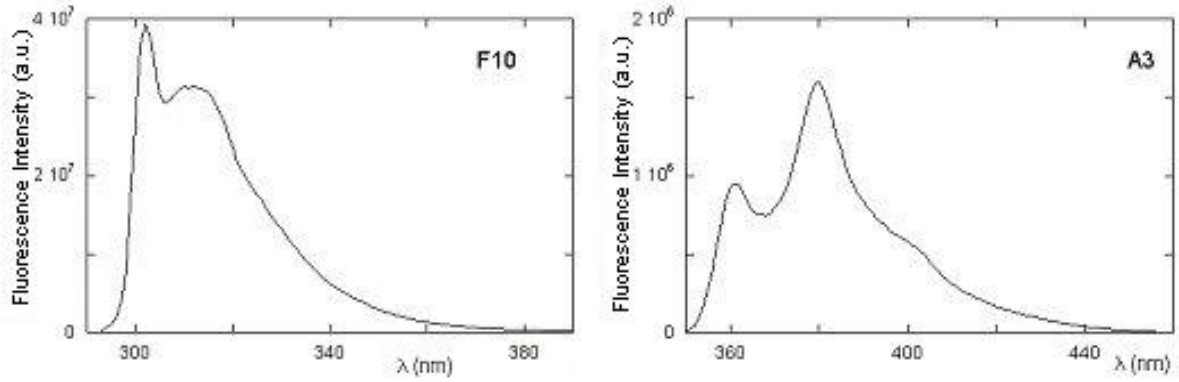

Figure 3.6 Emission spectra of F10 (left) and A3 (right).λ_{exc}=265nm for F10, and λ_{exc}=343 nm forA3. [F10]=5μM and [A3]= 7 μM (T=25°C)

The emission spectrum of Fmc in F10 closely resembles that of the well-characterized fluorene and Fmoc (fluorenyl-9-metyloxy-carbonyl) moieties (Pispisa *et al.*, 2000a and 2000c), exibiting two maxima at 301 nm and 315 nm. The emission of the azulenylalanine residue of A3, characterized by two maxima at 361 nm and 380 nm, differs only slightly from that of the isolated azulene chromophore (Venanzi *et al.*, 2004).

The quantum yields of the two probes are shown in Table 3.1; they are in good agreement with those reported in the literature (Pispisa *et al.*, 2000c; Pispisa *et al.*, 2002a; Venanzi *et al.*, 2004).

The time-decays of Fmc and Aal in the two analogs are shown in Figure 3.7. Both decays can be fitted by an exponential function, and the lifetimes, reported in Table 3.1, are substantially identical to those of Fmc (8.6±0.4 ns;

Pispisa *et al.*, 2000c) and Aal (0.85±0.05 ns; Venanzi *et al.*, 2004), used as references.

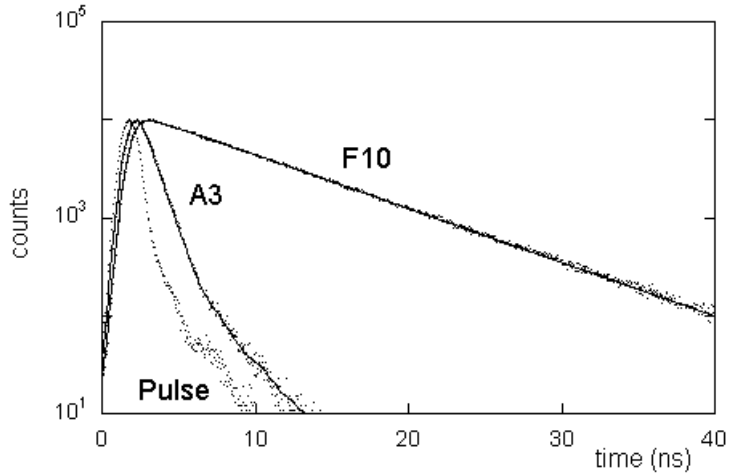

Figure 3.7 Decay curves of F10 (15 μM) and A3 (23μM) in methanol. Dots are experimental data which are fitted by the full lines. The lamp profile is also shown. F10: λ_{exc}=265 nm, λ_{em}=315 nm; A3: λ_{exc}=343 nm, λ_{em} = 380 nm (25°C).

Table 3.1 Quantum yields and emission decay times for the fluorene and Aal groups in F10 and A3 analogs.

peptide	quantum yield	decay time (ns)
F10	0.32 ± 0.01	8.1 ± 0.2
A3	0.042 ± 0.002	0.9 ± 0.1

Interestingly, all the spectral properties (absorption, CD, fluorescence) are not dependent on peptide concentration, at least up to 4 mM, thus indicating that, in methanol solutions, aggregation phenomena are not present. This conclusion is also supported by the observed monoexponential intensity decay shown in Figure 3.7, which is indicative of a homogeneous sample.

3.1.4 Peptide activity

In addition to the structural and spectroscopic properties of the analogs, we assayed their activity in membrane lysis. Figure 3.8 shows the peptide-induced

release of carboxyfluorescein entrapped inside ePC/cholesterol small unilamellar vesicles. These measurements will be discussed in detail in Section 3.6. Here it will suffice to say that the activity of labeled peptides is equivalent to that of Tric-OMe.

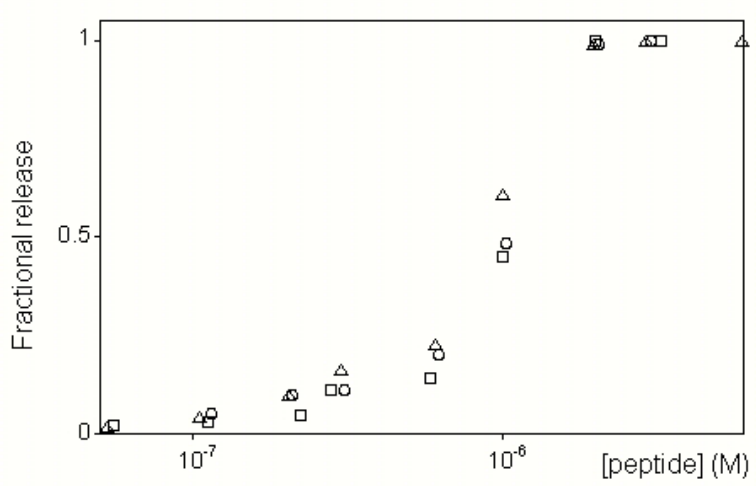

Figure 3.8 Peptide-induced release of carboxyfluorescein from ePC/cholesterol small unilamellar vesicles (3:2 molar ratio, 60μM total lipid concentration). Circles: Tric-OMe, triangles: F10, squares: A3. Fractional release (λ_{ex}=490 nm, λ_{em}=520 nm) was determined 20 minutes after peptide addition.

3.1.5 Summary

Derivatization of Tric-OMe with fluorescent labels does not affect significantly the structure and membrane-perturbing activity of the analogs. Furthermore, the spectroscopic properties of the probes covalently linked to the peptide chain closely resemble those of the isolated fluorophores.

3.2 Peptide behavior in water

To understand the mechanism of action of trichogin, characterization of this peptide in water, which is the solvent where the biological activity is exerted, is needed.

The primary structure of trichogin is such that hydrophobicity predominates. This is why the peptide is sparingly soluble in water: above 50 μM peptide concentration, water solutions of Tric-OMe, F10 and A3 become opalescent. Therefore, one may expect that aggregates form also at the much lower concentrations needed for antibiotic or membrane perturbing activity. In addition, we have observed a significant tendency of the peptides dissolved in water to be adsorbed on the walls of quartz, glass or plastic containers. In order to minimize this effect, which severely complicates spectroscopic studies in water, we pretreated cuvette walls with different materials.

3.2.1 Peptide adsorption

Hydrophilic polymers like poly(vinylalcohol) (Barret *et al.*, 2001), poly(ethyleneimine) (PEI) (Person *et al.*, 2003) or poly(ethyleneglycole) (PEG) adsorb irreversibly to the container walls, forming a stable film. This polar surface then prevents the adhesion of hydrophobic peptides. Therefore, we investigated the extent of peptide adsorption on cell walls after treating quartz and poly(methylmethacrylate) cuvettes with each of these polymers (see Section 2.2.1.5)

The kinetics of peptide adsorption, determined by the decrease of F10 fluorescence intensity, are shown in Figure 3.9.

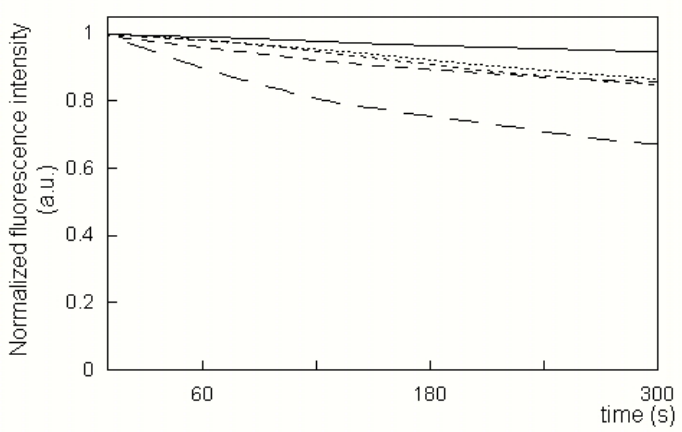

Figure 3.9 Kinetics of F10 adsorption on cuvette walls, as determined by the decrease in fluorene emission intensity ($\lambda_{exc.}$=265 nm, $\lambda_{em.}$= 302 nm; [F10]=1 μM). The curves refer to (from top to bottom) PMMA cuvette pretreated with PVA, untreated quartz cuvette, PMMA cuvette pretreated with PEG, untreated PMMA cuvette and PMMA cuvette pretreated with PEI). Peptide was dissolved in water at time zero, from a 1 mM methanolic solution.

From the results, it appears that peptide adsorption is almost completely suppressed by using PMMA cuvettes treated with PVA. Therefore, these conditions were employed in all experiments, allowing us to quantitatively characterize the behavior of trichogin and its analogs in water.

3.2.2 Peptide aggregation in water

3.2.2.1 UV-Vis absorption

Figure 3.10 compares the UV-Visible absorption spectra of a 6 μM solution in water and in methanol. The spectral shape in water strongly suggests scattering phenomena, very likely arising from aggregation effects.

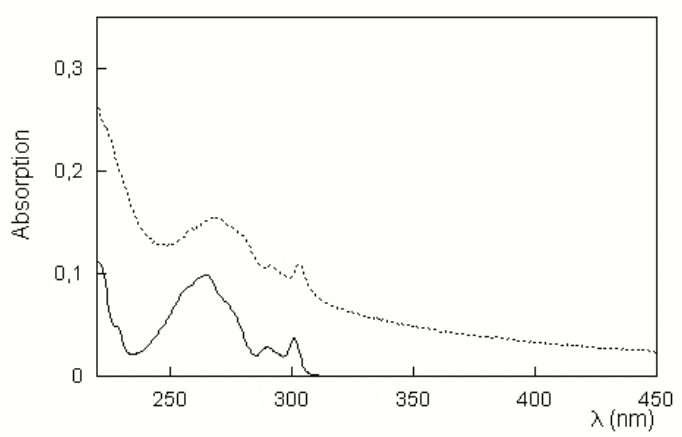

Figure 3.10 Absorption of a 6.0 μM F10 solution in water (dotted line) or methanol (solid line), 25°C.

3.2.2.2 Fluorescence spectroscopy

We performed time resolved fluorescence experiments on F10 in water because this technique is very useful for studying aggregation processes (Stella *et al.*, 2002) owing its sensitivity to heterogeneity effects.

The radiative decay of a fluorophore in a homogeneous medium follows a first-order kinetics. Therefore, as shown for F10 and A3 in methanol (Figure 3.7), the decay of fluorescence intensity is described by a mono-exponential function, such as:

$$I(t) = I_0 e^{-\frac{t}{\tau}} \tag{3.1}$$

where τ is called the fluorescence lifetime. However, when the fluorescent probe experiences ground-state perturbations, a multi-exponential decay is observed, i.e.:

$$I(t) = I_0 \sum_{i=1}^{n} \alpha_i e^{-\frac{t}{\tau_i}} \tag{3.2}$$

where α_i and τ_i are the normalized amplitude and lifetime of the i^{th} decay component, respectively. The normalized amplitudes, under the assumption

that no ground-state interaction leading to non-fluorescent species occurs, can be interpreted as the fraction of molecules decaying with the lifetime τ_i.

Figure 3.11 shows the time decay of F10 in buffer at different concentrations. For comparison, the decay of fluoren-9-acetic acid (Fmc-OH) in buffer is also reported.

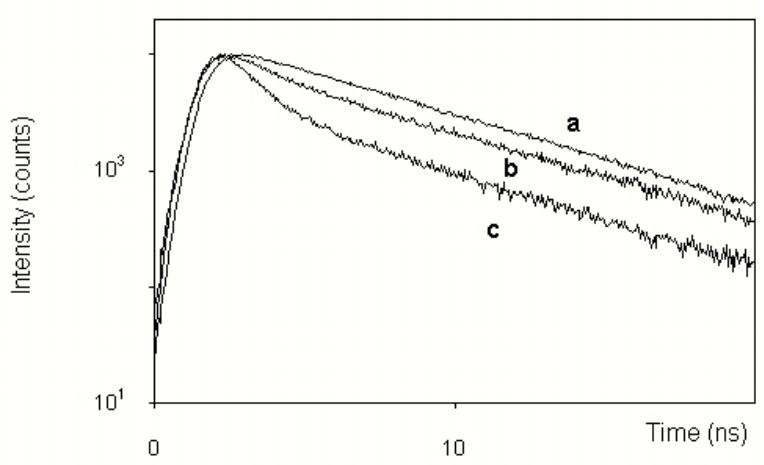

Figure 3.11 Intensity decay curves for Fmc-OH (11μM) (a), F10 (1.9 μM) (b), F10 (11μM) (c) in buffer. λ_{exc} = 265 nm, λ_{em} = 315 nm (20 nm bandwidth; cut-off filter at 305 nm; 25°C).

The decay of Fmc-OH is well described by a single exponential (τ = 5.6±0.1 ns χ^2 = 1.0), as expected for a homogeneous sample. At the lowest concentration studied (0.5 μM), F10 exhibits a very similar decay (data not shown) but, as the peptide concentration increases, a second decay component, characterized by a shorter lifetime, appears.

The analysis of the decay curves was carried out by processing all data simultaneously, using the "global analysis" procedure (Beechem *et al.*, 1991). All F10 fluorescence decay data can be fitted by assuming a double exponential function with lifetimes 5.6±0.1 ns and 0.87±0.08 ns (χ^2 = 1.0). The longest component coincides with the lifetime of the reference, so that it can be attributed to a peptide in a monomeric form. The relative weights of the two lifetime components depend markedly on peptide concentration, suggesting the presence of an aggregation equilibrium (Figure 3.12). In this case, the short lifetime would correspond to an oligomeric species.

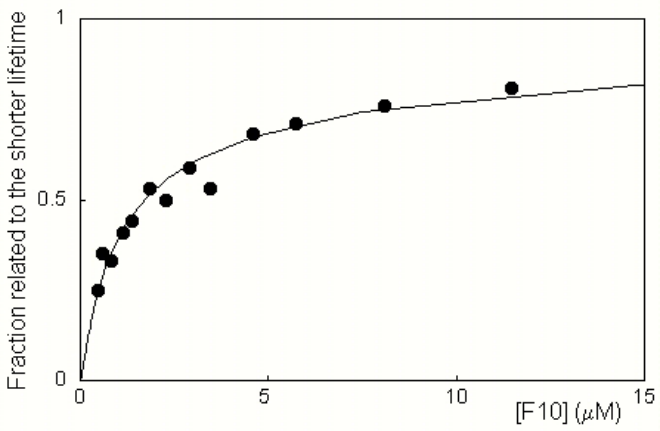

Figure 3.12 Pre-exponential factor associated to the shorter lifetime as a function of total peptide concentration. The experimental points are fitted according to equation (3.7) (solid line).

To verify this hypothesis, we tried to analyze these data according to a simplified model. Since the same lifetimes are observed at all peptide concentrations, we assume, to a first approximation, that only two species are present in solution, namely monomer and aggregate. This assumption means that the following equilibrium:

$$n\mathrm{M} \rightleftarrows \mathrm{M}_n \tag{3.3}$$

is highly cooperative, *i.e.* no intermediates are present.

In equation (3.3), n is the number of monomers in the aggregate, M_n. The equilibrium (aggregation) constant is defined as

$$(K_A)^{n-1} = \frac{X_a}{[X_m]^n} \tag{3.4}$$

where X_a and X_m are the molar fractions of aggregate and monomer, respectively.

One of observables is the pre-exponential factor of the shorter lifetime, which corresponds to the fraction of single peptide chains involved in the aggregates:

$$f_a = \frac{nX_a}{X_p} \tag{3.5}$$

where X_p is the total molar fraction of peptide, as given by

$$X_p = X_m + nX_a \tag{3.6}$$

By combining equations 3.3, 3.4 and 3.5, f_a can be obtained as a function of n, K_A and X_p:

$$f_a = n(1 - f_a)^n \left(K_A X_p\right)^{n-1} \tag{3.7}$$

The data reported in Figure 3.12 were fitted by equation (3.7), using a numerical iterative procedure, in which n and K_A are left as free fitting parameters. The best fitting was obtained with n = 2.3 and K_A = (3.4 ± 0.2) 10^7, as shown in Figure 3.12. The good agreement between experimental and calculated data confirms the hypothesis that the heterogeneous fluorescence decay may be ascribed to aggregation phenomena, while the short lifetime is associated to F10 molecules involved in the aggregates. It must be stressed that we have postulated a highly cooperative process, namely the absence of aggregates of varying sizes, so that n indicates only a lower limit to the number of peptide chains participating to the oligomeric species. Moreover, the results suggest that the size of aggregates is small.

The emergence of a second lifetime ensuing F10 aggregation may be due both to probe-probe or to probe-peptide interactions. To solve this problem, we analyzed the decay data in water by maintaining constant the total peptide concentration (4.6 μM) and varying the relative ratios of unlabeled (Tric-OMe) and labeled (F10) peptides, within the range of 0:4-2:2 (Table 3.2).

Table 3.2 Pre-exponential factor of the shorter lifetime for aqueous solutions of peptides at fixed total peptide concentration and varying ratios between F10 and Tric-OMe.

F10:Tric-OMe ratio	Aggregated fraction
4:0	0.86±0.09
3:1	0.83±0.08
2:2	0.83±0.08

As shown by the preexponential factor associated to the short lifetime component ("aggregated fraction"), within the experimental error, the time-resolved fluorescence curves do not change, thereby indicating that lifetime quenching is caused by peptide-probe interactions and not by interprobe interactions. Furthermore, these results suggest that Tric-OMe has an aggregation behavior similar to that of the labeled peptide, too.

The idea that aggregates in water are small was confirmed by fluorescence anisotropy experiments (Table 3.3). This quantity depends directly on the diffusional motions of the fluorophore (see Section 2.2.1.4), and therefore on the dimension of the molecule or supramolecular complex to which it is linked. Thus, association phenomena result in an increase in fluorescence anisotropy.

As shown in Table 3.3, the anisotropy of F10 in aqueous solutions is higher than in methanol, where the peptide is monomeric. Moreover, in water the anisotropy increases as the peptide concentration is increased, suggesting that aggregates form. However, the values of anisotropy are rather low at all concentration studied, as compared to the high limiting anisotropy value of fluorene (0.4), confirming that the aggregate size is small.

Table 3.3 Anisotropy values for several aqueous or methanol F10 solutions. λ_{exc} = 265 nm, λ_{em} = 320 nm (25°C).

Solvent	Concentration	Anisotropy
MeOH	5 μM	0.005±0.001
H_2O	0.5 μM	0.014±0.001
	5 μM	0.024±0.001

3.2.2.3 Circular dichroism

Circular dichroism experiments were performed to further characterize the aggregates. Figure 3.13 shows the CD spectra of F10 and Tric-OMe in water at peptide concentration of 4.6 μM. Both spectra are significantly different from those obtained in methanol, where self-association is absent, also because fluorene, which in the aggregates is interacting with the peptide chains, probably contributes with a strong induced dichroism.

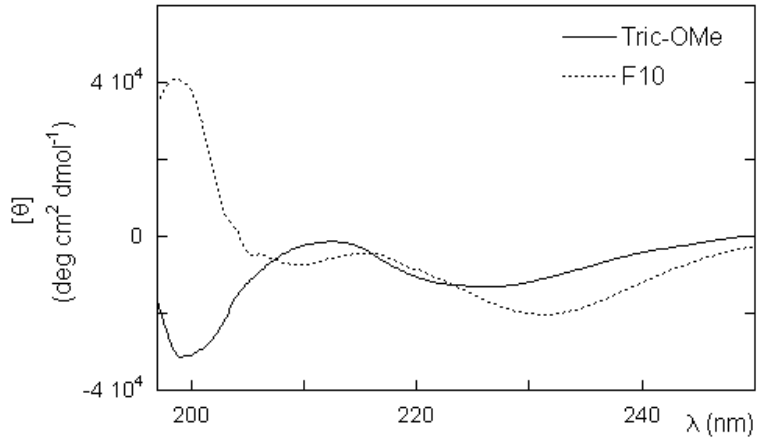

Figure 3.13 Far UV CD spectra of Tric-OMe (solid line) and F10 (dotted line) in water at 4.6 μM peptide concentration.

3.2.3 Summary

In water, trichogin has a strong tendency to self-associate [K_A = (3.4±0.2) 10^7], and the aggregates are rather small [n = 2.3].

3.3 Water-membrane partition

All models presented in recent years to describe the mode of action of antimicrobial peptides, suggest that the membrane permeation process takes place via two major consecutive steps: 1) peptides bind onto the surface of the membrane until a threshold concentration occurs and 2) they organize to achieve a permeation pathway (Shai, 2002; see Section 1.2). Therefore, the first important step in the study of the mechanism of action of an antibiotic peptide is to establish its affinity for membrane bilayer and the chemical and physical conditions that modulate this binding affinity (Epand and Epand, 2000).

3.3.1 Steady-state fluorescence experiments

The association of a peptide to membranes can be quantitatively described by the partition equilibrium between the aqueous and the lipid bilayer phase (White *et al.*, 1998; Coutinho and Prieto, 2003;Loura *et al.,* 2003; Santos *et al.*, 2003), according to the following expression:

$$K_P = \frac{X^P_{membrane}}{X^P_{water}} = \frac{\dfrac{[P]_{membrane}}{[L]+[P]_{membrane}}}{\dfrac{[P]_{water}}{[W]+[P]_{water}}} \cong \frac{[W][M]_{membran}}{[L][M]_{water}} \qquad (3.8).$$

K_p is the mole fraction partition coefficient, $X^P_{membrane}$ and X^P_{water} are the peptide molar fractions in the membrane and in the buffer, respectively, $[P]_{membrane}$ and $[P]_{water}$ are the bulk molar concentrations of peptide in the bilayer and water phases, respectively, and $[L]$ and $[W]$ are the molar concentrations of lipid and water.

The fraction of membrane-bound peptide can be easily obtained as an hyperbolic function of total lipid concentration, i.e.:

$$f_{membrane} = \frac{[P]_{membrane}}{[P]_{total}} = \frac{\frac{K_P}{[W]}[L]}{1 + \frac{K_P}{[W]}[L]} \qquad (3.9)$$

In our case, the membrane-water partition of the F10 analog was determined by steady-state fluorescence experiments, by measuring the change in the peptide emission intensity induced by the addition of increasing amounts of liposomes (White *et al.*, 1998), at fixed peptide concentration. This is possible if the observed fluorescence intensity, at a given peptide/lipid concentration, is a linear function of the molar fraction of the species present in the system. For instance, when only two species are present in the sample (e.g. peptide in water and membrane-bound), the emission intensity is proportional to the molar fraction of molecules bound to the membrane, as given by:

$$I_{observed} = f_{membrane} I_{membrane} + f_{water} I_{water} = f_{membrane}\left(I_{membrane} - I_{water}\right) + I_{water} \qquad (3.10).$$

Then one obtains:

$$\frac{I_{observed}}{I_{water}} = \left(\frac{I_{membrane} - I_{water}}{I_{water}}\right) f_{membrane} + 1 \qquad (3.11)$$

Figure 3.14 shows the partition curves measured at three different peptide concentrations (1.1, 11 and 30 μM).

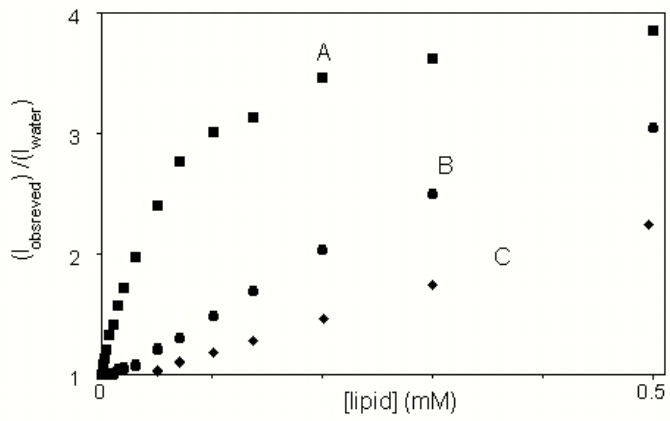

Figure 3.14 Membrane-water partition curves for F10, as detected by the fluorescence intensity ($I_{observed}$), normalized by the intensity measured in the absence of liposomes (I_{water}). Peptide concentration:1.1μM (A), 11μM (B), 30 μM (C). λ_{exc} =288 nm, λ_{em} =330 nm (25°C). Intensities were corrected for scattering effects according to Ladokhin *et al.* (2000) using water-soluble tryptophan as a reference.

These data show that, as peptide concentration increases, association with the phospholipid bilayer becomes less favored. However, on the basis of Equation 3.9, the binding curve should not depend on peptide concentration. Therefore, the observed behavior indicates that phenomena other than a simple partition equilibrium are present, such as aggregation in water and/or in the lipid phase. Consistently, we have already shown that aggregates are indeed present in the water phase but, at this time, it would be interesting to know whether the peptide associates to the membrane as a single species or also as aggregates. To this end, we performed binding experiments using the time resolved fluorescence technique.

3.3.2 Time-resolved fluorescence experiments

In contrast to steady-state experiments, in time-resolved measurements we chose to keep fixed the lipid concentration (0.2 or 2.0 mM), while varying peptide concentration.

At least three species are present in our system and contribute to the overall fluorescence: the monomer, the aggregate in water (see Section 3.2.2.2) and the membrane-bound peptide. Therefore, our system should exhibit a triple

exponential decay, with two lifetimes constrained to the values measured in water, and the third one corresponding to the membrane bound peptide.

Indeed, the experimentally determined decay are multiexponential (Figure 3.15), but a global analysis of the curves of F10 at a 2mM lipid concentration showed the inadequacy of a three-component model to describe the system under investigation. A high global χ^2 value (4.6) was obtained on assuming the third lifetime to be independent on peptide concentration ("global" parameter). If one allows it to vary, only a slight improvement is observed (χ^2 = 2.3), but the third lifetime exhibits a random behavior as a function of peptide concentration, confirming the inadequacy of this model (see Figure 3.15 A).

This result indicates that the fluorescence decay of membrane-bound peptides can not be described as a simple exponential function, and that some degree of heterogeneity is present in this phase too. Therefore, we tried to fit the data with a fourfold exponential function, with two components corresponding to monomer and aggregate in water (5.6±0.1 ns and 0.87±0.08 ns), and the other two to two other species, not yet identified, in the membrane phase. The latter two lifetimes were left to vary freely as global fitting parameters. In this case, a good fit is obtained, as judged by the global χ^2 value (0.95) and the distribution of residuals (Figure 3.15 B). The two recovered lifetimes associated to the membrane-bound species are 2.2 ± 0.2 ns and 7.0 ± 0.2 ns.

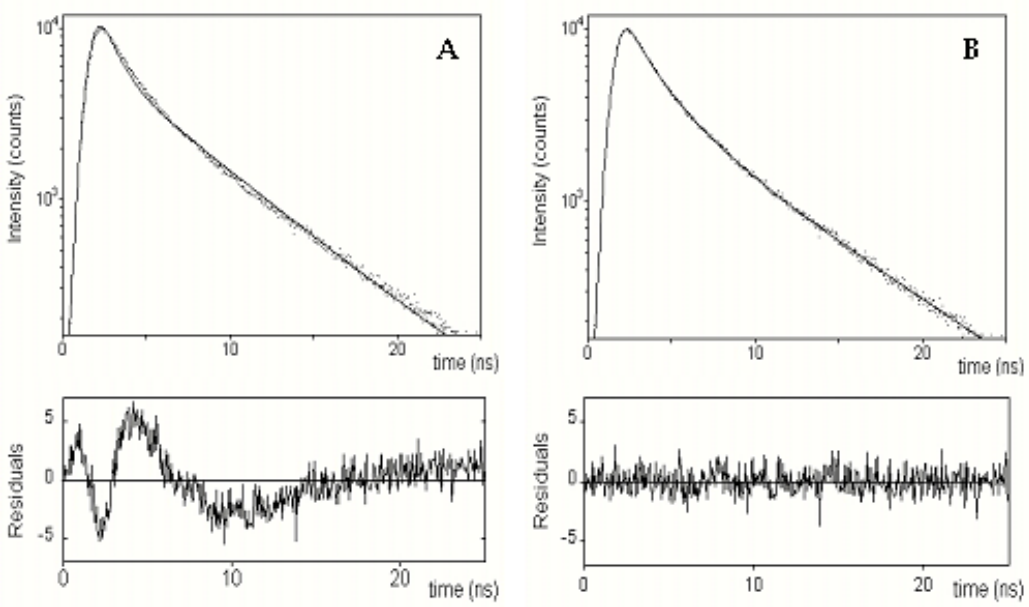

Figure 3.15 *Upper panel*: fluorescence decay intensity of F10 (50 μM) at lipid concentration 2mM; *A:* dots represent the experimental decay, while the solid line is the global fit with a triple exponential function*; B:* the solid line here is the sum of four exponential functions obtained as described in the text. *Lower panel:* distribution of the residuals associated to triple (*A)* and the quadruple *(B)* exponential global fits.

The molar fractions (the pre-exponential factors of equation 3.2) of each of the four lifetime component, in the presence of 2 mM lipid concentration, are reported in Figure 3.16. Each term shows a clear and distinctive dependence on peptide concentration.

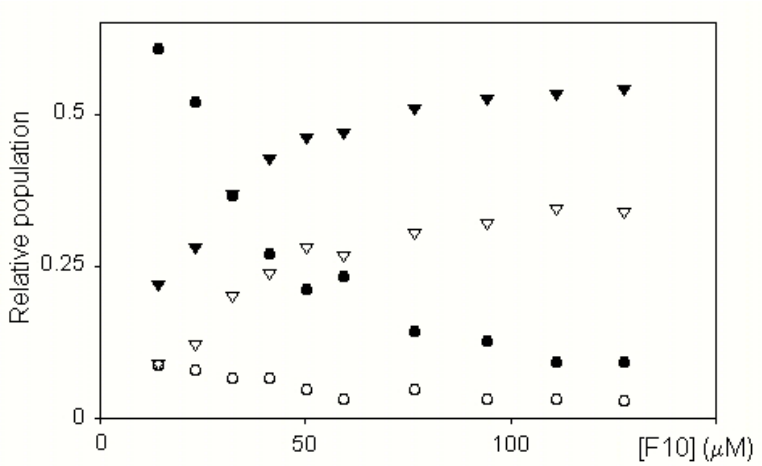

Figure 3.16 Pre-exponential factors, as determined from time-resolved fluorescence data for F10 in the presence of 2mM lipid concentration, corresponding to the following lifetimes: 0.87 ns *(open triangles)*, 2.2 ns *(solid triangles)*, 5.6 ns *(open circles),* and 7.0 ns *(solid circles).*

Similar results were obtained for F10 in 0.2 mM lipid concentration (global χ^2 = 1.09; Figure 3.17).

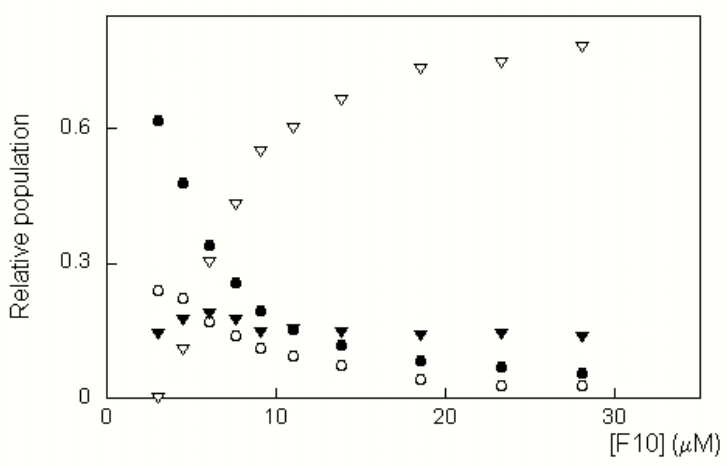

Figure 3.17 Pre-exponential factors, as determined from time resolved fluorescence data, for F10 in the presence of 0.2mM lipid concentration, corresponding to the following lifetimes: 0.87 ns *(open triangles)*, 2.2 ns *(solid triangles)*, 5.6 ns *(open circles),* and 7.0 ns *(solid circles).*

The observed heterogeneity in the membrane phase could be due, in principle, to several factors, such as a slow relaxation of the membrane, a ground state heterogeneity, resulting from different environments around the fluorophore, or different conformations of the peptide (Ladokhin and White, 2001). We analyze now each hypothetical contribution.

A slow relaxation of the environment of the fluorophore would indicate a rearrangement of the dipoles surrounding the probe, following the transition to the excited state. This could occur in a time scale comparable with the fluorescence lifetime, because of the high viscosity of membrane. Since, in this case, the environment of the fluorophore is changing with time, its decay becomes non-exponential.

A ground state heterogeneity would suggest that the probe experiences different perturbations before being excited, as due, for instance, to different positions in the membrane, or different conformations of the peptide.

The observation that the fluorescence decay of the membrane-bound peptide is strongly dependent on peptide concentration definitely rules out

conformational heterogeneity and solvent relaxation as the main reasons for the multi-exponential decay. Moreover, as shown in Figure 3.18, the emission spectrum of fluorene is almost insensitive to solvent polarity (Pispisa *et al.*, 2000c). This indicates that the excited state dipole is substantially coincident with that of the ground state. As a result, the slow solvent relaxation mechanism appears to be very unlikely.

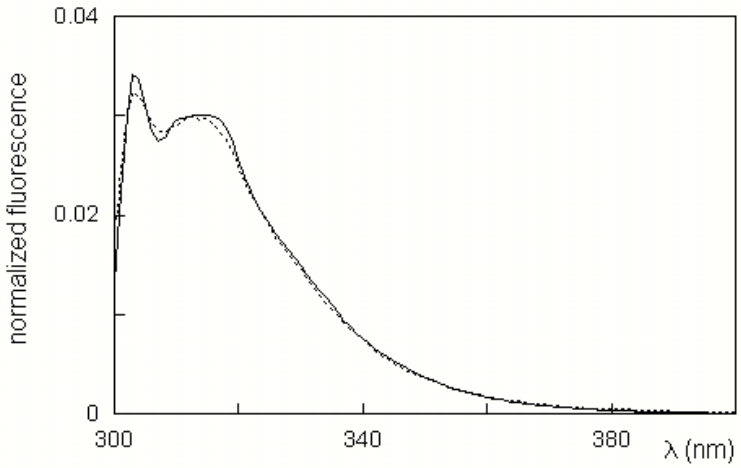

Figure 3.18 Normalized emission spectra of F10 at 0.5 μM concentration in water (dashed line) and in the presence of 0.2 mM lipids (solid line).

Finally, the dependence on peptide concentration of the multiexponential fluorescence decay strongly suggest that the heterogeneity arises from different aggregational states in the membrane phase, although the possibility of a concentration-induced change in orientation cannot be ruled out (Huang, 2000).

Our model is schematically presented in Scheme 3.1:

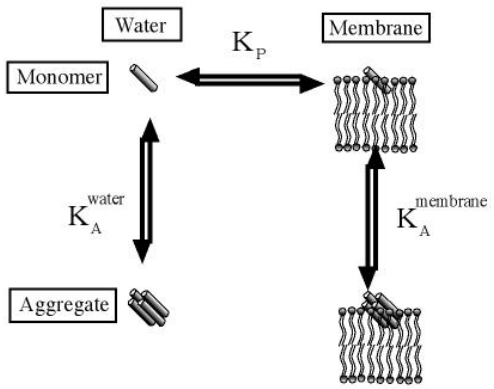

Scheme 3.1 Model of trichogin behavior in a water-membrane system.

The peptide is in equilibrium between a monomeric and an aggregated state, both in water and in the membrane phase. Monomers in the two phases are related by a partition equilibrium, while the situation is more complex in the case of aggregates. Due to the diversity of the water and membrane physico-chemical environments, it may be reasonably predicted that the aggregates in the two phases have different structure and/or size. Therefore, they can not be related by a simple partition equilibrium. All the same, the three equilibria described above are sufficient to define the relative concentration of the four species (monomer and aggregate in the two phases) and predict a dependence of peptide-membrane association on total peptide concentration, as experimentally observed from partition experiments (see Section 3.3.1).

Time-resolved data allow us to know the molar fraction of each species. Accordingly, we have fitted our data with a four component function, which is in agreement with the model described in Scheme 3.1. However, we still need to associate the two lifetimes, corresponding to membrane-bound peptides, to the monomeric and aggregated species. The data reported in Figures 3.16 and 3.17 show that the weight of the longest lifetime observed in the membrane phase (7.0 ± 0.2 ns) decreases as peptide concentration increases. Therefore, this lifetime corresponds to the membrane-bound monomer, while the other component (2.2 ± 0.2 ns) may be assigned to the oligomer. This hypothesis is supported by the finding that the aggregated form is substantially quenched with respect to the monomer, as already observed in water. Furthermore, both species have a significantly longer lifetime in the membrane phase than in water, as expected from the increase in fluorescence intensity caused by membrane binding.

Having associated fluorescence lifetimes and peptide species, it is now possible to check whether the data reported in Figure 3.16 follow the model of Scheme 3.1. The easiest way is to analyze each of the three proposed equilibria separately.

The fraction of peptide molecules in each of the four species, corresponding to the preexponential factors determined in the time-resolved experiments can be defined as follows:

$$\alpha_{monomer}^{water} = \frac{[M]_{water}}{C_p}; \qquad \alpha_{monomer}^{membrane} = \frac{[M]_{membrane}}{C_p};$$
$$\alpha_{aggregate}^{water} = \frac{n[M_n]_{water}}{C_p}; \quad \alpha_{aggregate}^{membrane} = \frac{n'[M_{n'}]_{membrane}}{C_p} \tag{3.12}$$

where n and n' are the numbers of monomers (designed as M) forming the aggregates (M_n) in water and in membrane, respectively, C_p is the peptide molar concentration. The concentration of the species are calculated considering the total volume of the solution.

The equations used to describe aggregation or partition equilibria were reported in previous sections. Monomer partition, for instance, should follow Equation 3.9, and should be independent on peptide concentration. The fraction of membrane-bound monomers can be calculated from the experimental data as follows:

$$f_{membrane-bound\,monomer} = \frac{\alpha_{monomer}^{membrane}}{\alpha_{monomer}^{membrane} + \alpha_{monomer}^{water}} \tag{3.13}$$

This fraction is shown in Figure 3.16. As expected for a simple partition equilibrium, it does not depend on peptide concentration (Equation 3.9), confirming our model. From its value, the partition constant K_P is (1.3±0.3)10^5 is obtained.

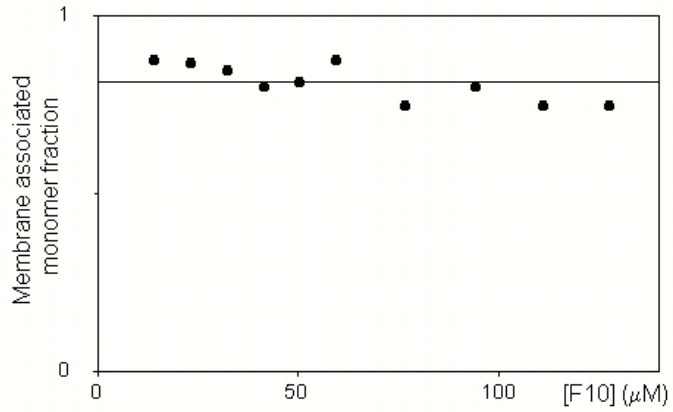

Figure 3.19 Water-membrane partition equilibria of monomeric F10 in the presence of 2mM lipid concentration. The continuous line is the fit obtained according to equation 3.9.

On the other hand, the fraction of aggregated peptide, which should follow Equation 3.7, and the peptide molar fraction in each phase can be calculated according to the following equations:

$$
\begin{aligned}
f_{aggregate}^{water} &= \frac{\alpha_{aggregate}^{water}}{\alpha_{monomer}^{water} + \alpha_{aggregate}^{water}} \\
X_p^{water} &= \left(\alpha_{monomer}^{water} + \alpha_{aggregate}^{water}\right)\frac{C_p}{[W]} \\
f_{aggregate}^{membrane} &= \frac{\alpha_{aggregate}^{membrane}}{\alpha_{monomer}^{membrane} + \alpha_{aggregate}^{membrane}} \\
X_p^{membrane} &= \left(\alpha_{monomer}^{membrane} + \alpha_{aggregate}^{membrane}\right)\frac{C_p}{[L]}
\end{aligned}
\qquad (3.14)
$$

Figures 3.20 A and B report these data for the water and membrane phases, respectively.

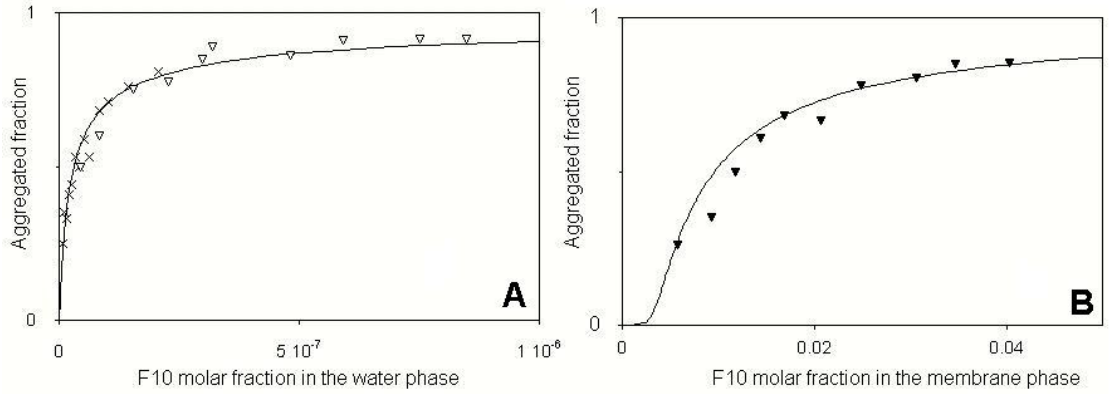

Figure 3.20 *(A)* Aggregation equilibrium of F10 in water (triangles), as obtained by time-resolved data in the presence of membranes (lipid concentration: 2 mM). For comparison, the data measured directly in buffer (crosses) are also shown.
(B) Aggregation equilibrium of F10 in the membrane phase (lipid concentration: 2 mM). The continuous line is a fit of these data according to equation 3.7

From the results it appears that the data describing aggregation in water (observed from the measurements reported in Figure 3.16) are in very good agreement with those experimentally observed in the same solvent, in the absence of membranes (Figure 3.12, Section 3.2.2.2). This finding strongly

supports the proposed model. On the other hand, the curve describing the aggregation equilibrium in the membrane (Figure 3.20 B) shows that aggregation in this phase is much less favored as compared to water, and exhibits a marked sigmoidal shape. By using equation 3.7, we obtain the values of n=8.0 and $K_A^{membrane}$=154±8 (continuous line in Figure 3.20 B), showing that aggregates in the membrane phase are larger than in water (K_A^{water} = (3.4±0.2) 10^7, n_{water}=2.3; see Section 3.2.2.2).

The good agreement between the experimental and calculated aggregation and partition equilibria confirm the idea that the heterogeneity observed for the peptide fluorescence decay in the membrane phase is primarily due to the formation of aggregates.

3.3.3 Summary

Time-resolved fluorescence data show that trichogin tends to self-associate not only in water, but also in the membrane phase.

3.4 Peptide aggregation in membrane: FRET experiments

To validate the idea that the peptide forms aggregates in the membrane phase, we took advantage of the ability of analogs F10 and A3 to act as a donor-acceptor resonance energy transfer (FRET) pair.

The efficiency of the FRET phenomenon is strongly dependent on the interprobe distance and orientation (see Section 2.2.1.2). This property can then be used to determine the presence of aggregates in the membrane as the transfer efficiency is expected to vary significantly on going from a monomeric random distribution of peptide to an aggregate (Strahilevitz *et al.*, 1994; Schuman *et al.*, 1997).

We performed time-resolved fluorescence experiments at fixed F10 and lipid concentration (2 μM and 2mM respectively), by increasing the A3 concentration. The quenching efficiency caused by the FRET phenomenon was determined by the decrease in average fluorescence decay–time of the donor as a function of the acceptor concentration. Time resolved fluorescence measurements are preferred over the steady state experiments, in order to avoid inner-filter effects caused by acceptor absorption (Pispisa *et al.*, 2003).

The experimentally determined energy-transfer efficiencies are shown in Figure 3.22. These values are compared with the efficiencies theoretically expected in the case of a random distribution of peptides in liposomes (dashed line in Figure 3.22). To calculate these theoretical energy transfer efficiencies, one assumes that peptides are located in the surface of both leaflets of the membrane, considered as bidimensional layers (Fung and Stryer, 1978), and that quenching across the bilayer, peptide diffusion during the donor excited state lifetime, excluded volume effects and non coplanarity of donor and acceptor do not hold. Indeed, interlayer FRET can be neglected because the Förster radius is 22 Å (see below), as compared to a 44 Å bilayer thickness (Schuman *et al.*, 1997), and peptide diffusion in the membrane is not significant in a nanosecond fluorescence timescale (Kusba *et al.*, 2002). Finally, excluded

volume effects, or non-coplanar donor and acceptor, if present, would only lead to a decrease in theoretical transfer efficiency.

Using this model, the intensity decays for a random distribution of donors and acceptors is given by:

$$I_{DA}(t) = I_D^0 \exp\left[-\frac{t}{\tau_D} - \Gamma\left(\frac{2}{3}\right)\frac{C}{C_0}\left(\frac{t}{\tau_D}\right)^{\frac{1}{3}}\right] \qquad (3.15)$$

where τ_D is the donor decay in the absence of acceptors, $\Gamma\left(\frac{2}{3}\right)$ is the gamma function, C is the acceptor concentration and C_0, defined as $(\pi R_0^2)^{-1}$, is the acceptor concentration corresponding to 66% transfer efficiency.

The efficiency of energy transfer can be then calculated:

$$E = 1 - \frac{\int_0^\infty I_{DA}(t)dt}{\int_0^\infty I_D(t)dt} \qquad (3.16)$$

Calculation of the Förster distance (R_0) in the membrane requires knowledge of spectral properties of the probes, such as donor quantum yield and acceptor molar extinction coefficient. However, the experimental determination of these quantities is complicated by the strong scattering present in liposome suspensions. Therefore, they were measured in decanol, the organic solvent whose dielectric properties more closely mimic the interior of a membrane (White *et al.*, 1998).

Figure 3.21 shows the overlap of F10 emission and A3 absorption in this medium, where the quantum yield of the F10 donor is 0.33±0.01. With these data, an R_0 of 22 ± 1 Å was obtained.

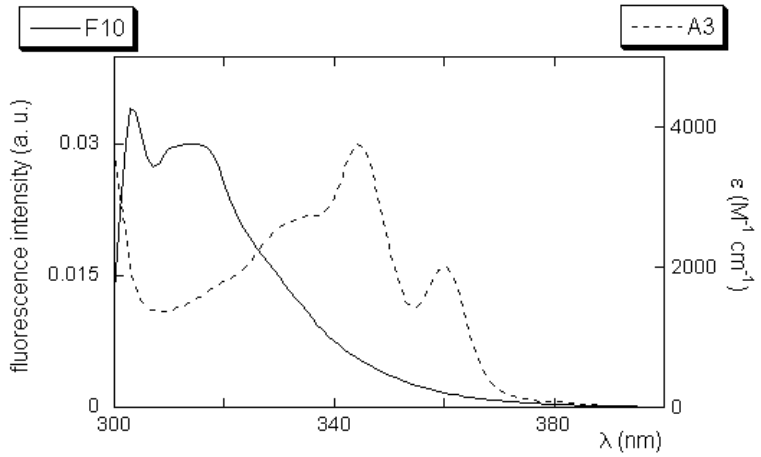

Figure 3.21 Normalized emission spectrum of F10 and absorption spectrum of A3 in decanol.

Finally, we assume a per lipid surface area of 95.6 Å^2 (Lis *et al.*, 1982) while the average decay time of F10 in the presence of liposomes (2mM lipid concentration), and in the absence of A3 (τ_D) is 6.5 ns.

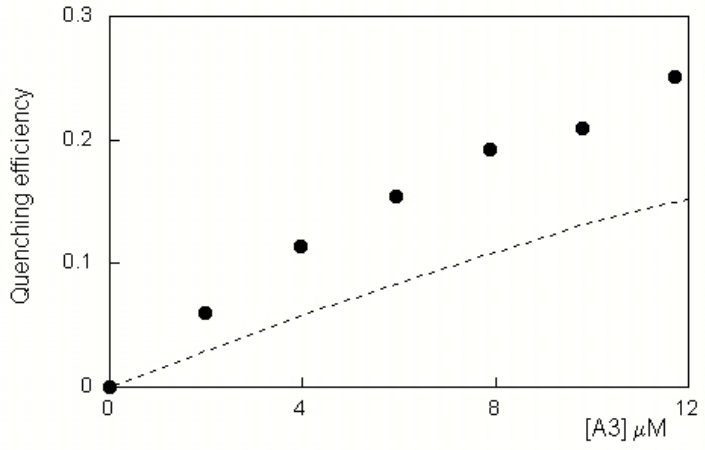

Figure 3.22 Intermolecular RET efficiency between F10 and A3 analogs in the membrane (lipid concentration 2mM, [F10] = 2μM; full circles), as a function of acceptor-labeled peptide (A3). For comparison, the quenching efficiency for a random distribution of peptide in the bilayer is reported as a dashed line(see text).

As a result (Figure 3.22), a large deviation of the experimental points from the theoretical curve is observed, strongly suggesting that peptide aggregates are present in the membrane.

3.4.1 Summary

FRET experiments confirm the formation of peptide aggregates in the membrane.

3.5 Structural features of trichogin in membrane

3.5.1 Circular dichroism experiments

To determine whether membrane-association induces a perturbation in the secondary structure of the peptide, we performed circular dichroism meaurements on the Tric-OMe analog, in order to avoid the possible induced dichroism due to the fluorophores. Experiments were carried out using a 1 mm path length cell. Therefore, a 97 μM peptide concentration was needed in order to obtain a good CD signal. Liposomes were added up to a 1 mM concentration, which maximizes the membrane-bound peptide fraction, while keeping scattering artifacts absents, as checked by preliminary experiments (see Section 2.2.3).

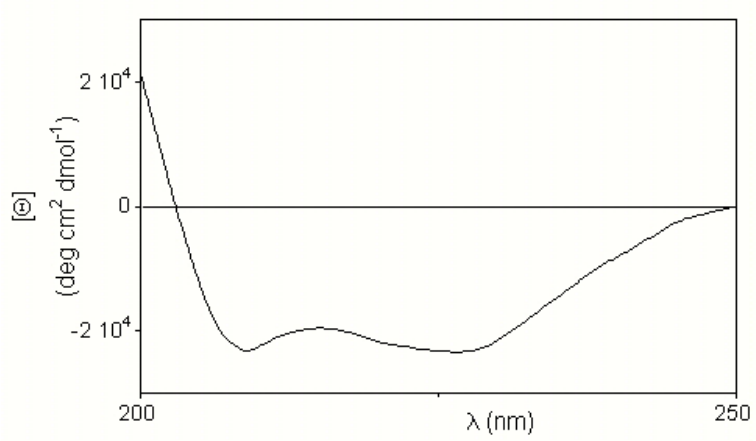

Figure 3.23 CD spectrum of Tric-OMe in a water solution of ePC/cholesterol liposomes. ([Tric-Ome] =97 μM, [Lipid] = 1mM)

The CD spectrum, shown in Figure 3.23, is the typical spectrum of an α-helix. Therefore, membrane binding seems to favor this conformation with respect to the mixed $3_{10}/\alpha$ helix present in methanol. However, it is worth noting that, according to the aggregation and partition equilibria previously determined, the experimental conditions for CD measurements are not suitable to get the spectrum of a single species, but rather the spectral patterns are the sum of the

contributions of all species. Nevertheless, a transition towards the α-helix of the peptide by membrane association seems likely. To confirm this idea, the secondary structure of trichogin in the membrane was investigated by FTIR-ATR measurements.

3.5.2 ATR-FTIR measurements

Attenuated total reflection Fourier transform infrared (ATR-FTIR) absorption provides informations about the conformation and orientation of proteins and peptides in a lipid environment. Experimentally, all the spectra were performed covering the germanium crystal with a monolayer of POPC/trichogin 20:1. Moreover, the ATR element was modified, placing over the plate a homemade gas-tight cover containing a holder for D_2O, in order to saturate the compartment with D_2O vapors and allow the exchange with water(see Section 2.2 for details).

The equilibration time necessary to achieve a complete exchange (190 min) was determined recording the spectra of the lipid film alone in the presence of D_2O as a function of time (Figure 3.24) and following the increase of the D-O absorption (2500 cm^{-1}) and the contextual decrease of the O-H stretching signals (3400 cm^{-1}) (Figure 3.25).

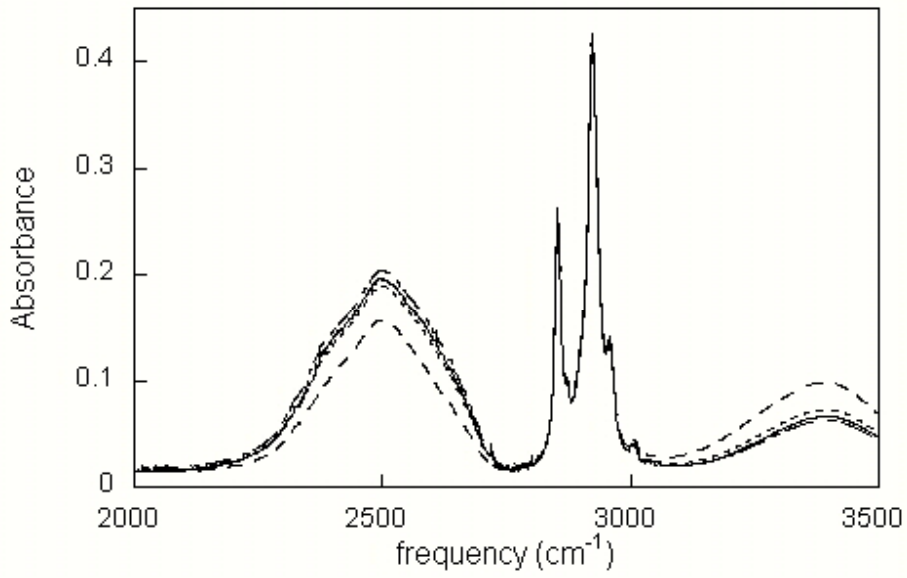

Figure 3.24 IR spectra of the lipid alone after 25 minutes (dashed line), 90 minutes (dotted line), 140 minutes (straight line) and 195 minutes (dashed dotted line) after the addition of 0.6 mL D_2O in the cell.

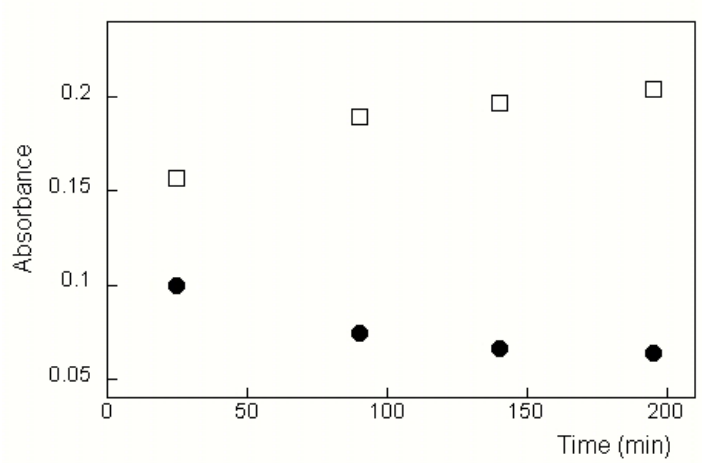

Figure 3.25 Plot of absorbance as a function of time at 2500 cm^{-1} (corresponding to the O-D stretching frequency; empty squares) and at 3400 cm^{-1} (corresponding to the O-H stretching frequency; filled circles).

It must be pointed out that no variation of the symmetric and antisymmetric lipid methylene absorption (2850 and 2920 cm^{-1} respectively) was observed during the D_2O/ H_2O exchange process, indicating that the degree of membrane hydration remains constant.

The ATR-FTIR spectrum of the peptide-containing membrane, before and after equilibration with D_2O, is reported in Figure 3.26.

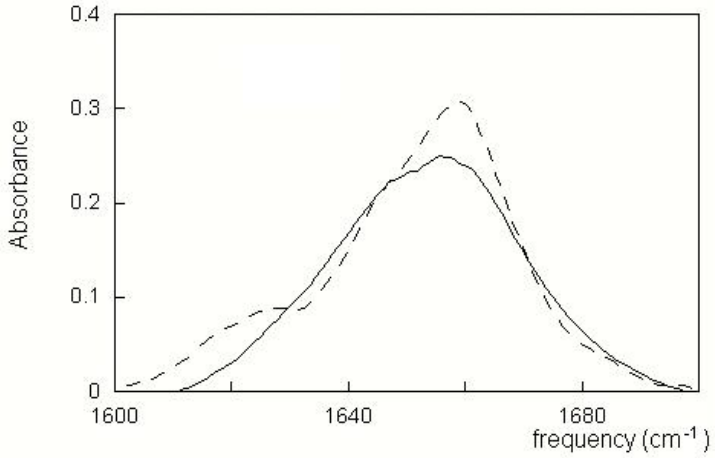

Figure 3.26 ATR-FTIR spectra in the amide I region of trichogin in the presence of POPC lipids 1:20, after 20 minutes (straight line) and 3 hours (dashed line) the addition of D_2O vapours in the cell.

Both spectra have a maximum at approximately 1655 cm^{-1} indicating that the α-helical conformation is predominant. It is interesting to mention that a transition towards an α-helical conformation following membrane association has been reported in the literature for a wide number of antimicrobial peptides. The membrane environment conformational equilibria towards ordered structures, very likely because intramolecular hydrogen bonds are favored by the absence of solvent competition. (Shai, 2002; White *et al.*, 1998; Ladokhin and White, 1999).

3.5.3 Summary

CD and IR results suggest that membrane binding brings about a conformational transition towards α-helix.

3.6 Active species in membrane

3.6.1 Carboxyfluorescein release

Trichogin kills bacteria by permeabilizing their membranes. Therefore, an easy way to characterize its activity is to measure the peptide-induced membrane leakage in model systems, such as liposomes

Trichogin activity was investigated by performing leakage experiments on carboxyfluorescein(CF)-loaded large unimellar vesicles as a function of F10 concentration, at the same lipid concentrations as that used in the previously described time-resolved fluorescence experiments (0.2mM and 2mM).

Figure 3.27 shows several carboxyfluorescein release curves obtained at different F10 and lipid concentrations. The release kinetics is very complex, and it will be investigated in detail in chapter 3.10. However, a phenomenological measure of peptide activity can be given by the fractional release at a fixed time. We determined the percentage of release 20 minutes after peptide addition.

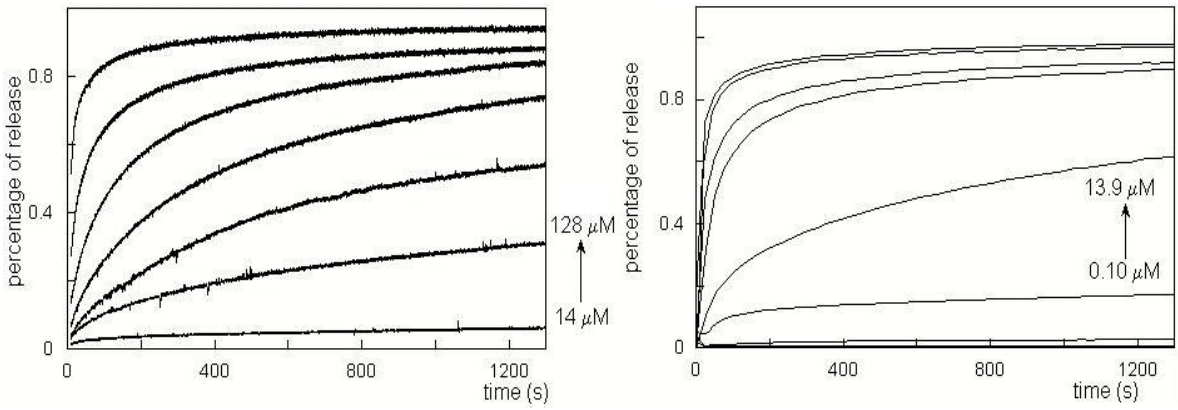

Figure 3.27 Kinetics of carboxyfluorescein release after addition of peptide (time= 0 s), as a function of F10 concentration. *Left panel*: release at [Lipid]=2mM and [F10]=14 μM; 23 μM; 32 μM; 41 μM; 59 μM; 91 μM; 128 μM (from bottom to top); *right panel*: [Lipid]=0.2mM and [F10]=0.10 μM; 1.2 μM; 2.3 μM; 3.7 μM; 4.7 μM; 6.9 μM; 10.8 μM; 13.9 μM (from bottom to top).

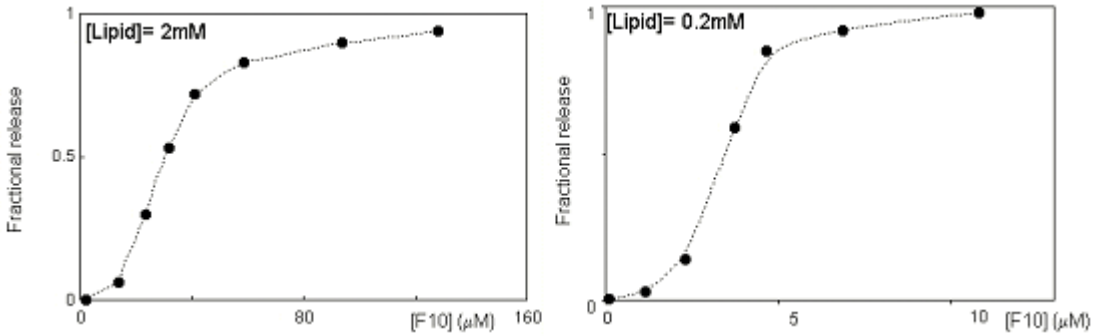

Figure 3.28 Fractional release of entrapped carboxyfluorescein 20 minutes after F10 addition to 2 mM *(left panel)* or 0.2 mM (*right panel*) lipids.

Figure 3.28 reports the fractional release 20 minutes after peptide addition. This fraction increases sigmoidally as peptide concentration increases, suggesting the occurrence of a cooperative phenomenon: liposomes are not significantly perturbed until a critical concentration is reached.

3.6.2 Activity–aggregation relationship.

In Sections 3.3 and 3.4, we demonstrated that trichogin is present in membranes both as a monomer and an aggregate, the latter being probably responsible for the cooperative behavior observed in peptide activity. To investigate which of the membrane-bound species is responsible for the membrane permeabilizing activity, we studied the peptide-induced leakage in more detail.

The results are reported in figure 3.29 and 3.30.

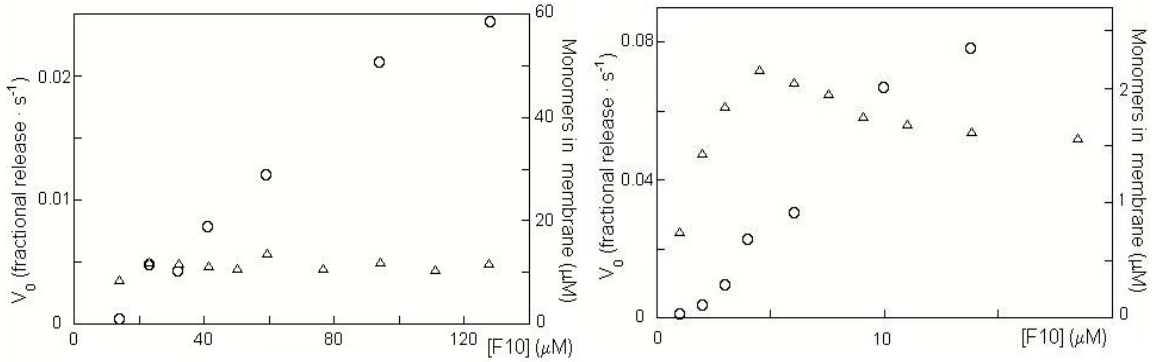

Figure 3.29 Comparison between the behavior of membrane perturbing activity (initial rate of liposome release; empty circles, left scales) and of the concentration of membrane bound monomer (triangles, right scales), as a function of total peptide concentration, in the presence of ePC/cholesterol LUV, 2mM (left panel) and 0.2mM (right panel).

Figure 3.29 compares the peptide concentration dependence of the initial rate of liposome leakage, and of the concentration of monomeric, membrane-bound peptide (determined from the data of Section 3.4) as a function of total trichogin concentration. No correlation is observed between the two quantities. By contrast, when the aggregate bound to the membrane is considered (Figure 3.30), a very good correlation is observed, indicating that the aggregated peptides are responsible for membrane leakage.

This finding is very similar to what has been observed for peptides like alamethicin and GALA, which make pores formed by peptide oligomers (Huang, 2000; Fattal *et al.*, 1994).

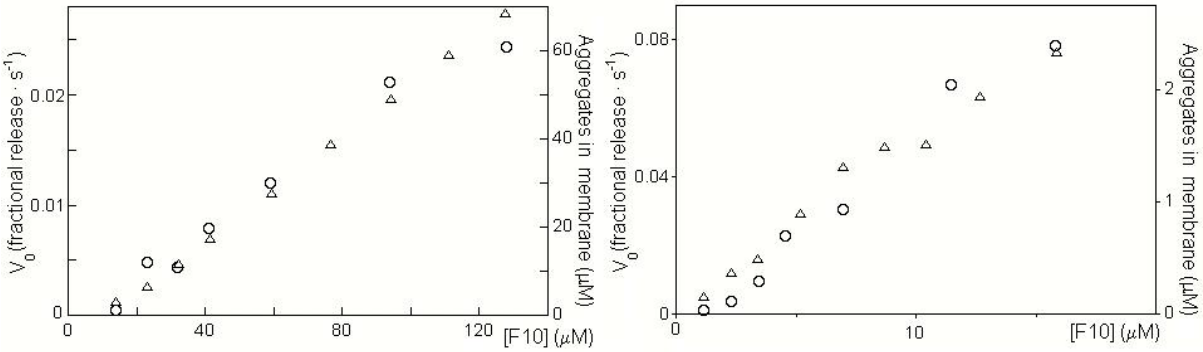

Figure 3.30 Comparison between the behavior of membrane perturbing activity (initial rate of liposome release; empty circles, left scales) and of the concentration of membrane bound aggregate (triangles, right scales), as a function of total peptide concentration, in the presence of ePC/cholesterol LUV, 2mM (left panel) and 0.2mM (right panel).

3.6.3 Summary

Comparison between trichogin activity and concentration of membrane-bound species in vesicles shows that biological activity is due to peptide aggregates.

3.7 Topology in membrane

In the previous Section we have shown that membrane leakage is caused by trichogin aggregates. However, in order to define the molecular details of the mechanism of action, additional structural information, such as the position of trichogin inside the membrane bilayer, is needed (Wimley and White, 2000).

As reported in the introduction, trichogin is only ~ 2 nm long in its helical conformation, and it is too short to span the membrane. Therefore, one may wonder whether the peptide is present only in the outer layer of the liposomes, or if, at equilibrium, it is able to translocate across the membrane, spreading out over the whole bilayer.

To answer this question, we devised a set of experiments, in which FRET efficiency was measured between F10, acting as a donor, and a phospholipid analog (C6-NBD-PC; see Table 2.2 in Section 2.1.1) introduced into the membrane and labeled with a fluorophore (NBD), which acts as energy-transfer acceptor. This acceptor can be introduced selectively in one layer only (asymmetric labeling) or in both layers of the membrane, allowing us to discriminate the position of trichogin.

This translocation assay will be described in detail later on. However, its successful application requires some prerequisites, which will be discussed in the next two Sections. They are the measurement of the Förster energy-transfer distance for the donor-acceptor couple employed, preparation of symmetrically and asymmetrically labeled vesicles, and the determination of peptide-induced lipid mixing, which could perturb the asymmetric labeling of the membrane and invalidate the assay.

3.7.1 Förster distance between F10 and NBD moieties

One requirement for our translocation assay is that the Förster energy-transfer distance for the fluorophore couple employed is significantly shorter than the bilayer thickness. If this is not the case, the measured transfer efficiency would not be very sensitive to the position of the peptide into the membrane. The

Förster distance R_0 can be calculated from Equation 2.10, which requires the determination of several spectral properties of the two probes.

The excitation and emission spectra of C6-NBD-PC inserted in ePC/Cho (1:1 molar ratio) liposomes are shown in Figure 3.31 A, while in Figure 3.31 B the overlap of the emission of F10 and the absorption of C6-NBD-PC in decanol is reported.

Quantum yield of the fluorene donor was determined in a decanol solution (see Section 3.4), obtaining a value of 0.33±0.01. The molar absorbance of C6-NBD-PC was measured in the same solvent and a value of 1.4 was used for *n*, representing the refractive index of the membrane environment (Strahilevitz *et al.*, 1994; Schuman *et al.*, 1997).

By using these parameters, an R_0 value of 24 Å was obtained, which satisfies our requirement, since the bilayer thickness is 42 Å (Lis *et al.*, 1982).

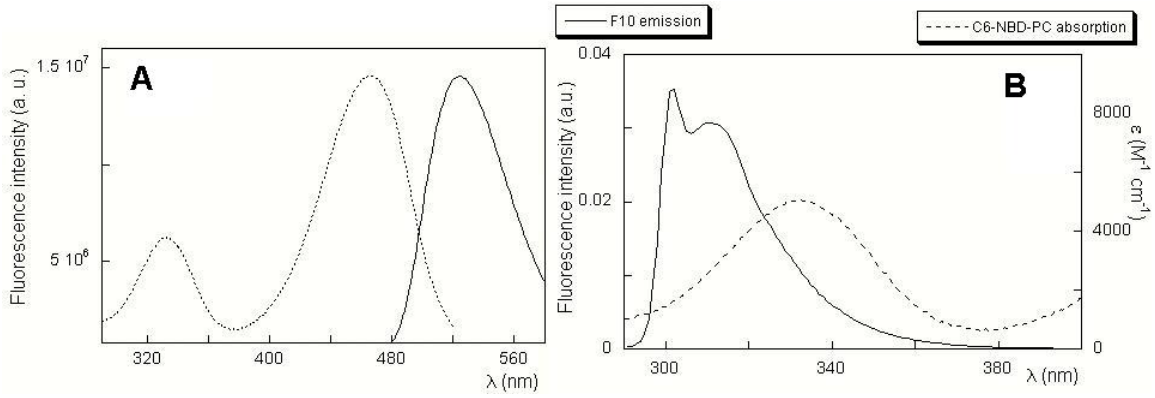

Figure 3.31 A). Emission (solid line, λ_{exc} = 467 nm) and excitation (dotted line, λ_{em} = 522 nm) spectra of the NBD moieties in C6-NBD-PC in ePC/Cho (1:1 molar ratio) liposomes. B). Overlap between the normalized to unity emission spectrum of F10 (solid line) and the absorption spectrum of C6-NBD-PC in decanol (dotted line)

3.7.2 Preparation of NBD-labeled liposomes

Liposomes containing the fluorescent lipid C6-NBD-PC in both layers were obtained by adding 1% (mol/mol) C6-NBD-PC to the initial chloroform solution.

Liposomes labeled in the external layer only were prepared by adding an aliquot of a concentrated ethanolic solution of C6-NBD-PC to preformed, unlabelled vesicles (Matsuzaki *et al.*, 1996), in order to obtain a 0.5 % label

molar fraction (1% in the outer layer only). This vesicle solution was then incubated, under gentle stirring, for at least two hours at room temperature. The final ethanol concentration was always below 1 %.

Liposomes containing the fluorescent label in the internal layer only were obtained by chemically quenching the external NBD of symmetrically labeled vesicles with dithionite. Dithionite ions are able to reduce the NBD group to ABD (7-amino-2,1,3-benzodiazol-4-yl), which is not fluorescent (McIntyre and Sleight, 1991). Under the proper experimental conditions, this reaction is much faster than the time necessary for dithionite to cross the bilayer, so that only the NBD groups lying at the external surface of the liposomes are chemically quenched. The kinetics of NBD quenching was followed by measuring fluorescence intensity (Figure 3.32). A plateau value was reached in approximately 1 minute, at a fluorescence intensity corresponding to approximately half of the initial value. In test experiments, we verified that this plateau corresponds to complete quenching of external NBD, since a second addition of dithionite to the final liposome solution caused no further fluorescence reduction (Figure 3.32, inset). After the plateau was reached, a second extremely slow kinetics was observed, corresponding to dithionite diffusion across the membrane. However, under our experimental conditions, the two kinetics have time scales which differ by at least two orders of magnitude. Therefore, after the plateau was reached, excess dithionite was rapidly removed by gel filtration.

The fluorescence emission of the final internally labeled liposomes was about 45% of the emission intensity of the starting symmetrically labeled vesicles, indicating that only a minor quenching of the C6-NBD-PC in the internal layer occurred. In the case of externally labeled liposomes, the fluorescence intensity was 51% of the emission of doubly labeled vesicles, indicating a correct degree of labeling.

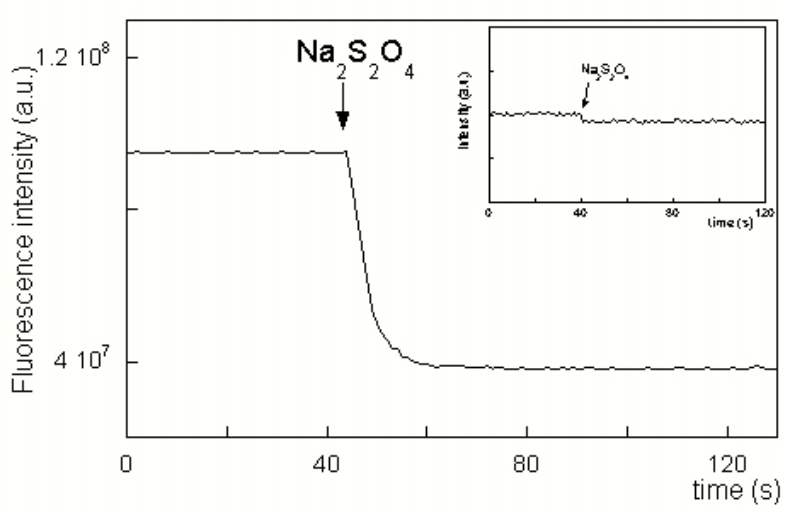

Figure 3.32 C6-NBD-PC emission decrease in symmetrically labeled liposomes ([Lipid] = 4 mM) after addition of 80 mM dithionite (arrow). λ_{ex}= 460 nm, emission, λ_{em}= 522 nm, T = 25°C. *Insert :*after gel filtration, a second dithionite addition did not cause further fluorescence decrease.

3.7.3 Peptide-induced lipid flip-flop

The transbilayer translocation of phospholipids (flip-flop) is very slow, with half times for flip-flop ranging from hours to weeks (Fattal *et al.*, 1994). However, many membrane perturbing agents can cause a huge enhancement of this rate, so that the lipid translocation process is complete in just a few minutes.

To check whether this is also the case of trichogin, we used a method based on the capability of the protein bovine serum albumin to extract the C6-NBD-PC labeled phospholipid analog from the outer layer of liposomes (Marx *et al.*, 2000; Valcarcel *et al.*, 2001). Binding by BSA causes a strong quenching of NBD fluorescence which can be easily followed spectroscopically.

The amount of BSA needed to the extract all the C6-NBD-PC present in the liposomes was established by carrying out binding experiments, following the variation of NBD emission intensity as a function of BSA concentration (the operating conditions were the same of subsequent flip-flop experiments). The result is shown in Figure 3.33.

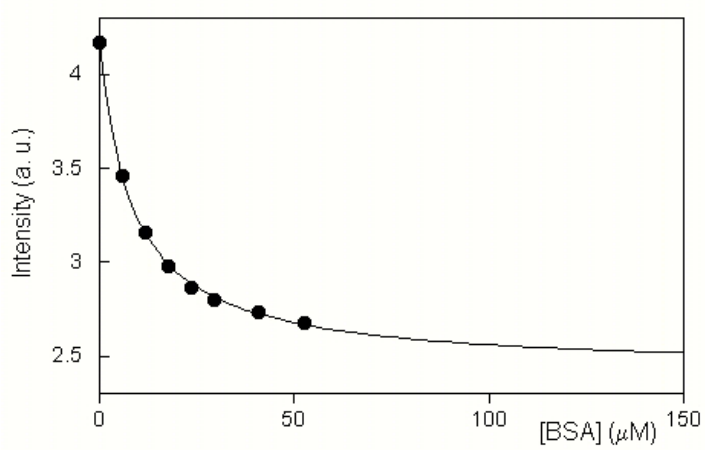

Figure 3.33 Extraction of C6-NBD-PC inserted in ePC/cholesterol liposomes (0.2 mM lipid concentration, 1% label molar ratio) by BSA binding, as detected by the decrease in NBD fluorescence intensity. λ_{exc}=470, λ_{em}=522 nm. Data are fitted according to the Langmuir binding model (equation 3.17, solid line)

The experimental data are fitted according to a Langmuir binding model (Equation 3.17):

$$I = I_0 + (I_\infty - I_0)\frac{KC}{1+KC} \tag{3.17}$$

where I is the NBD intensity measured at a given BSA concentration, and I_0 and I_∞ are the emission signals corresponding to the free labeled lipid and to complete binding,.

On the basis of the calculated binding constant (K=0.118±0.004 μM^{-1}), we used a BSA concentration of 0.2 mM in our flip flop experiments. Under these conditions, more than 96% of labeled lipids are bound to the protein.

Lipid flip-flop experiments were performed as described in Section 2.2.1.5. The results obtained in the case of F10 are shown in Figure 3.34.

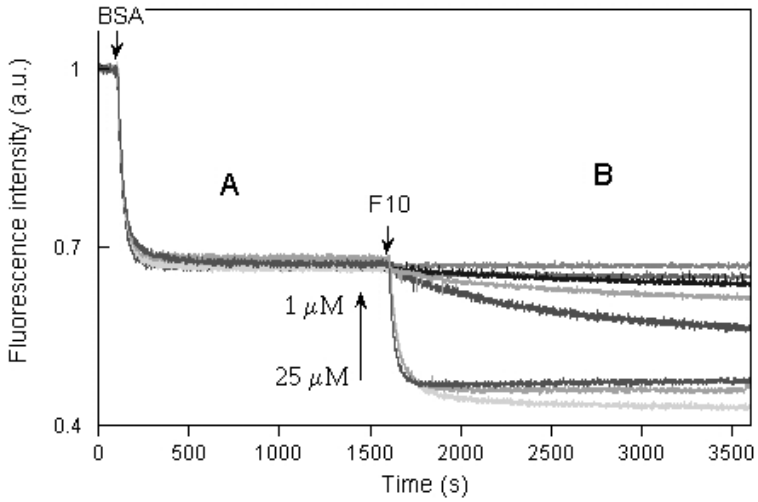

Figure 3.34 Lipid translocation assay. The first arrow indicates the time when BSA (0.2 mM) was added to a liposome suspension (0.2 mM lipid concentration), containing the labeled lipid C6-NBD-PC (1% molar ratio). NBD emission intensity was recorded as a function of time. BSA extraction of C6-NBD-PC located in the outer layer of the liposomes results in a first decrease in fluorescence intensity. The second arrow indicates the time when different concentration of analog F10 were added. Peptide-induced lipid flip-flop brings new C6-NBD-PC molecules to the outer layer, so that a further decrease in emission intensity is observed. Peptide concentrations (from bottom to up): 25 μM, 16 μM, 11μM, 7.0 μM, 4.5 μM, 3.5 μM, 2.0 μM, 1.0 μM.

As indicated by the decrease in NBD emission intensity, addition of F10 (part B of the graph) induced lipid translocation from the inner layer to the outer layer of the vesicles, to an extent depending on the amount of the peptide. However, it is interesting to note that below 1 μM of F10 no flip-flop is observed. Therefore, this is the upper limit that can be used in the peptide translocation assay.

Another interesting point is shown in Figure 3.35, where the peptide-induced flip-flop rate is compared with peptide membrane-perturbing activity.

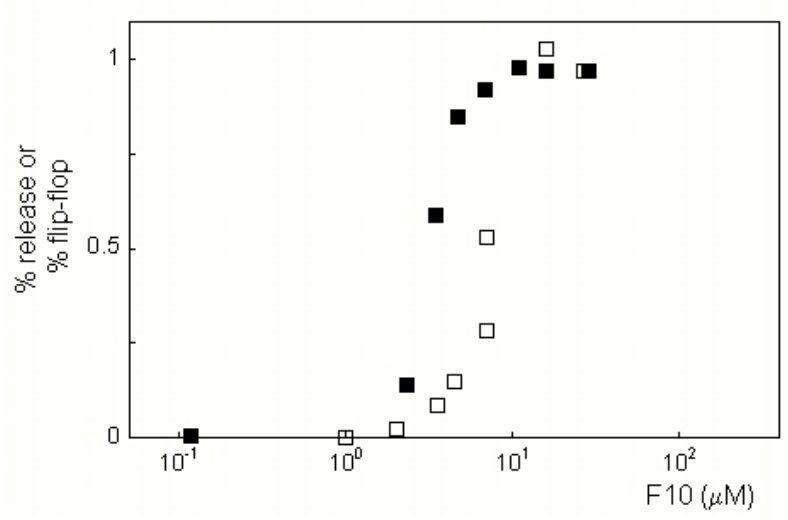

Figure 3.35 Comparison between the peptide concentration dependence of F10-induced membrane leakage (filled squares) and lipid flip-flop (empty squares).

The two phenomena occur approximately at the same peptide concentration range, in agreement with the results reported for pore forming peptides like magainin, GALA and alamethicin (Matsuzaki *et al.*, 1995a; Fattal *et al.*, 1994). The pore formation process brings about defects in the hydrophilic/hydrophobic lipid packing, which leads to lipid flip-flop. Interestingly, this phenomenon is not observed for ion-carrier peptides such as valynomicin (Fattal *et al.*, 1994).

3.7.4 Translocation experiments

The experiments described in the previous Sections provided all the prerequisites for the peptide translocation assay, which uses three different types of vesicles, containing the C6-NBD-PC fluorescent lipid: symmetrically labeled liposomes (DL), outer layer labeled liposomes (OL), and inner layer labeled liposomes (IL).

As already seen, for fluorene-NBD pair, the Förster energy transfer distance is 24 Å. Moreover, the fluorophore of C6-NBD-PC is located in the region of the polar headgroups (Wolf *et al.*, 1992; Abrams and London, 1993; Mazeres *et al.*, 1996). Since the FRET phenomenon has an inverse sixth power dependence on distance, the 50% quenching efficiency being at the Förster radius (Pispisa *et al.*, 2002b; Pispisa *et al.*, 2003) and the thickness of the bilayer is 42 Å (Lis *et*

al., 1982), we can reasonably conclude that a peptide located in the outer layer or a peptide distributed in the whole bilayer will be quenched very differently when associated to the three liposome preparations discussed above.

The fluorescence quenching results expected in the presence or in the absence of peptide translocation are presented schematically in Figure 3.36.

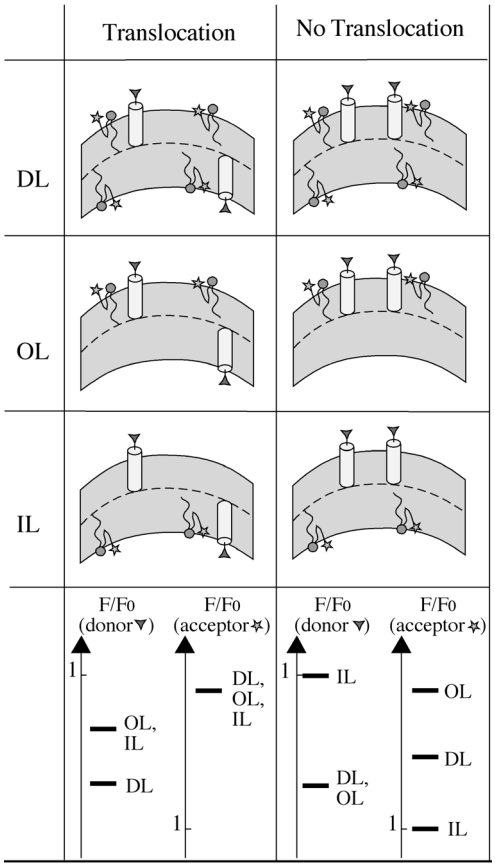

Figure 3.36 Schematic description of the translocation experiments, in which three different liposomes preparations are used: double labeled (DL), with a fluorescent lipid in both layers, and outer layer labeled (OL) or inner layer labeled (IL), in which the fluorophore is in one layer only. The peptide is shown as a cylinder, while the fluorophores are represented as a triangle (donor) or a star (acceptor).

The figure describes the decrease in peptide fluorescence (F), when interacting with these three liposome preparations, with respect to a sample containing unlabeled liposomes (F_0), where energy transfer is absent. Similarly, the increase in lipid fluorescence caused by peptide binding is represented.

Quenching of peptide fluorescence is determined by measuring the emission intensity F in the presence of acceptor labeled liposomes (DL, OL or IL), and comparing it to the fluorescence measured with unlabeled vesicles (F_0), when RET is absent. On the other hand, the increase in acceptor emission caused by

FRET is determined by measuring the lipid fluorescence in the presence (F) and in the absence (F_0) of fluorescent peptides.

When the peptide translocates across the membrane, it is approximately equidistributed in both layers. Therefore, half of the peptide interacting with IL or OL vesicles will be located in a layer void of acceptors (labeled lipids). For this reason, the quenching efficiency caused by these two types of vesicles will be approximately half of that caused by symmetrically labeled liposomes (DL), where all peptides are surrounded by RET acceptors. The relative increase in lipid fluorescence as due to peptide binding, will be the same in all cases, since all labeled lipids will be surrounded by peptide donors.

In the absence of translocation, all the peptide molecules are located in the outer layer. In this case, IL vesicles will cause a negligible quenching of peptide fluorescence and the effect of OL and DL liposomes will be the same, since both these vesicles have the same amount of acceptors in the outer layer. The increase in lipid fluorescence, on the other hand, will be different in all three cases, since OL, DL and IL have 100%, 50% or 0% of their acceptors surrounded by peptide donors, respectively.

This description evidences that our approach allows a clear-cut discrimination between the cases in which the peptide is equally distributed in both layers, and those in which it lies in the external layer only. The experimental results obtained for the F10 analog are reported, in Figure 3.37. It is easily recognizable from a comparison of Figures 3.36 and 3.37 that the peptide is able to completely translocate across the membrane.

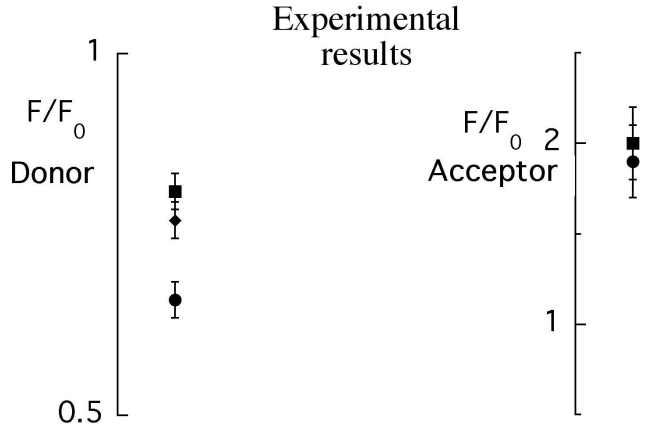

Figure 3.37 Experimental fluorescence variation in peptide translocation experiments (see legend to Figure 3.36). Results obtained in the case of analog F10, under the following experimental conditions: [F10] = 0.5 μM; [lipid]= 0.2 mM, C_6-NBD-PC =1% (DL) or 0.5% (IL and OL) mol/mol; λ_{exc} = 290 nm; cut-off filter at 295 nm. The reported values are the average of multiple experiments. DL: circles, OL: squares, IL: diamonds.

At the end of the translocation experiments, i. e. after peptide addition and after the emission intensities reported in Figure 3.37 were determined, we verified again that peptide insertion did not perturb the asymmetric distribution of phospholipids, by adding 0.2 mM of bovine serum albumin to the vesicles (see previous Section). The results are shown in figure 3.38: no NBD quenching is observed for IL liposomes, demonstrating that no C6-NBD-PC is accessible from the outside, while a significant fluorescence decrease is observed for both OL and DL liposomes. The quenching efficiency of OL vesicles doubles that of DL liposomes, in agreement with the different fraction of the labeled lipids which is located in the outer layer in the two cases. Therefore, as expected, no significant amount of lipid flip-flop is induced by trichogin at the very low concentration used, and the initial lipid asymmetry is preserved during the translocation experiments.

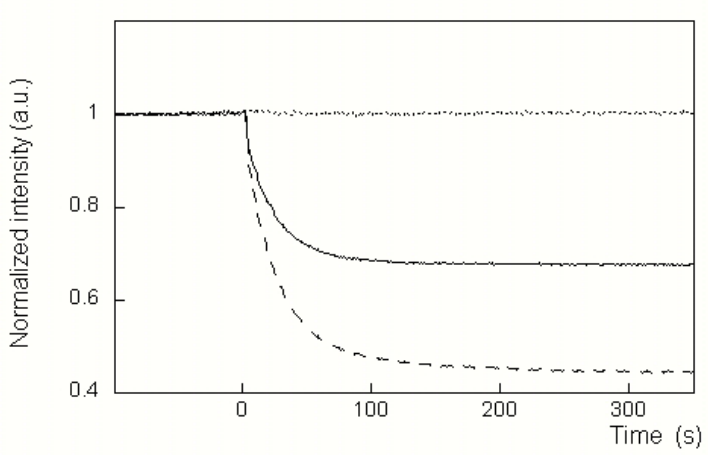

Figure 3.38 Kinetics of C_6-NBD-PC extraction by bovine serum albumin (BSA), after F10 addition. BSA (0.2 mM) was added at time zero. Continuous line: DL liposomes; dashed line: OL liposomes; dotted line: IL liposomes. Fluorescence intensities have been normalized to their value before BSA addition. λ_{ex}=460, λ_{em}=522 nm.

It should be noted that the translocation experiments were performed at a peptide concentration so low that liposome leakage is absent (see Figure 3.28, Section 3.6.1). Therefore, trichogin translocation is not related to its activity, as for other peptides, such as magainin, which form so-called toroidal pores (Matsuzaki *et al.*, 1991, 1996)).

3.7.5 Summary

FRET experiments using symmetrically and asymmetrically NBD-labeled lipids have shown that trichogin is located on both leaflets of liposomes, even at concentration so low that no membrane perturbing activity is observed. At higher concentrations, trichogin induces lipid translocation to an extent directly correlated to peptide activity.

3.8 Peptide depth and orientation

In order to determine the orientation and position of trichogin within the lipid bilayer, several experiments were performed with the fluorescent analogues, by using both water-soluble and lipid-attached quenchers.

3.8.1 Iodide quenching

Fluorescence quenching by the water soluble iodide ion, which acts by a collisional mechanism (Lakowicz, 1983), is used to determine the degree of accessibility of a given fluorophore from the water phase. This can be obtained by comparing the iodide quenching efficiency when the peptide is free in solution or is bound to a membrane (Castanho and Prieto, 1995).

In the case of an homogeneous sample, the mathematical relation between the fluorescence intensity of the probe (F) and the quencher concentration ([Q]) can be expressed as:

$$F = \frac{F_0}{1 + k_Q[Q]} \tag{3.18}$$

where F_0 is the fluorescence when no quencher is present and k_Q is the quenching constant. This equation can be rearranged in a linear form, known as Stern-Volmer equation:

$$\frac{F_0}{F} = 1 + k_Q[Q] \tag{3.19}$$

Our experiments were performed at a peptide and lipid concentrations chosen to ensure an almost complete binding of trichogin to the membrane (see Section 2.2.1.5). However, it is important to note that, at this very low peptide/lipid ratio, the analogs are not active and no membrane leakage is

observed. For comparison, quenching was also measured in the absence of membranes. The results are shown in Figure 3.39.

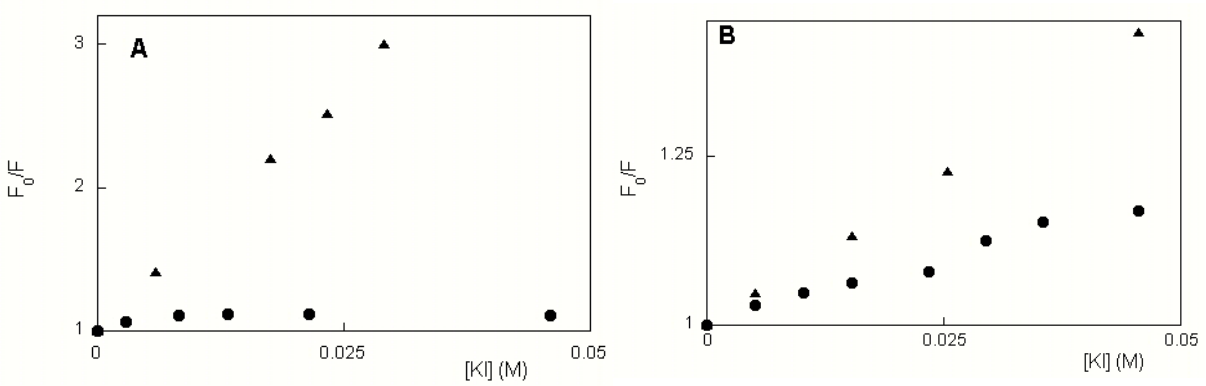

Figure 3.39 Stern-Volmer plots of I^- induced quenching. *Panel A*: F10 (1.2 μM) in water (triangles) and in the presence of liposomes (circles, [lipid]=2 mM); λ_{exc} = 280 nm, λ_{em} = 304 nm. *Panel B*: A3 (1.0 μM) in water (triangles) and in the presence of liposomes (circles); λ_{exc} = 280 nm, λ_{em} = 382 nm.

In both cases, the quenching caused by the iodide ion dissolved in water is significantly reduced by the presence of liposomes, indicating that the peptides are inserted into the membrane, but are still partially accessible to the quencher. The azulene fluorophore contained in A3 seems to be somewhat more accessible than F10, probably because it is more polar.

3.8.2 Depth dependent quenching

A more detailed information on the position of a fluorophore within a membrane can be obtained by the method of depth-dependent quenching (Ladokhin, 1997; London and Ladokhin, 2002).

In this case, fatty acids or phospholipids carrying quenchers (usually bromine atoms or nitroxide groups), selectively linked to different positions along the acyl chains, are incorporated in the liposomes. Therefore, the quenchers are at relatively fixed depths in the bilayer (Vogel *et al.,* 2003). Since bromine or nitroxide derivatives quench by a short distance mechanism, the extent of quenching is maximum when the fluorescent probe in the peptide and the

quencher are placed at the same depth in the vesicles. In this case, only membrane-bound peptides are quenched, and therefore complete binding of the peptides to the membrane is not a strict requirement.

In our depth-dependent quenching experiments, we have compared the degree of quenching resulting from the interaction of trichogin fluorescent analogs with different liposomes, containing lipid-linked quenchers at various positions along their chain. For comparison, emission intensities of the analogs were determined also when interacting with unlabeled vesicles (see Section 2.2.1.5).

3.8.2.1 Quenching experiments using dibromide derivatives

A first set of experiments was performed with liposomes entirely composed by ePC phospholipids marked by bromine atoms in position 6-7, 9-10 and 11-12 of the fatty acyl chain (see Figure 3.40). Diffraction experiments (McIntosh and Holloway, 1987) have shown that the bromine atoms are located at 11.0 Å, 8.3 Å and 6.6 Å, from the bilayer center, respectively.

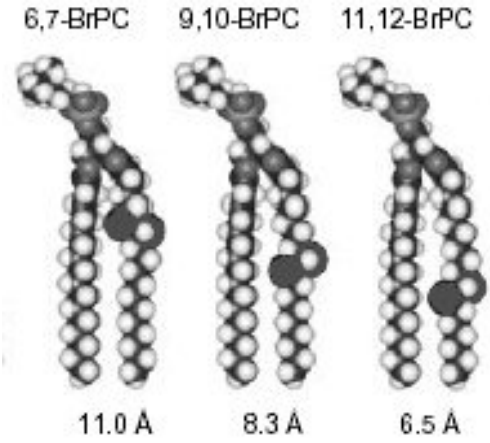

Figure 3.40 3D representation of the dibromide derivatives used

The quenching measurements were carried out at three different peptide concentrations spanning the whole activity range, being able to cause a leakage of vesicle entrapped carboxyfluorescein equal to 0%, 50% and 100%, respectively, 20 minutes after peptide addition (see Figure 3.28 in Section

3.6.1). Therefore, these concentration values were chosen to investigate a possible coupling of peptide position in the bilayer with membrane perturbing activity.

Table 3.4 F10 quenching efficiency as a function of the dibromide position along the lipid chain ([Lipid] = 0.2 mM; λ_{exc} = 290 nm, λ_{em} = 300-400nm).

[F10]	6-7 DiBr-PC	9-10 DiBr-PC	11-12 DiBr-PC
0.5μM	0.79±0.01	0.83±0.01	0.68±0.01
3.5μM	0.82±0.02	0.85±0.01	0.69±0.01
10.8μM	0.77±0.01	0.80±0.02	0.65±0.01

Table 3.5 A3 quenching efficiency as a function of the dibromide positions along the lipid chain ([Lipid] = 0.2 mM; λ_{exc} = 290 nm, λ_{em} = 350-450nm).

[A3]	6-7 DiBr-PC	9-10 DiBr-PC	11-12 DiBr-PC
0.5μM	0.47±0.01	0.42±0.01	0.06±0.01
3.5μM	0.22±0.01	0.26±0.02	0.02±0.01
10.8μM	0.18±0.01	0.25±0.02	0.01±0.01

In both cases, and at all concentration studied, a similar quenching efficiency is observed with lipids labeled in position 6-7 and 9-10 in the lipid chain, while a significantly lower quenching was obtained with 11-12 labeled lipids. This suggests that our probes are located within the membrane, but close to the polar headgroups region. However, these results are not conclusive, because the labeled lipids used do not span the whole membrane thickness.

3.8.2.2 Quenching experiments using doxyl derivatives

A more detailed study was then performed under the same experimental conditions ([lipid] = 0.2 mM, [F10,A3] = 0.5, 3.5, 10.8 μM), but using 1-palmitoyl-2-stearoyl-(n-doxyl)-*sn*-glycero-3-phosphocholine (see Table 2.2 in Section 2.1) as quencher. Lipids with a doxyl moiety linked in different positions along the acyl chain were used i. e. labeled in position n = 5, 7, 10, 12, 14 and

16, which correspond to distances from the center of the bilayer of 12.2 Å, 10.0 Å, 7.7 Å, 5.9 Å, 4.0 Å and 2.3 Å, respectively (Vogel *et al.*, 2003).

Figure 3.41 shows the results of these experiments for F10.

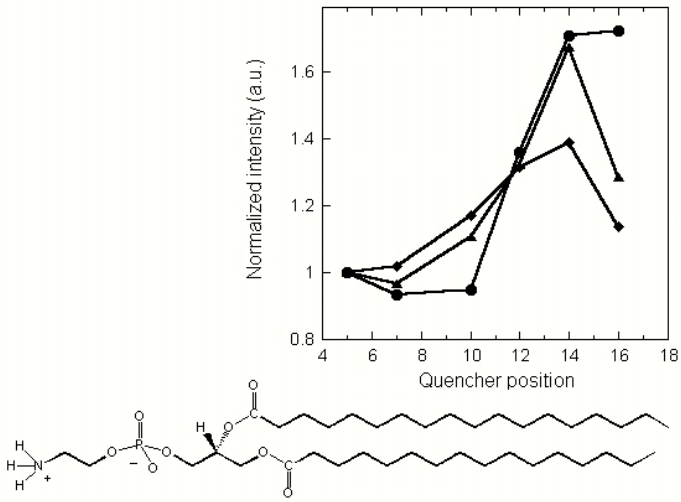

Figure 3.41 Relative quenching of F10 by phospholipids labeled with doxyl moieties at different depths. The positions of the quencher along the stearic chain are graphically reported in the bottom part of the Figure, in correspondence to their value on the X-axis of the plot**.** Fluorescence intensities are normalized by the intensity measured in the presence of liposomes containing lipids labeled at position 5. Peptide concentration 0.5 μM (full circles); 3.5 μM (crosses); 10.8 μM (empty symbols), lipid concentration 0.2 mM. Errors are within 2%

At the lowest concentration studied, the highest decrease in fluorescence intensity is caused by the quencher in position 7, which corresponds approximately to the same position within the membrane for which maximum quenching was recorded with brominated lipids. However, as the peptides concentration increases, reaching values high enough to cause liposome leakage, the relative quenching due to the deepest quencher increases significantly. This effect was not observed with brominated lipids, because in that case we did not have such a deep quencher.

Interestingly, an increase in the relative quenching efficiency of a quencher located deep in the membrane as peptide concentration increases, is observed also for analog A3, in which the fluorescent label is close to the N-terminus rather than to the C- terminus of the peptide, as in F10 (Figure 3.42).

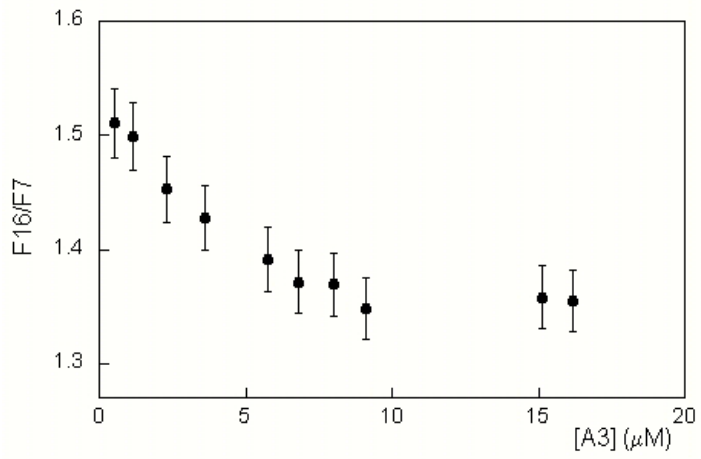

Figure 3.42 Relative quenching of A3 by phospholipids labeled with doxyl moieties at position 16 or 7. The ratio of fluorescence intensities measured for the peptide interacting with the two liposome preparations is reported as a function of A3 concentration. Lipid was 0.2 mM.

A similar set of experiments on F10, but using different lipids to label membranes (i.e. 5- or 16-doxyl-stearic acids at a 7% molar ratio) and a different lipid concentration (2 mM) (Figure 3.43), gave rise to comparable results. On increasing peptide concentration up to values that are able to cause liposome leakage (see Figure 3.28 on Section 3.6.1), the fluorophore becomes, on average, more accessible to the quencher positioned close to the bilayer center.

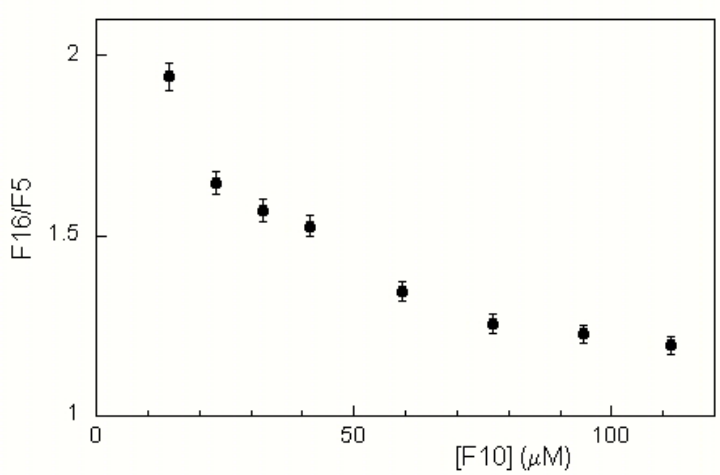

Figure 3.43 Relative quenching of F10 by phospholipids labeled with 5- or 16-doxyl-stearic acid. The ratio of fluorescence intensities measured for the peptide interacting with the two liposome preparations is reported as a function of F10 concentration. Lipid was 2 mM.

Taken together, these data are consistent with the results obtained with dibromide labeled liposomes, indicating a preferential location of the fluorophores close to the membrane surface. However, in the case of doxyl labeled lipids, the presence of a quencher very close to the bilayer center allowed us to detect the presence of a peptide population deeply buried within the membrane, which becomes more relevant as peptide concentration increases to values able to bring about liposome leakage. Since the same behavior is observed for F10 and A3, having the fluorescence probes at the opposite ends of the peptide, one may conclude that trichogin insertion into the membrane has not a preferential direction.

Previous studies seem to contradict the finding that trichogin, at a high peptide/lipid ratio, inserts into the lipid bilayer. In particular, Epand *et al.* (1999b) performed experiments in which the quencher aminoacid TOAC (4-amino-4-carboxy-2,2,6,6-tetramethylpiperidino-1-oxyl) was introduced in the peptide sequence, and liposomes were labeled with phosphatidylcholine analogs bearing the fluorophore BODIPY (4,4-difluoro-4-bora-3a,4a-diaza-S-indacene) at different positions along the acyl chain. They showed that fluorescence quenching is independent on both the position of the quenching residue along the peptide chain, and on the peptide/lipid ratio. These results were interpreted by assuming that trichogin lays parallel to the membrane surface, at all concentrations investigated. However, it has been conclusively shown that the BODIPY group attached to phospholipids "has a clear tendency to locate in the polar headgroup region of the bilayer", irrespective of its position along the acyl chain (Kaiser and London, 1998). We are, therefore, inclined to think that in the study by Epand a transition in peptide orientation could not have been observed, even if it was present. This is confirmed by the absence of any clear dependence of fluorescence quenching on the BODIPY position along the lipid acyl chain (Figure 2 of Epand *et al.*, 1999b)), indicating that the fluorescent lipid analogs employed do not allow the peptide position in the membrane to be determined. On the other hand, our study does not suffer from this limitation, because the use of doxyl labeled lipids and fatty acids is a very well established methodology for determining the membrane position of

fluorescent probes (Ladokhin, 1997; London and Ladokhin, 2002). In addition, recent structural results have shown that doxyl groups linked to phospholipid chains have a depth distribution in the membrane bilayer that is approximately centered at the chain position of the probe (Vogel *et al.*, 2003).

3.8.3 Orientation-aggregation relationship

In Section 3.4, we have shown that, as the peptide concentration increases, peptide aggregation takes place into the membrane, and that these oligomers are responsible for membrane leakage. The question, therefore, arises as to whether all the processes driven by peptide concentration (i.e. membrane perturbation, peptide aggregation and orientational transition) are correlated.

To answer to this question, we carried out a proper analysis of the depth-dependent quenching experimental data, that allows us to obtain quantitative information regarding the fraction of peptide deeply inserted into the membrane. From the experiments reported in Figure 3.43, regarding F10, we calculated the quantity

$$\frac{I(5)-I(16)}{C_p^l} \tag{3.20}$$

where $I(5)$ and $I(16)$ are the fluorescence intensities of F10 measured in the presence of lipids labeled with a quencher at position 5 or 16, respectively, and C_p^l is the concentration of peptide bound to the membrane, as obtained from the data reported in Section 3.3.2. This quantity has a linear relationship with the fraction of peptide deeply inserted into the membrane, as shown below.

If we assume that two different peptide positions in the membrane are present (S for superficial and D for deep), the fluorescence intensity measured in the presence of lipids labeled at position 5 or 16 will be given by

$$\begin{aligned} I(5) &\propto C_p^w \Phi^w + C_p^l \left[\alpha_D \Phi_D^l E_D^5 + (1-\alpha_D)\Phi_S^l E_S^5\right] \\ I(16) &\propto C_p^w \Phi^w + C_p^l \left[\alpha_D \Phi_D^l E_D^{16} + (1-\alpha_D)\Phi_S^l E_S^{16}\right] \end{aligned} \tag{3.21}$$

where C_p^w and C_p^l is the peptide concentration in water and in the lipid phase, respectively, α_D is the fraction of membrane-bound peptide located deeply in the bilayer, Φ the fluorophore's quantum yield in the different states and E_i^j the quenching efficiency of the fluorophore located in state i by quencher j. To eliminate the contribution from the unbound peptide, we calculate the difference between the two intensities, and divide by C_p^l:

$$\begin{aligned}\frac{I(5)-I(16)}{C_p^l} &\propto \alpha_D \Phi_D^l E_D^5 + (1-\alpha_D)\Phi_S^l E_S^5 - \alpha_D \Phi_D^l E_D^{16} - (1-\alpha_D)\Phi_S^l E_S^{16} = \\ &= \alpha_D \left[\Phi_D^l \left(E_D^5 - E_D^{16}\right) - \Phi_S^l \left(E_S^5 - E_S^{16}\right)\right] + \Phi_S^l \left(E_S^5 - E_S^{16}\right)\end{aligned} \tag{3.22}$$

Therefore, one has:

$$\frac{I(5)-I(16)}{C_p^l} = \alpha_D A + B \tag{3.23}$$

where A and B are constants.

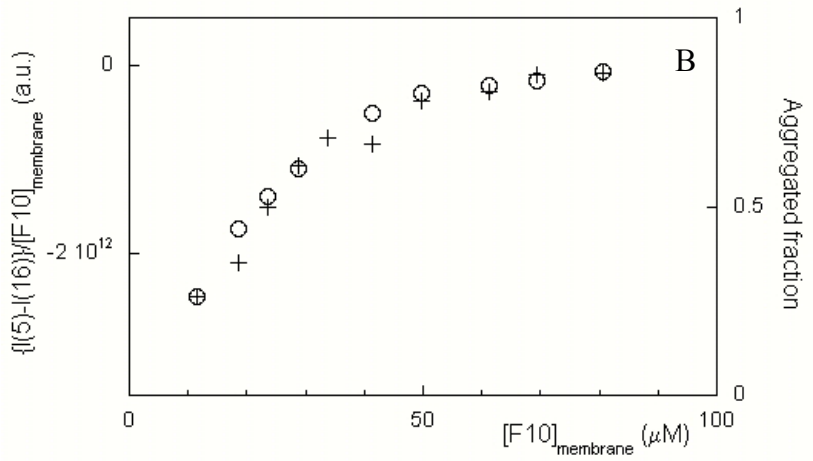

Figure 3.44 Comparison between the fraction of membrane-bound, aggregated peptides (crosses), and that of peptides deeply inserted into the membrane (empty circles) at 2mM lipid concentration as a function of F10 concentration (see text).

Figure 3.44 compares the peptide concentration dependence of this quantity and of the fraction of membrane-bound aggregated peptide, at 2mM lipid concentration. The finding that there is a remarkable correlation between the two sets of data is a strong indication that only two peptide states are present in the membrane: a monomeric, surface bound and inactive form and an

inserted, aggregated state, causing membrane leakage. The interconversion between these two states is driven by peptide concentration.

It is worth stressing that such coupling between membrane insertion and peptide aggregation suggests the presence of a strong driving force for peptide self-association in the inserted state, so that monomeric peptides are present on the surface only.

3.8.4 Summary

Fluorescence quenching measurements, performed by using water soluble quenchers and quenchers positioned into the membrane at different depths, indicate that at low peptide/lipid ratios trichogin is located close to the polar headgroups region. However, by increasing peptide concentration until liposome leakage is observed, a cooperative transition takes place and a significant fraction of the peptide becomes deeply buried into the bilayer.

Remarkably, this change in peptide depth is strictly coupled with peptide aggregation. It can be therefore, concluded that the increase in trichogin concentration brings about a two-state transition from a monomeric, surface bound and inactive form to a buried aggregated state, responsible for membrane leakage and bioactivity.

3.9 Mechanism of action

Having determined the dependence trichogin behavior on its concentration and the position that it attains within the membrane, we addressed more in detail its mechanism of action.

3.9.1 Membrane micellization?

The first question was whether trichogin acts like a detergent, causing a complete breakdown of the membrane (micellization) when a threshold concentration is reached. If this was the case, then a drastic decrease in particle size would be expected for the liposome suspension. This can be detected by measuring the intensity of light scattered at 90° by the vesicle suspension, before and after peptide addition (Jones and Cossins, 1990), because, as it is well known, the scattered intensity depends strongly on the particle size.

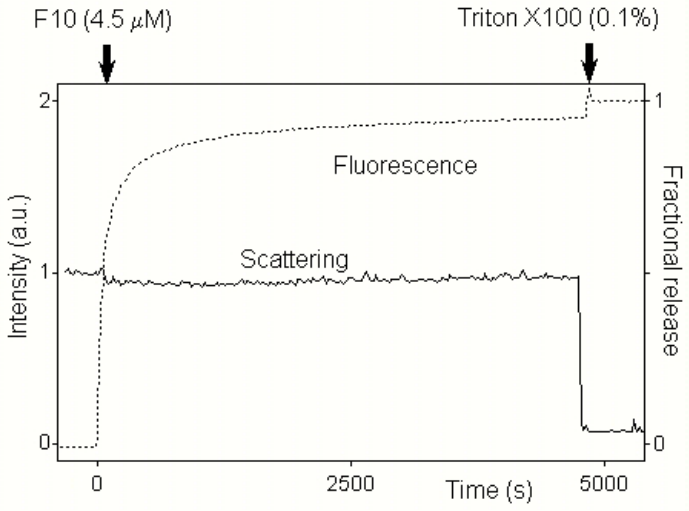

Figure 3.45 Kinetics of carboxyfluorescein release. Comparison between the time evolution of the dye fluorescence and the liposome scattering signal ($\lambda_{exc}=\lambda_{em}$= 600 nm). The two arrows indicate the times corresponding to the addition of F10 and of Triton X-100, respectively.

When a detergent, such as Triton, is added to a liposome solution, the scattered intensity decreases almost to zero (Figure 3.45). On the other hand, when F10 or Tric-OMe is added at concentrations high enough to determine an

almost complete release of the carboxyfluorescein entrapped in liposomes, the observed changes in the intensity of scattered light are minor (less than 10 %), thus indicating that vesicle size is not significantly perturbed. Both these results suggest that trichogin is not acting by membrane micellization, an hypothesis supported by many other experimental findings too.

For instance, trichogin-induced membrane leakage is size-selective. We have compared the release of carboxyfluorescein (CF, molecular weight 376, diameter ~ 1nm) and that of Texas Red-labeled dextrans (TRD, average molecular weight 10000, diameter ~ 4nm). Within the peptide concentration range where complete CF release is attained, TRD release is definitely minor. Also this partial release could be due to the polydispersity of the poysaccharide chain. The observed dependence of trichogin-induced release on the size of entrapped molecules can not be reconciled with a mechanism involving complete breakdown of the membrane.

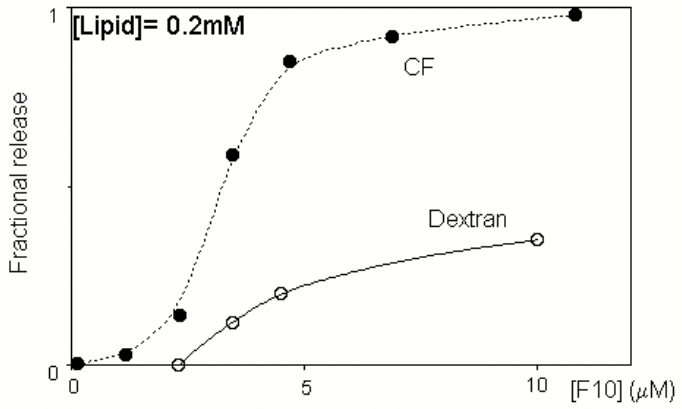

Figure 3.46 Comparison of carboxyfluorescein (CF) and Texas Red-labeled dextran (<M.W.> = 10000) fractional release, 20 minutes after F10 addition. Lipid concentration = 0.2 mM.

Finally, direct visualization of trichogin-induced leakage, by means of giant unilamellar vesicles (GUVs) prepared by electroformation (see section 2.1.4), further confirms the idea that micellization does not take place.

Carboxyfluorescein release experiments after the addition of Tric-OMe 6μM were initially performed.

GUVs have a size comparable to a cell, and therefore they are visible by optical microscopy. The possibility to substitute the filter set of the fluorescence

microscope during the release experiments (see Section 2.1.6.2), allows us, by choosing an opportune lipid marker, to follow almost simultaneously the fate of the entrapped dye and that of the bilayer, after peptide addition. In particular, since the spectral characteristics of carboxyfluorescein (whose excitation and emission maximum are λ_{exc}=492 nm and λ_{em}= 520 nm, respectively; see Figure 3.47 A) are consistent with the spectral bandpasses of the "blue" excitation filter set, a lipid marker matching the spectral characteristics of the "green" filter set had to be used to label the giant liposome. Therefore, GUVs were marked with 1% molar ratio of the Rhodamin-labeled lipid N-Rho-PE, whose absorption and fluorescence spectra are reported in Figure 3.47 B.

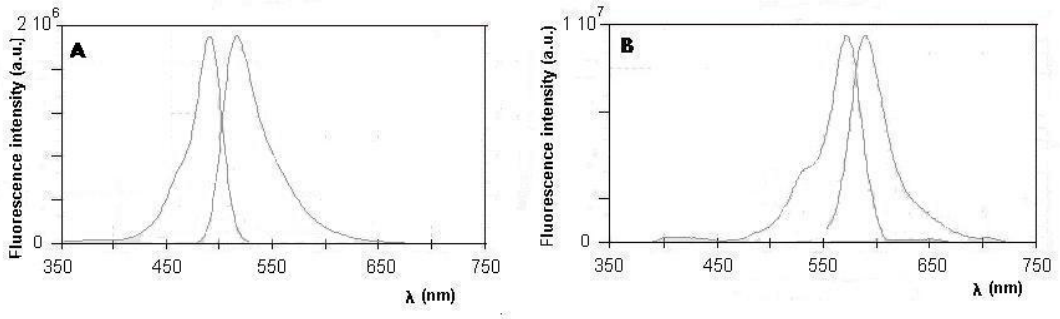

Figure 3.47 Excitation and emission spectra of (A) carboxyfluorescein (3 μM; λ_{exc} = 470 nm; λ_{em} = 550 nm) and (B) N-Rho-PE labeled liposomes (20μM; λ_{exc} = 520 nm; λ_{em} = 640 nm) in water.

The results of the release experiments are shown in Figure 3.48.

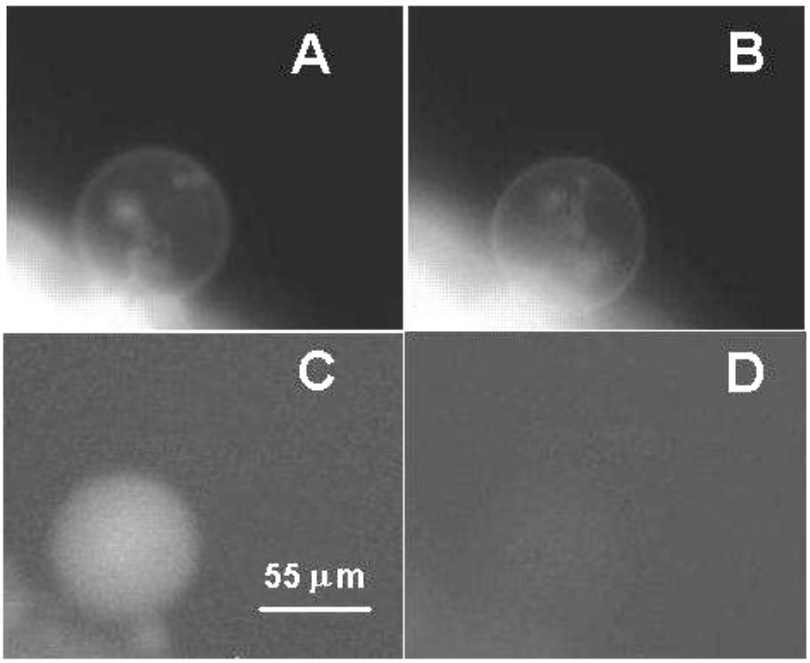

Figure 3.48 Giant unilamellar vesicle before (left) and few minutes after (right) peptide addition ([Tric-OMe] = 6 μM). Upper and lower panels show the emission of rhodamine labeled phospholipids and of carboxyfluorescein entrapped inside the vesicle, respectively (40x magnifying objective).

The figure shows that, after peptide addition (Tric-OMe at 6μM concentration), carboxyfluorescein entrapped inside the liposomes is released in a few minutes, while the lipid bilayer remains intact.

The same kind of release experiments were performed entrapping Texas-Red labeled dextran inside GUVs. The spectral characteristics of Texas Red (see Figure 3.49 A) are such that its absorption and emission maxima of Texas-Red fall within the spectral bandpass of the "green" filter set. As a consequence, to be able to simultaneously observe the status of the membrane, we chose a different lipid marker with respect to the previous experiments. This implies that the marker must have absorption and emission characteristics consistent with the spectral bandpasses of the "blue" filter set. For this purpose, the lipid N-NBD-PE (λ_{exc}=467 nm, λ_{em}= 530 nm, Figure 3.49 B) was chosen.

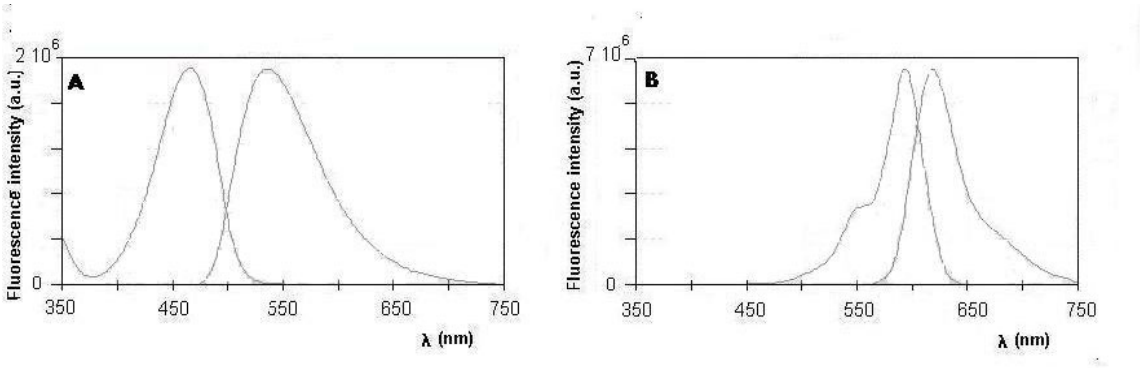

Figure 3.49 Excitation and emission spectra of (A) N-NBD-PE labeled liposomes (20 μM; λ_{exc} = 350 nm; λ_{em} = 550 nm) and (B) Texas-Red dextran (18 μM; λ_{exc} = 545 nm; λ_{em} = 660 nm) in water.

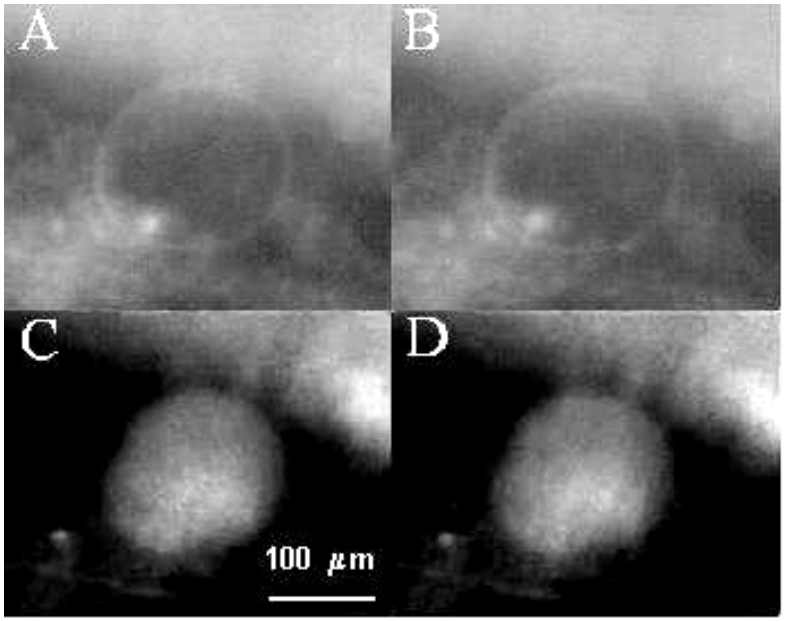

Figure 3.50 Experiment on giant unilamellar vesicles. (A) and (B) NBD-PE labeled bilayer (5% molar ratio) before and after addition of Tric-OMe (6 μM). During the same experiment the fluorescence of Texas-Red labeled dextran (18 μM), entrapped in liposomes, is followed, before and after trichogin addition (panels C and D, respectively). As shown in panels B, and D, the peptide does not induce neither vesicle breakdown nor the release of markers (40x magnifying objective).

Figure 3.50 shows the results of these experiments: the addition of Tric-OMe did not induce any release of the marker, and any liposomes breakdown.

These results confirm that the trichogin-induced leakage is size selective and is not due to liposome lysis.

3.9.2 ION-CARRIER?

To assess the possibility that trichogin acts via an ion carrier mechanism we performed leakage experiments using model membranes of very different viscosities, because the activity of ionophores operating as carriers decreases significantly with increasing membrane viscosity. This because the high rigidity of the bilayer severely hinders peptide diffusion across it (Pregel *et al.*, 1995; Boheim *et al.*, 1980).

A great difference in membrane viscosity can be easily obtained by using liposomes composed by lipids in the gel or in the liquid crystalline phase (see Section 2.1.2). For instance, DMPC and POPC vesicles have their melting transition at 26°C and -2°C, respectively (Rosoff 1996; Szoka and PapahadJopoulos, 1980). Therefore, it should be possible to find a working temperature at which DMPC is in the gel phase while POPC is in the liquid crystalline state. However, the values of temperature reported above refer to pure lipids, so that, as a preliminary step, we have to determine the influence of peptide binding on the lipid transition temperature, studying the phase transition of DMPC vesicles in the absence and in the presence of different concentrations of peptide.

3.9.2.1 Effects of trichogin on the DMPC phase transition.

To follow the membrane phase transition, we made use of the emission spectrum of the fluorescent membrane probe 6-dodecanoyl-2-dimethylaminonaphatalene (Laurdan). In Figure 3.51, the fluorescence spectra of this probe in DMPC liposomes at different temperatures (above and below the phase transition) are shown.

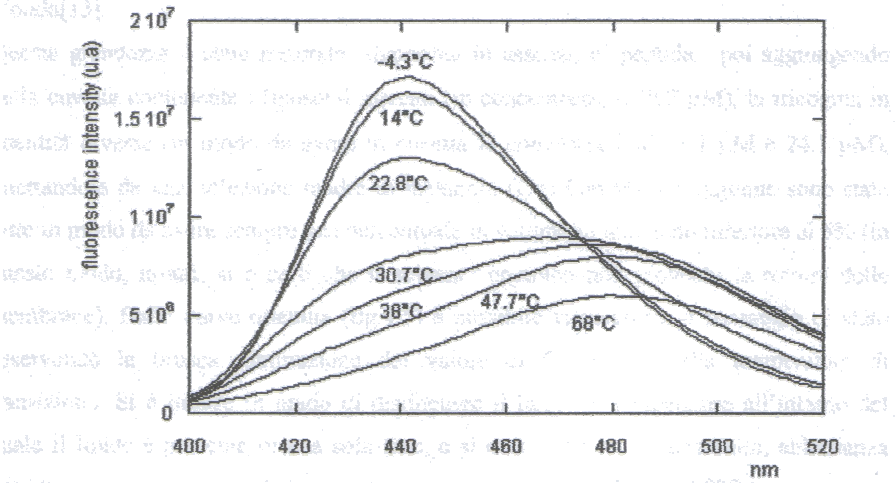

Figure 3.51 Emission spectra of Laurdan in DMPC liposomes ([Lipid] = 0.2 mM), at different temperatures (λ_{exc}= 382 nm).

The emission maximum of this fluorophore displays a red shift from 440 nm, when the membrane is in the gel phase, to 490 nm, in the liquid crystalline phase. The physical origin of this large spectral shift in Laurdan emission can be attributed to dipolar relaxation phenomena, originating from the sensitivity of the probe to the polarity of the environment (Parasassi *et al.,* 1991). In the membrane liquid-crystalline phase, water molecules can penetrate at the level of the bilayer glycerol backbone, where the probe is located, and reorientate themselves along the Laurdan excited state dipole, stabilizing it. On the other hand, in the gel phase, water permeation is hindered owing to the tightly packed phospholipid moieties (Parasassi *et al.,* 1998).

Experimentally, the change in Laurdan spectral shape can be expressed as:

$$GP = \frac{I_{440} - I_{490}}{I_{440} + I_{490}} \tag{3.24}$$

where I_{440} and I_{490} are the fluorescence intensities measured at 440 and 490 nm, and GP is the so-called "general polarization" for the apparent similarity of its definition to that of fluorescence polarization.

We performed the experiments measuring the GP values of DMPC liposomes containing Laurdan at a concentration that has been reported to not affect the

membrane phase transition (Abrams and Yager, 1993) i.e. 5% molar ratio, in the temperature range from –5°C to 80°C.

The results are shown in figure 3.52.

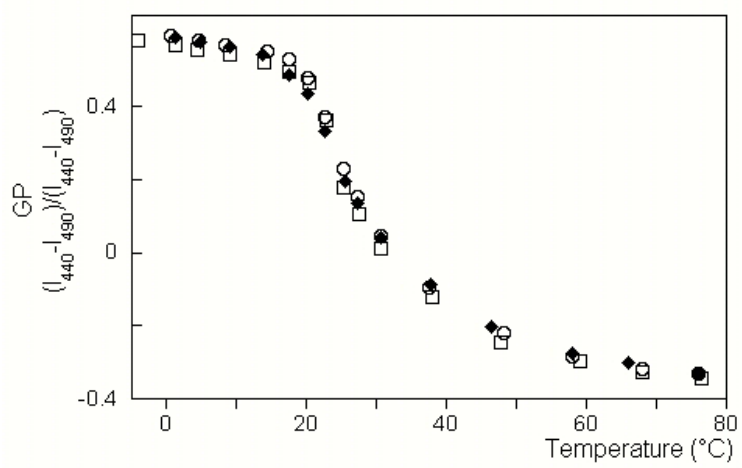

Figure 3.52 GP values as a function of temperature for DMPC liposomes (0.2mM) containing 5% molar ratio of Laurdan, in absence (empty squares), and in the presence of 11.1 μM (empty circles) and 24.1 μM (filled diamonds) of Tric-OMe.

The S-shaped curve, corresponding to the phospholipid phase transition, is not affected by trichogin, at least up to a concentration as high as 24.1 μM.

This result is in good agreement with that found for other antibiotic peptides, like the pore-forming alamethicin and magainin, which at a similar peptide/lipid ratio do not induce any significant perturbation in the lipid phase transition (Matsuzaki *et al.*, 1998; Lee *et al.*, 1984).

A more quantitative determination of the transition temperature can be obtained by a proper analysis of the GP data. The lipid phase transition is not a first order transition, and therefore, in the temperature range corresponding to the melting process both phases are present and contribute to the signal, according to the following formula:

$$GP(T) = X \cdot GP_{gel} + (1 - X) \cdot GP_{liquid} \qquad (3.25)$$

where X is the molar fraction of lipids in the gel phase, GP_{gel} and GP_{liquid} are the generalized polarization in the gel and in the liquid-crystalline phase, respectively. However, inspection of Figure 3.52 reveals that there is a

temperature dependence of the GP values of the pure phases. To account for this temperature effect, we employed a linear extrapolation of the GP values of the pure gel or of the pure liquid-crystalline phase at all temperatures, as obtained by a linear fit of the data points below 15 °C or above 50 °C, respectively. By substituting these linear extrapolations to the GP values of the pure phases in equation 3.25, it has been possible to calculate the fraction of lipids in the gel phase, as shown in Figure 3.53.

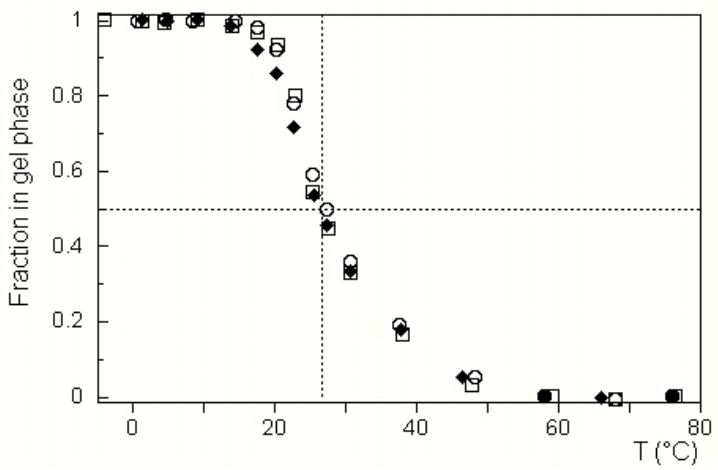

Figure 3.53 Fraction of lipids in gel phase as a function of temperature, for DMPC liposomes (0.2mM). All conditions are those reported in Figure 3.52.

All curves have the same transition temperature, within experimental errors (26.5 ± 0.5 °C), which is in agreement with the literature data.

3.9.2.2 Release experiments with membranes of different viscosities

On the basis of the results of the previous Section, we performed carboxyfluorescein release experiments at 15° C, where POPC and DMPC are in the liquid-crystalline and gel phase, respectively. The phase transition curves reported in the previous Section show that at 15 °C more than 98% of DMPC lipid molecules are in the gel state. It is important to note that membrane viscosity differs substantially between these two systems. For instance, measurements of lipid lateral diffusion (performed at 15 °C) have yielded diffusion coefficient values of 3.5 10^{-8} cm^2 s^{-1} and of 7 10^{-11} cm^2 s^{-1} for POPC and DMPC, respectively (Tocanne *et al.*, 1994). In addition, besides using DMPC and POPC, experiments were performed also with vesicles formed by ePC and

cholesterol in a 1:1 molar ratio. Cholesterol is known to induce collective order in the acyl-chain conformations of lipid molecules (Miao *et al.*, 2002) broadening the phase transition temperature.

The results are reported in Figure 3.54, which shows the fractional release 20 minutes after peptide addition.

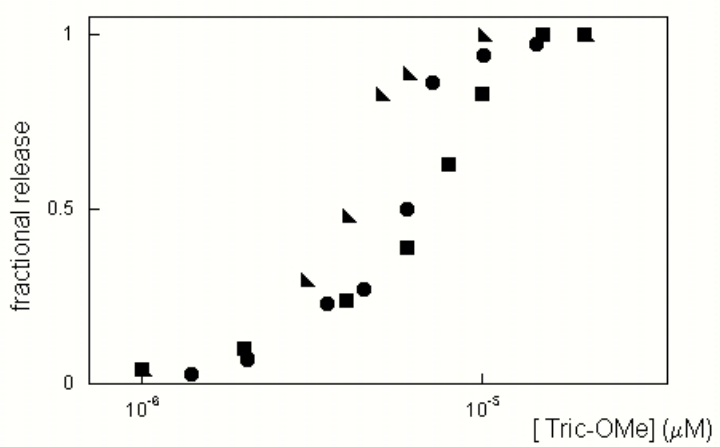

Figure 3.54 Tric-OMe induced leakage of carboxyfluorescein entrapped inside vesicles formed by DMPC (triangles), POPC (squares), and ePC/ Cholesterol (1:1 molar ratio, circles). Fractional release was determined 20 minutes after peptide addition. Total lipid concentration 0.2mM

No clear dependence on membrane viscosity is observed for trichogin activity, since a similar leakage is obtained with POPC and ePC/cholesterol membranes, while a somewhat higher permeability is induced in DMPC vesicles, which are in the ordered gel state.

Similar results were reported, for channel forming peptides, such as alamethicin and gramicidin A, in contrast with the carrier valynomicin, whose activity stops abruptly below the membrane melting temperature (Boehim *et al.*, 1980).

These results rule out the idea that trichogin could act as ion-carrier. Interestingly, even the activity of peptides which induce membrane leakage by forming toroidal pores in the membrane, such as magainin, is favored by a lower bilayer viscosity (Matsuzaki *et al.*, 1991). Therefore, our observation of a slightly higher trichogin activity in the rigid DMPC membranes is a further confirmation that the carpet-like mechanism is unlikely.

3.9.3 Pore formation?

3.9.3.1 BLM measurements

The most direct demonstration of pore formation is the experimental determination of the ion current that can flow through such a pore. This is made possible by planar lipid bilayer membranes (BLMs), which have been in use for more than three decades for the study of active proteins and peptides. In particular, if trichogin acts by forming pores, then discrete current jumps should be observed, corresponding to opening and closing events. In the case of well-defined channels, these current jumps will be approximately of the same size, while if pores of different sizes are formed (as in the case of toroidal pores) a higher variability should be observed.

A preliminary set of BLMs experiments on membranes formed by 1,2-diphytanoyl-sn-glycerophosphocoline has been performed in the laboratory of Dr. Giancarlo Menestrina (see Section 2.2.6), keeping the peptide concentration constant and varying the applied voltage in the range -120÷+120 mV.

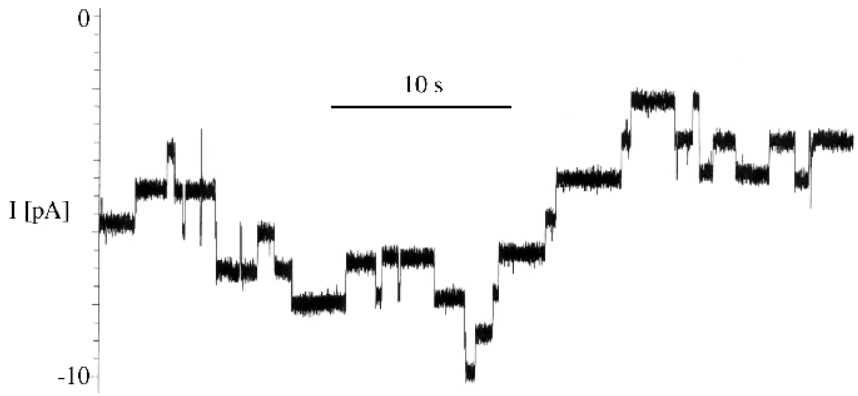

Figure 3.55 Single channel current fluctuations at +120 mV applied voltage. [Tric-OMe]=2.7 μM.

Figure 3.55 reports a typical current curve: independently on the applied voltage, the measured intensity varies with time in a stepwise fashion, through discrete current jumps. Additionally, a conductivity of 9±1 pS was estimated from the statistical analysis of the pore distribution.

These results would suggest that well-defined channels form. However, they represent a single set of experiments only, and, up to now, we were unable to

reproduce them. BLMs are known to be often poorly reproducible and therefore, we decided to address this problem with voltage clamp experiments on GUVs, an approach presenting also additional advantages which will be explained in greater detail in the following Section.

3.9.3.2 Voltage-clamp experiments

Black lipid membranes experiments give very useful informations about the activity of antibiotic peptides and their behavior under an applied voltage. However this technique is scarcely reproducible because of the low stability of the planar membrane. On the other hand, as shown in this thesis, spectroscopic measurements provide a wealth of information on peptides interacting with membranes. This assumes a particular relevance considering that the more powerful structural approaches of X-ray crystallography and multidimensional NMR are of very difficult applicability to membrane systems.

An experimental approach allowing both electrophysiological and spectroscopic measurements on the same system would be ideal for the study of membrane-perturbing agents. We tried to develop this idea by using GUVs for voltage-clamp experiments, normally performed with cells.

As reported above, GUVs are very stable liposomes characterized by a diameter in the micrometer range, like cells (Figures 3.56 and 3.57).

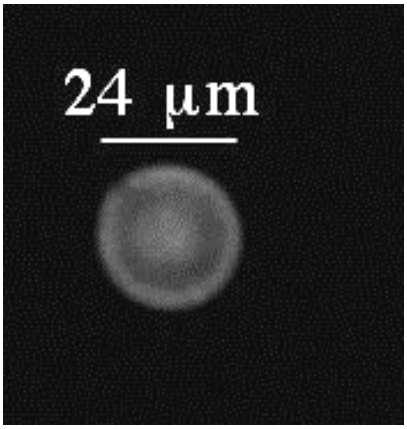

Figure 3.56 Microscopic image of a Giant Unilamellar Vesicle (ePC 30%, ePG 10%, Cho 25%, NBD-PE 10%).

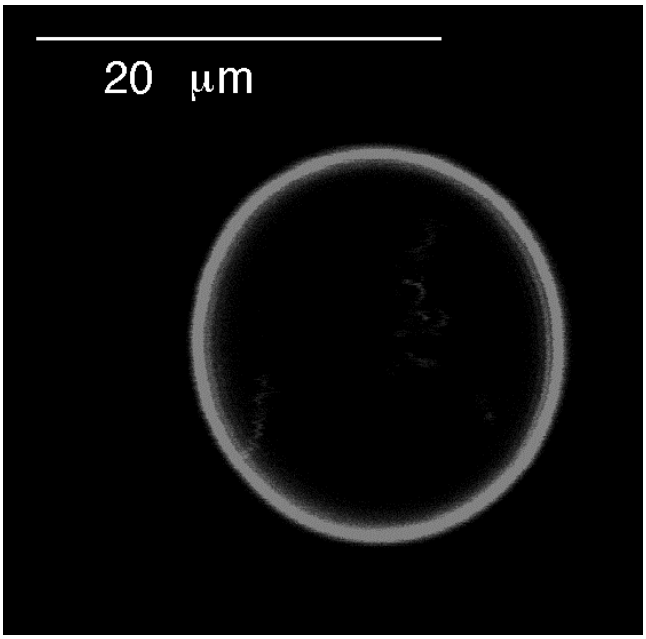

Figure 3.57 Confocal fluorescence microscopic image of a giant unilamellar liposome (ePC 30%, ePG 10%, Cho 25%, NBD-PE 10%).

Therefore, we thought that it would be possible to use them in a technique which uses microelectrodes to measure the electrophysiological properties of cell membranes.

A typical voltage clamp apparatus for single cell measurements is shown in Figure 3.58 and consists in a glass pipette electrode sealed onto the vesicle so to be in contact with its internal solution, and the counterelectrode immersed in the external bath, both connected to a measuring circuit.

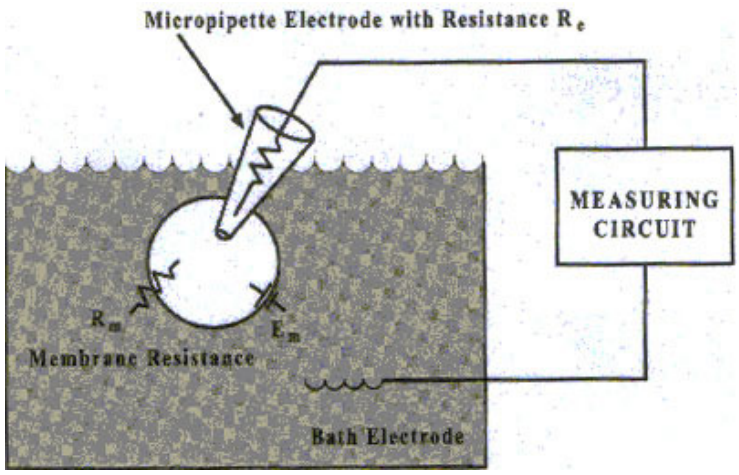

Figure 3.58 Schematic representation of the apparatus for voltage-clamp measurements.

The name ”voltage clamp” indicates the fact that in these experiments, like in those involving BLMs, the membrane voltage is under control (i.e. “clamped”), and the transmembrane current required to maintain that voltage is measured: by holding the membrane potential constant, the investigator ensures that the current is linearly proportional to the conductance being studied (First Ohm’s law). Therefore, regarding the electrophysiological measurements the two techniques are equivalent. The only difference is that here a micropipette must form an extremely tight seal with the membrane, and then break it, in order to allow the contact of the electrode with the internal solution. Successful electrophysiological measurements are strongly dependent on the effectiveness of this seal, so our effort was directed to the development of GUVs suitable for this purpose.

To this end, several issues must be considered: the giant liposomes should be stable to mechanical solicitations (in order not to be disrupted by the insertion of the glass electrode); moreover, the seal between the micropipette and the membrane must be characterized by an high impedance and, finally, to facilitate vesicles manipulation, their diffusive motions must be limited. As far as the microscopic investigation is concerned, the optimal experimental condition required the possibility to distinguish the multilamellar vesicles from the unilamellar ones and to follow the “fate” of the peptides inserted in liposome as well as the bilayer itself. Lastly, it is desirable to obtain GUVs as stable as possible.

Experimentally, in our case, electrophysiology experiments on GUVs were performed in collaboration with the laboratory of Dr.Rispoli (Ferrara University). The voltage clamp apparatus is equipped with a microscope which can be used to visualize GUVs in transmission or by fluorescence emission, after excitation with visible or UV light. For this last purpose we used an observation chamber formed by a quartz slide, 0.1mm thick and silanized, to avoid liposome adsorption.

The giant liposomes were synthesized by the gentle hydration method (2.1.4), which allows the use of high ionic strength buffers, as required for current

measurements. Our first experiments were with GUVs composed of ePC 90%, ePG 10% in 5mM PIPES, 100 mM KCl, 1mM EDTA, pH7 buffer. In this way we obtained GUVs with diameters around 10 μM, that remain stable for several weeks, when stored at 4 °C.

Incorporation of 10% anionic lipids like ePG in the vesicles is needed for several reasons: it helps the separation of different lipid layers and the formation of unilamellar vesicles, it avoids liposome aggregation and fusion, and finally it favors interaction with the voltage-clamp micropipette, for the formation of a tight seal. However, charged liposomes can be induced to aggregate by the presence of trace metal ions in the solution. To avoid this, the chelating agent EDTA was added to the preparation buffer (1mM).

With these liposomes it was possible to form a tight seal with the micropipette containing the electrode, with resistances up to 2 GΩ. However, experiments were severely complicated by the high mobility of the vesicles in the observation chamber, which made the seal formation very difficult. This is easily shown by calculating the diffusion coefficient for a GUV. According to the Stokes-Einstein equation,

$$D = \frac{kT}{f} \tag{3.26}$$

Here f is the frictional coefficient, which for a sphere can be expressed as:

$$f = 6\pi\eta a \tag{3.27}$$

where η is the solvent viscosity (89 cPoise for water) and a the vesicle radius (5 μm). This results in a diffusion coefficient of 0.5 $\mu m^2/s$, which shows that these vesicles move significantly in the microscope field, complicating an optimal visualization and their blockage with the micropipette

To solve this problem, we caused liposome precipitation at the bottom of the observation chamber, by using buffers containing 0.5 M saccharose inside the

vesicles and 0.5 M glucose outside. These solutions are equiosmolar but have slightly different densities (1.171 g/ml and 1.090 g/ml, respectively).

In the presence of a density difference, the concentration of liposomes decays exponentially as a function of the height:

$$C(h) \propto e^{-\frac{h}{\lambda}} \tag{3.28}$$

where λ is

$$\lambda = \frac{kT}{Vg\Delta\rho} \tag{3.29}.$$

λ is a function of the temperature (T), the volume of the solution (V) and the difference between the densities of the liposomes and of the buffer ($\Delta\rho$).

In our case, by approximating liposome density with that of the internal solution, λ is approximately 10 nm, i.e. even lower than the liposome radius. Therefore, under these conditions all vesicles should settle at the bottom of the observation chamber. This is what was actually observed in our experiments, where, after a few minutes, all vesicles are on the bottom quartz plate, and remain stationary for the rest of the experiment.

Unfortunately, the lipid composition of these liposomes gave rise to GUVs which were too elastic and, once sealed to the micropipette, were excessively deformed, causing problems when the vesicles had to be broken and altering the conductivity measurements.

At first, the use of liposomes containing an increasing fraction of cholesterol was investigated as a way to obtain membranes stable under the introduction of the micropipette. As reported above, this steroid is known to be able to induce collective order in the acyl-chain conformations of lipid molecules (Miao *et al.*, 2002). The preparations analyzed were:

- ePC 65% + ePG 10% + Cho 25%

- ePC 55% + ePG 10% + Cho 25% + NBD-PE 10%(or dansyl-PE 10%)
- ePC 30% + ePG 10% + Cho 50% + NDB-PE 10%

where NDB-PE and dansyl-PE stand for phosphatidylethanolamine labeled with nitrobenzoxadiazole and dansyl, respectively.

Cholesterol has effectively strengthened the vesicles, which could more easily be perforated without exploding or being deformed. Membranes containing 50% cholesterol resulted more robust than those containing 25% only. However 50% is the maximum amount of cholesterol which can be inserted in a membrane without having precipitation (Akashi, 2003).

Successively, the possibility of using lipids which at room temperature are in the gel phase, i.e. lipids having a melting temperature higher than 25 °C, was exploited. In particular, vesicles containing an high proportion of DPPC (dipalmitoylphosphatidylcholine; T_m = 60°C), which at T_{amb} is in the gel phase, were investigated, preparing liposomes of the following compositions:

- DPPC 95% + NBD-PE 5%
- DPPC 90% + ePG 5% + NBD-PE 5%.

Even in the absence of ePG, a sufficient number of unilamellar vesicles were obtained. However, these GUVs have proved to be unsuitable, since it was not possible to seal them to the micropipette. One hypothesis is that, as we could not add too much ePG in order not to lower excessively the transition temperature, the weakly charged membranes are not enough reactive towards the charged groups in the glass and cannot adhere well.

Almost all the GUV preparations reported above included also a portion of phospholipids labeled with fluorescent probes. It has to be pointed out that the introduction of fluorescent phospholipids did not change the GUVs resistance to mechanical solicitations or the possibility to penetrate them with the pipette. Even if GUVs are visible also in transmission, the inclusion of fluorescent probes has allowed a high visualization sensibility, resulting from a significant increase in contrast, and a better discrimination between unilamellar and multilamellar vesicles, because of difference in intensities (Figure 3.59).

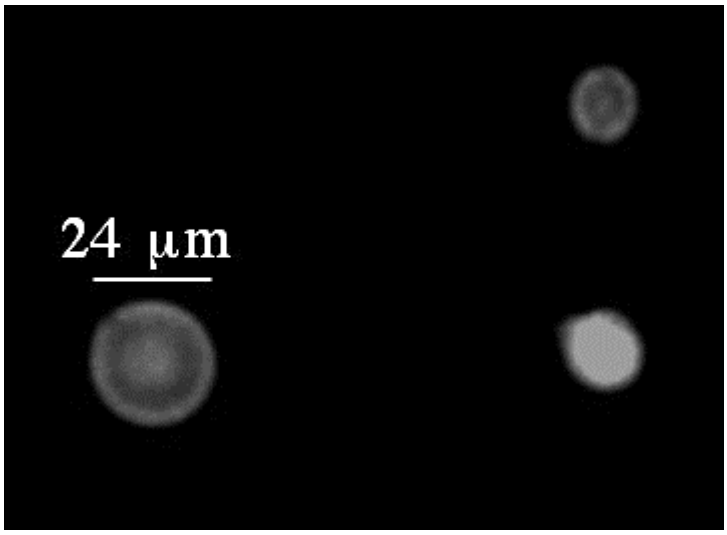

Figure 3.59 Fluorescence microscopic image of giant vesicles. Differences in the emission intensity allow to discriminate between unilamellar and multilamellar liposomes (ePC 30%, ePG 10%, Cho 25%, NBD-PE 10%).

In addition, the use of fluorescent probes permits to test the feasibility of coupling spectroscopic and conductimetric measurement on this kind of systems which, as anticipated in the introduction to this Section, would provide a powerful way to investigate the molecular details of membrane perturbation by antimicrobial agents.

Experimentally, the best visualization has been obtained with the NBD probe, whose quantum yield, (λ_{exc}=470 nm) was 10 fold higher than that of dansyl (λ_{exc}=360 nm).

At present, voltage-clamp experiments have only been carried out on giant vesicles alone (i.e. without any peptide added). A picture representing, on different scales, the micropipette perforating a giant liposome is reported in Figure 3.60 (the pipette for peptide microperfusion is also shown).

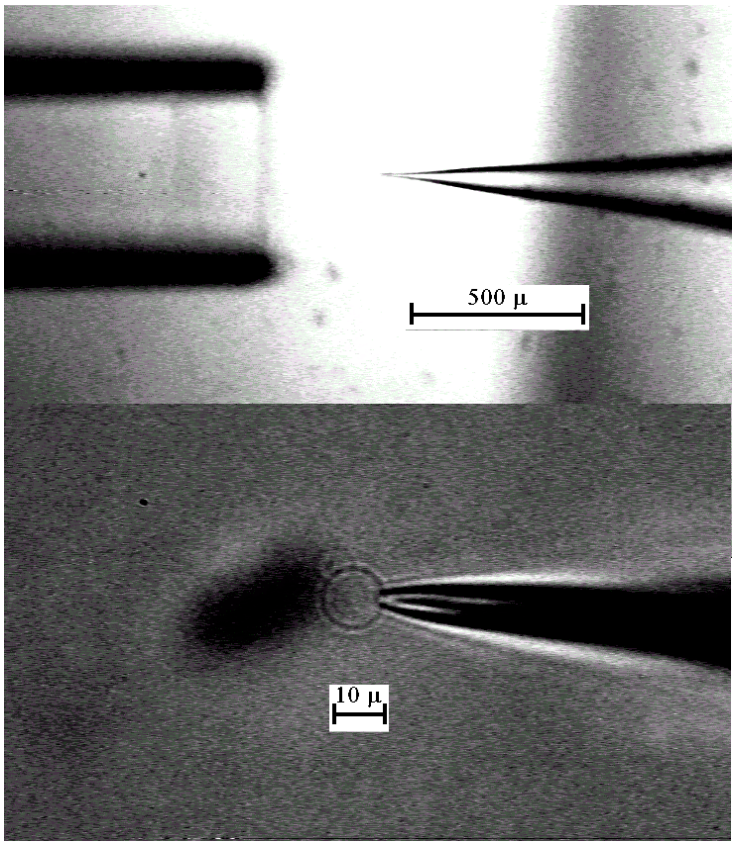

Figure 3.60 Microscopic image of voltage clamp apparatus, at two different scales, showing the micropipette inserted in giant vesicle and the peptide-perfusing pipette.

The curves reporting the current intensity measured on a giant liposome at different applied voltages are shown in Figure 3.61.

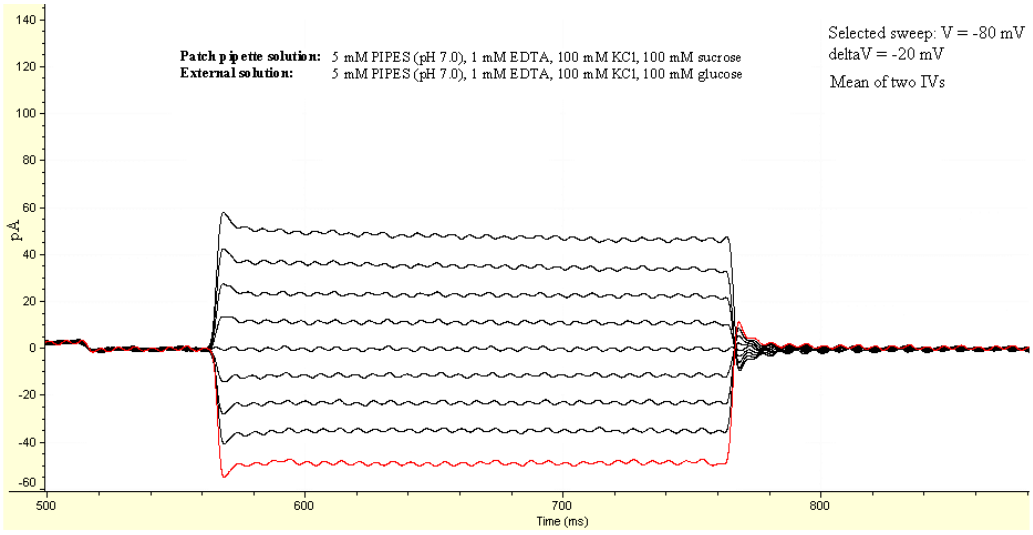

Figure 3.61 Current intensities as a function of time. Curves are registered under different applied voltages, that are from the bottom upwards: -80mV, -69mV, -40mV, -20mV, 0mV, 20mV, 40mV, 60mV, 80mV respectively.

Phospholipidic membranes can be considered as ohmic conductors; thus their resistance can be easily obtained plotting the current intensities in Figure 3.61 as a function of the applied voltages (Figure 3.62) and computing the reciprocal of the slope of the resulting straight line.

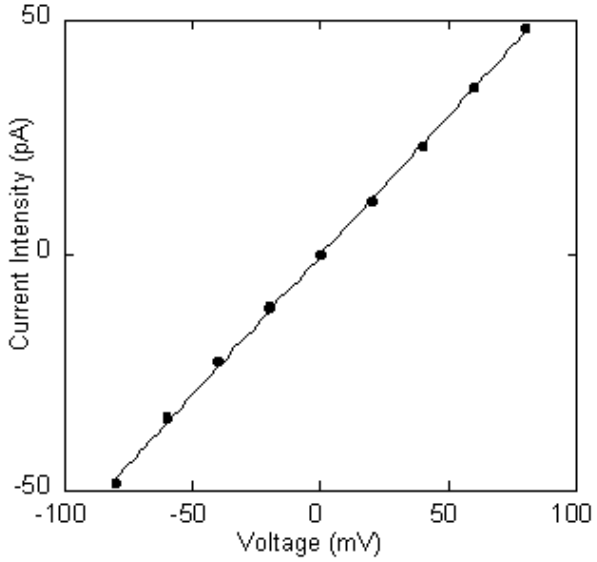

Figure 3.62 Voltage clamp experiments. Graph of measured current intensity versus applied potential; T = 25°C.

From the data reported in Figures 3.61 and 3.62, a resistance value of 1.7 GΩ was calculated, confirming the tight seal between micropipette and vesicle.

Having set up a suitable set of experimental conditions, the successive step will be to repeat these measurements in the presence of trichogin.

3.9.4 Summary

Different experiments have been performed to univocally define the peptide mode of action. Light scattering measurements and release experiments on giant unilamellar vesicles allowed to rule out micellization as the trichogin membrane perturbation mechanism. On the other hand, an ion-carrier mode of action was also excluded, after peptide-induced leakage experiments using liposomes of different viscosities. Indeed, voltage-dependent measurements on

BLMs suggest that trichogin acts by forming channels of well-defined size. In order to have further confirmation of this mechanism, voltage-clamp measurements on giant vesicles are at present being performed.

3.10 Analysis of the release kinetics

Further information regarding the molecular details of trichogin mechanism of action can be obtained from the analysis of the kinetics of peptide-induced carboxyfluorescein (CF) release.

From a purely phenomenological point of view, two main results emerge. The first is that, as already shown in Section 3.6, the time courses of carboxyfluorescein efflux from liposomes are rather complex, and simple functions are unable to fit the data (Matsuzaki *et al.,* 1995b; Schwarz *et al.,* 1987). In particular, it is shown in Figure 3.63 that, while in the simplest case (dye efflux from a single pore) the time evolution of carboxyfluorescein signal is expected to be monoexponential, experimentally this function was unable to fit the observed release kinetics. Indeed, a good fit could be obtained only with a stretched exponential function (Figure 3.63, curve b), which is defined as:

$$\%\,Release(t) = 1 - exp\left[-(k_0 t)^a\right] \tag{3.30}$$

where k_0 is a leak rate coefficient, and a is a constant. However, this phenomenological equation does not correspond to any physical model.

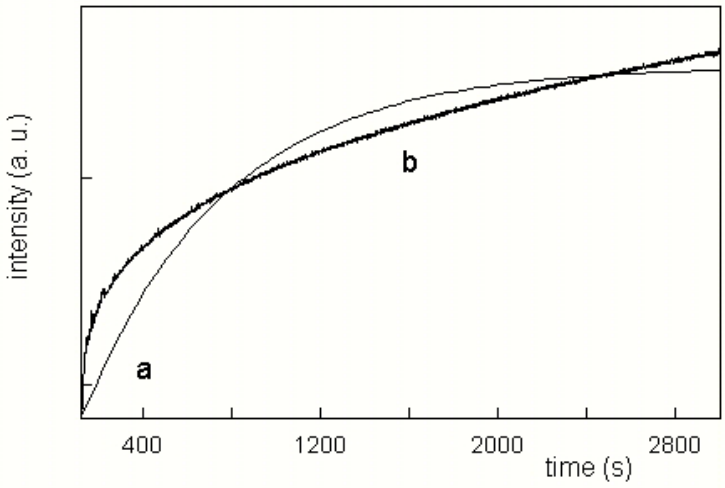

Figure 3.63 Analysis of the CF release kinetics (0.2mM lipid concentration) after the addition of F10 2μM according to: a) a single exponential function and b) a stretched exponential curve.

The other important observation is that the investigated efflux kinetics appeared to be rather slow, occurring in the minutes range, and, interestingly, did not stop, but continued until complete release was reached, even at the lowest peptide concentrations displaying some activity (an example is shown in Figure 3.64).

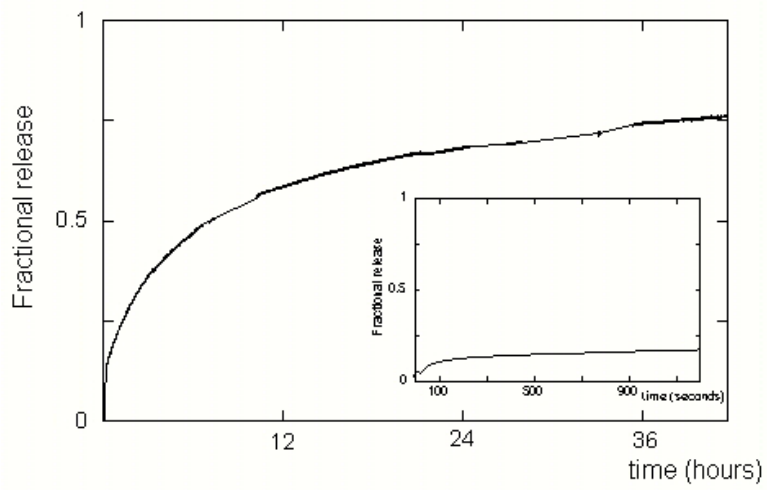

Figure 3.64 Kinetics of the release from loaded vesicles at [F10]= 2 μM and [Lipid] = 0.2 mM. Note that after 40 hours the carboxyfluorescein efflux out of liposomes did not stop. 20 minutes after peptide addition, the fractional release was less than 0.20 (*inset*).

Similar behavior has been observed for several other peptides, like alamethicin and GALA, even if, up to now, no unambiguous explanation for it was found. Anyway, the observation that the release goes slowly to completeness contrasts with a toroidal pore mode of action: in the latter case, the pore formation is accompanied by peptide translocation from the outer to the inner leaflet, so that the peptide surface concentration decreases below the threshold value necessary to form a pore; as a consequence the release stops (see Section 1.2).

Having observed these two phenomenological results (slow kinetics described by a stretched exponential function), our aim was then to look for a physical interpretation of the findings.

To this end, we first had to identify what process occurs in the time scale of the release phenomenon, so to be rate determining. As dye efflux is only the

last step in the process of trichogin interaction with vesicles, we wanted to know first in which time scale the peptide binding to membranes occurs. Therefore, we performed stopped-flow experiments.

3.10.1 Stopped flow experiments

Stopped flow allows the kinetic of a reaction to be followed continuously in the millisecond to second time scale, after rapid mixing of the reactants. In particular, we have studied the kinetics of binding of F10 to liposomes symmetrically labeled with C6-NBD-PC at different peptide concentrations, examining different time ranges (1 s and 20 seconds).

As shown in Section 3.3.2, several processes other than binding (for instance, aggregation in water) can result in a variation of the F10 emission intensity. Therefore, in order to focus only on peptide association to the liposomes, we chose to follow the increase of NBD fluorescence intensity (FRET acceptor) after its interaction with membrane-bound F10 (Fmc: FRET donor). However, this way of operating results in a recorded signal which is not linearly dependent on the membrane-bound peptide concentration. As a consequence, the kinetics can only be used to determine the time-scale of the binding process.

The results on doubly labeled liposomes as a function of the peptide concentration are reported in Figure 3.65 A and B.

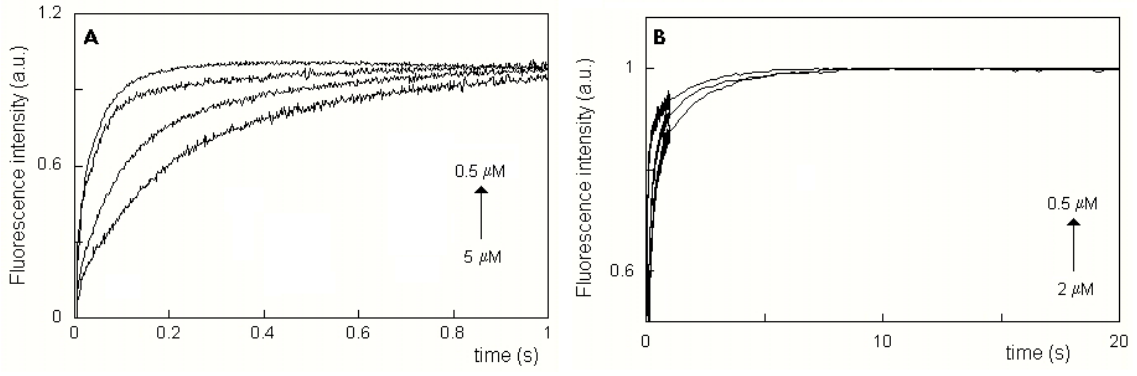

Figure 3.65 Normalized NBD emission intensities as a function of time [1s (A), 20s (B)] after the addition of F10 at 0.5 μM, 1 μM, 2μM and 5μM concentration to C6-NBD-PC 1% in 0.2 mM total lipid concentration. In (B) only the kinetics corresponding to the three lower concentrations are shown. (λ_{exc} = 265 nm, emission cut-off filter at 385 nm, 25°C).

Also in these short time scales, the kinetics appear to be very complex, as expected due to the several phenomena involved, like, for example, association to the membrane, changes in the secondary conformation, trichogin aggregation and translocation. Moreover, the curves are strongly different on varying the amount of F10 added, suggesting that peptide concentration-dependent phenomena like aggregation are involved.

However all of these kinetics are fast and, independently on peptide concentration, there is no further change in emission intensity for times > 5 seconds. Therefore, water-membrane partition of the peptide can not be the rate-determining step in membrane-leakage.

3.10.2 Analysis of the pore lifetime

After ruling out peptide binding to the membrane as the possible rate-determining step we focused our attention on the pore opening and closing process.

Indeed, liposomes containing pores cannot be seen like a homogeneous system, but rather as a macroscopic system composed of several non interacting subunits - the carboxyfluorescein release from each vesicle being independent from the others. Since liposomes are comparatively small systems the fluctuations become relevant.

If the pores remain open for a time sufficient for the complete depletion of a vesicle, then only completely full or completely empty liposomes are present ("all-or-none" process). In this case, the duration of the pore open state, the size or the number of channels in a given vesicle are not relevant. On the other hand, if only a fraction of the liposome contents are released during the average pore lifetime (graded process), the kinetics of pore opening and closing could be rate limiting.

To verify if trichogin-induced release occurs by a gradual mechanism or an "all-or-none" process, we determined the variation of the emission intensity of the carboxyfluorescein still entrapped inside vesicles after partial release.

Experimentally, after incubation with F10 (2 μM) for 20 minutes, vesicles (lipid concentration = 0.2 mM) were separated by gel filtration from the released marker and then the increase of CF emission intensity after addition of a detergent, Triton X-100 (due to the dequenching of the fluorophores signal, as explained in Section 2.1.6.1) was measured and compared to that observed on liposomes where no peptide was added. If the dye leaked out in an all-or-none fashion, then fluorescence of the dye remained entrapped in liposomes should be as quenched as it was before peptide addition, and consequently the increase in emission intensity after TX-100 addition would be the same. On the contrary, if the leakage was gradual, then the dye remaining in the liposomes should be partially dequenched, leading to a lower increase in CF intensity after the addition of Tx-100, with respect to that observed before peptide addition.

Our experiments showed that the change in CF emission after partial release was only 34% of that obtained when no peptide was added, indicating that the dye leaks in a graded mode. This, in turn, suggests that the lifetime of the pore is not sufficiently long to permit a complete CF release. However, BLM experiments (Section 3.9.3.1) have shown that the fluctuations leading to the opening and closing of the pores, have a time scale below 1s. At the same time, an estimate of the time needed for complete release of the marker from a single liposome can be obtained applying the first Fick's law. Accordingly, the diffusion-mediated flow of fluorescent molecules through an open pore can be described as :

$$-\frac{dn^*}{dt} = A_p \frac{D_0}{d}\left(C^* - C\right) \tag{3.31}$$

where n^* is the amount (mole numbers) of the marker material at time t inside a given liposome, C^* and C stand for marker concentration at the internal and external pore bounds, respectively, D_0 is the diffusion coefficient of carboxyfluorescein, d is thickness of the membrane, and A_p is the pore cross-sectional area. Assuming liposomes as regular spheres with radius R, we obtain

the expression for the characteristic lifetime of complete release from a single pore (ϕ):

$$\phi = \frac{4}{3}\pi R^3 \frac{d}{A_p D_0} \qquad (3.32)$$

In our case, R = 50 nm (radius of the pores of polycarbonate extrusion filters), d = 4 nm (Lis *et al.*, 1982) and $D_0 = 2.17 \cdot 10^{-8}$ nm^2/s (Mastuzaki *et al.*, 1995). A_p can be calculated on the basis of the results reported in Section 3.6 where we demonstrated the pore diameter to lie in the interval 1-4nm; accordingly, 0.80 nm^2 $\leq A_p \leq$ 12.6 nm^2. Substitution of these parameters into the equation 3 gives values of 0.8 ms $\leq \phi \leq$ 12 ms. It should be pointed out that this is just a very rough estimate, because we have assumed free diffusion of carboxyfluorescein through the pore, even though this is probably not the case. Anyway, from these consideration it is reasonable to assume that both pore opening and the release of marker from the open pore are processes happening on a time scale much faster than the observed release kinetics. This is in good agreement with average pore lifetimes reported for alamethicin (1-5 ms; Brachais *et al.,* 1995), magainin (~ 15 ms; Mastuzaki *et al.,* 1996) and sticholysin I (1-10 ms; Tejuca *et al.,* 1998). Therefore, the slow release time scale can not be ascribed to the kinetics of pore opening and closing. Another phenomenon, possibly involved in pore formation, must be present.

In Section 3.3 we have demonstrated that, in a water-membrane system, the peptide is involved in several concomitant equilibria. This means that trichogin partition to the membrane is a dynamic process and, as a consequence, peptide exchange among vesicles is likely to occur.

Experimentally, the existence of rapid exchange phenomena was evidenced, for example, by observing the abrupt interruption of the carboxyfluorescein release kinetics (Figure 3.66), after addition of an excess of unloaded vesicles (10:1 molar ratio). Peptide exchange between the liposomes causes a high dilution of its concentration in the membrane, resulting in a loss of activity.

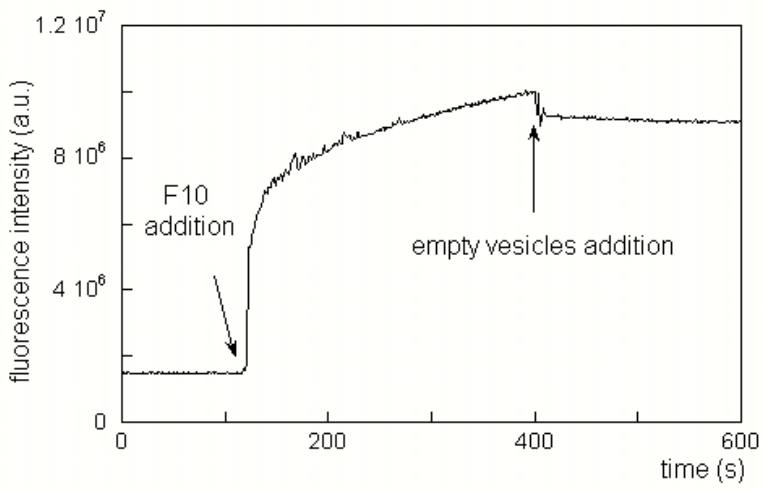

Figure 3.66 F10 induced carboxyfluorescein release ([F10]= 2μM, [lipid] = 0.2mM) was stopped by the addition of 2mM unloaded vesicles. T= 25°C

Peptide exchange between vesicles has important consequences on the release kinetics, since it will cause fluctuations in the number of peptide molecules present in a given liposome. If the number of peptide molecules on each vesicle is rather low, a large fraction of vesicles will contain no pores at a given time. However, due to fluctuations in the number of peptide molecules in a given vesicle, the threshold concentration for peptide aggregation and pore formation can be reached. This could be the rate-determining step for depletion of that liposome. In other words, the slow kinetics observed could be a consequence of the long time that an "inactive" vesicle has to wait before fluctuations lead to an amount of bound peptide sufficient to induce leakage.

Additionally, these results allow a physical interpretation of the stretched exponential function used to fit the kinetic data. As demonstrated by Huber (Huber, 1985) a stretched exponential function is applicable to systems with channels opening and closing with time, provided that the correlation time of these fluctuations is much longer than the relaxation time.

3.10.3 Summary

Trichogin-induced relase kinetic curves can be represented as a stretched exponential evolution characterized by a significant slow time constant. Peptide partition to membrane and the opening or closing of pores have been ruled out as the rate determining steps, based on stopped-flow experiments and theoretical calculations. All the findings suggest, instead, that the process the time scale of the release kinetics is determined by the long time that a vesicle not containing any pores has to wait, before fluctuations in the peptide distribution bring to it enough peptide molecules to form a channel.

4

“That’s all, Folks!”
Warner Bros Inc. – Looney Tunes

Conclusions

In this thesis work, the mechanism of membrane perturbation of the lipopeptaibol trichogin GA IV has been investigated by using two fluorescent synthetic analogs called F10 and A3.

The use of these analogs allowed us to take advantage of the high versatility of fluorescence spectroscopy to investigate in great detail each of the processes involved in the peptide-membrane interaction. As a consequence, we have been able not only to determine the mode of action of trichogin, but also to outline a general approach to investigate the mechanism of membrane perturbation by other antimicrobial agents.

The principal results of our research are summarized below.

As shown by time-resolved fluorescence, in a water-membrane system four different trichogin species are present, namely the monomeric and the aggregated form in each of the two phases. Experimentally, we were able to determine the constants regulating the equilibria among these species. Furthermore, the comparison of these results with carboxyfluorescein release experiments, showed that liposome perturbation is due only to peptide aggregates in the lipid phase. Therefore, the ratio between the total peptide and lipid concentration is inadequate to describe membrane perturbation, since the fraction of membrane-bound aggregates (which is the only active species) depends on all aggregation and partition equilibria.

This is an important and generally applicable finding. Indeed, in the literature the activity of a peptide is often reported as a function of ratio between total peptide and lipid concentrations. However, only the concentration of membrane-bound, active peptide is relevant. Therefore, this approach can give rise to misleading interpretations. For instance, Toniolo *et al.* reported that the dependence of trichogin-induced leakage on peptide/lipid ratio is different when experiments are performed at 60 μM or 600 μM lipid concentration (Toniolo *et al.*, 1996). This result is easily understood on the basis of the partition data presented here, as it is due to a difference in the fraction of membrane-bound, active peptides.

On the other hand, these results are important also for the future design of more active peptides. Indeed, when introducing one or more modifications on a pre-existent antimicrobial agent, the simultaneous existence of multiple partition and aggregation equilibria, which can positively or negatively affect its membrane perturbing ability, has to be taken into account. For example, increasing the total hydrophobicity of the peptide does not always lead to a parallel increase in its activity. In the case of trichogin, on increasing the number of methylene groups of the N-terminal lipid moiety from 1 to 16 (and consequently the hydrophobicity of the peptide), the affinity for membrane reaches a maximum for the chain length of 8-10 carbon atom and then decreases abruptly. Our results allow us to interpret this finding as due to an increase in the fraction of aggregated peptide in water which, as reported in Section 3.3, reduces the affinity of trichogin for the membrane phase.

The second important result obtained in this study is that trichogin activity is due to the formation of channels made up of aggregated peptides, as demonstrated by several observations. In particular, light scattering measurements and microscopic observation of giant unilamellar vesicles allowed us to exclude a detergent-like mode of action, while release experiments performed on membranes of different viscosity ruled out an ion-carrier mechanism. Additionally, further activity experiments have shown the release to be size-dependent, while preliminary studies on BLMs have provided a direct evidence of channel formation.

Finally, topology experiments using depth-dependent fluorescence quenchers have shown that membrane-bound trichogin can exist both in a superficial and an inserted form. The relative amount of the latter, which increases with peptide concentration, is strictly correlated with the fraction of membrane-bound aggregated peptides. This finding is a strong indication that only two peptide states are present in the membrane, a monomeric surface-bound and inactive form and an inserted aggregated state causing membrane leakage. The interconversion between these two states is driven by peptide concentration and does not involve stable intermediates.

This is a fundamental result, as it provides an extremely detailed information on the trichogin mechanism of action at the molecular level. Indeed, it relates the occurrence of aggregates in the membrane phase to a concentration-induced change in orientation, both processes being involved in the definition of the peptide active state (pore formation). It has to be pointed out that this is the first time that such a strict correlation between these three phenomena (aggregation-insertion-activity) is directly observed.

The concentration-driven trichogin insertion can be explained by considering the elastic perturbation of the lipid membrane caused by the surface-absorbed peptides. The energy of surface-absorption starts with a negative binding contribution, due to the attraction between the horizontally oriented amphipathic peptide and the hydrophilic/hydrophobic interface of the lipid bilayer. However, with increasing peptide concentration, it increases with a positive quadratic term, due to the elastic deformation of the bilayer. Therefore, as the amount of peptide increases, a threshold is reached after which a transmembrane orientation becomes thermodynamically favorable (Huang *et al.*, 2000; Chen *et al.*, 2002). It is worth noting that the structural features of the transmembrane state depend on the charge state of the peptide under study. The insertion into the apolar region of the membrane is feasible for neutral or weakly charged peptides, such as trichogin or alamethicin, while for highly charged peptides, such as magainin, it is very unfavorable (Zemel, 2003 and 2004; Yang *et al.*, 2001; Shai, 2002).

The observed coupling between membrane insertion and peptide aggregation suggests the presence of a strong driving force for peptide self-association in the inserted state, so that monomeric peptides are present on the surface only. The lipid membrane plays a key role in mediating the attractive interactions between transbilayer inclusions, as elucidated in detail by several theoretical and experimental studies (Aranda-Espinoza *et al.*, 1996; Lagüe *et al.*, 2000). One explanation can once again be found in the elasticity theory: as a result of the quadratic elastic deformation term, the energy cost increases if two surface adsorbed peptides aggregate. The opposite is true in the case of inserted peptides, where self-association decreases the total free energy, as

demonstrated theoretically and experimentally shown by X-ray lamellar diffraction measurements with Gramicidin in thick bilayers (Huang 1995, Harroun *et al,* 1999).

In addition, aggregation processes appear to be favored by the so-called "hydrophobic mismatch", which consists in a difference between the size of the peptide backbone and the hydrophobic bilayer thickness. The situation in which the hydrophobic length of a transmembrane helix is shorter than the dimension of the hydrophobic core of the bilayer (negative mismatch, as in the case of trichogin), implies an unfavorable exposure of hydrophobic acyl chain segments to polar moieties. As a consequence, significant rearrangements such as aggregation, can occur to achieve an energetically more favorable configuration (de Planque and Killian, 2003; Killian, 1998).

Furthermore, trichogin aggregation in membrane can also be driven by specific interactions between the sequence motif GxxxG of adjacent helices. Recent studies have shown the GxxxG sequence motif (where G stands for glycine and x for any aminoacid) to induce specific association of transmembrane helices, and helix association is even more favored if bulky residues occupy the sequence positions just before or after the two glycines (Curran and Engelman, 2003). In this sequence motif, the glycine residues are located on the same face of the helix, allowing close packing of two helices. Moreover, the lack of side chain atoms in glycine residues results in no loss of side-chain enthropy upon dimerization at these positions. Finally, the possibility of hydrogen bond formation between the glycine $C_{\alpha}H$ and CO groups of another helix has been suggested (Curran and Engelman, 2003).

Based on all these considerations, trichogin mechanism of action can be graphically summarized as shown in Figure 4.1: the increase of peptide concentration induces a transition from the surface-bound inactive monomeric form to a labile intermediate transmembrane-oriented monomer which, being very unstable in the lipid phase, aggregates almost instantaneously.

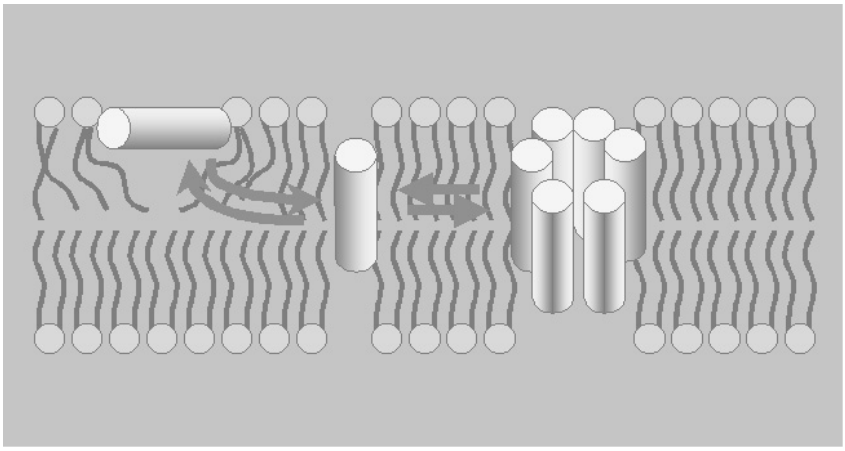

Figure 4.1 Schematic representation of trichogin mode of action.

In conclusion, the activity model that seems congruent with all the evidences available at the moment is the so-called "barrel-stave" mechanism of pore formation, the same followed by alamethicin. In this model, peptide helices inserted in a transmembrane orientation associate as the staves in a barrel, to form a water-filled channel.

We have collected several informations regarding the pore structure, *i.e.* that its diameter is in the 1-4 nm range and that it is formed by at least 8 trichogin units in α-helical conformation held together by specific interactions. However, some structural details are still missing. In particular, since trichogin is too short to span the bilayer, a complex supramolecular structure must be envisaged for the formation of a membrane channel, as for example, an assembly of head-to-head and/or head-tail dimers perpendicular to the plane of the bilayer (Didonè, 2001). The elucidation of this structure requires additional investigations, that are underway.

Additionally, within this research work an experimental system, which will allow spectroscopic and voltage-clamp experiments to be carried out simultaneously on giant unilamellar vesicles, was developed and set up. As demonstrated by this thesis, spectroscopic techniques provide a wealth of structural information, while electrophysiological measurements can supply functional data. Currently, we are performing the first experiments on liposomes in the presence of trichogin and other antibiotic peptides.

5

"Τις ουν ο τροπος του καλως τε και μη γραφειν;
δεομεθα τι, ω Φαιδρε, Λυσιαν ο περι τουτων
εξετασαι και αλλον οστις πωποτε τι γεγραφεν
η γραψει, ειτε πολιτικον συγγραμμα ειτε ιδιωτικον,
εν μετρωι ως ποιητης η ανευ μετρου ως ιδιωτης"
Plato - Phaedrus

"What is good, Phaedrus, and what is not good…
Need we ask anyone to tell us these things?"
Robert M. Pirsig - Zen and the art of motorcycle maintenance

Bibliography

Abrams, F. S., and E. London. 1993. *Extension of the parallax analysis of membrane penetration depth to the polar region of model membranes: use of fluorescence quenching by a spin-label attached to the phospholipid polar headgroup*. Biochemistry. 32:10826-10831

Abrams, S. B., and P. Yager. 1993. *Perturbation of chain melting transition of DPPC by galactose, agarose, and laurdan as determined by differential scanning calorimetry*. Biochim. Biophys. Acta 1146:127-135

Akashi, K., Miyata, H., Itoh, H., and K. Kinosita Jr. 1996. *Preparation of giant liposomes in physiological conditions and their characterization under an optical microscope*. Biophys. J. 71:3242-3250

Akashi, K., Miyata, H., Itoh, H., and K. Kinosita Jr. 1998. *Formation of giant liposomes promoted by divalent cations: critical role of electrostatic repulsion*. Biophys. J. 74:2973-2982

Anderson, D. J., Hanson, P., McNulty, J., Millhauser, G., Monaco, V., Formaggio, F., Crisma, M., and C. Toniolo. 1999. *Solution structure of TOAC-labeled trichogin GA IV peptide from allowed (g » 2) and half-field electron spin resonance*. J. Am. Chem. Soc. 121:6919-6927.

Andrès, E, and J. L. Dimarcq. 2004. *Cationic antimicrobial peptides: update of clinical development*. J. Intern. Med. 255:519-520.

Angelova, M. I. and D. S. Dimitrov. 1986. *Liposomes electroformation*. Faraday Discuss. Chem. Soc. 81:303-312

Aranda-Espinoza, H., Berman, A., Dan, N., Pincus, P., and S. Safran. 1996. *Interaction between inclusions embedded in membranes*. Biophys. J. 71:648-656.

Auvin-Guette, C., Rebufatt, S., Prigent, Y., and B. Bodo. 1992. *Trichogin GA IV, an 11-residue lipopeptaibol from Trichoderma longibrachiatum*. J. Am. Chem. Soc. 114:2170-2174.

Barret, D. A., Hartshorne, M. S., Hussain, M. A., Shaw, P. N., and M. C. Davies. 2001. *Resistance to nonspecific protein adsorption by poly(vinyl alcohol) thin films adsorbed to a poly(styrene) support matrix studied using surface plasmon resonance*. Anal. Chem. 73:5232-5239.

Beechem, J. M., Gratton, E., Ameloot, M., Knutson, J.R., and L. Brand. 1991. *The global analysis of fluorescence intensity and anisotropy decay data: second generation theory and programs*. In: Topics in Fluorescence Spectroscopy, Volume 2: Principles. J. R. Lakowicz, editor. Plenum Press, New York. 241-305.

Blondelle S. E., Lohner, K. and M. Aguilar. 1999. *Lipid-induced conformation and lipid-binding properties of cytolytic and antimicrobial peptides: determination and biological specificity*. Biochim. Biophys. Acta 1462:89-108.

Boheim, G., Hanke, W., and H Eibl. 1980. *Lipid phase transition in planar bilayer membrane and its effect on carrier- and pore-mediated ion transport*. Proc. Natl. Acad. Sci. USA 77:3403-3407.

Brachais, L., Davoust, D. and G. Molle. 1995. *Conformational study of a synthetic analog of alamethicin. Influence of the conformation on ion channel lifetimes*. Int. J. Pept. Protein Res. 45:164-172

Bree, A., and R. Zwarich. 1969. *Study of some excited singlet and triplet electronic states of fluorene*. J. Chem. Phys. 51:903-912

Bulet, P., Stöcklin, R., and L. Menin. 2004. *Anti-microbial peptides: from invertebrates to vertebrates*. Immun. Rev. 198: 169-184.

Cantor, R.C. and P.R. Schimmel. 1980. *Optical activity*. In Biophysical chemistry. Part II. W.H. Freeman and Co. Press. San Francisco. 409-432.

Carpino, L. 1993. *1-Hydroxy-7-azo-benzotriazole. An efficient peptide coupling additive*. J. Am. Chem. Soc. 115: 4397-4398.

Castanho, M, and M. Prieto. 1995. *Filipin fluorescence quenching by spin-labeled probes: studies in aqueous solution and in a membrane model system*. Biophys. J. 69:155-168.

Chattopadhyay, A. and E. London. 1987. *Parallax method for direct measurement of membrane penetration depth utilizing fluorescence quenching by spin-labeled phospholipids*. Biochemistry 26:39-45.

Chen, R. F., and J. R. Knutson. 1988*. Mechanism of fluorescence concentration quenching of carboxyfluorescein in liposomes: energy transfer to nonfluorescent dimers*. Anal. Biochem. 172:61-77.

Chen., F. Y., M. T. Lee, and H. W. Huang. 2002. *Sigmoidal concentration dependence of antimicrobial peptide activities: a case study on alamethicin*. Biophys. J. 82:908-914.

Chugh, J. K. and B. A. Wallace. 2001. *Peptaibols: models for ion channels*. Biochem. Soc. Trans. 29:565-571.

Coutinho, A., and M. Prieto. 2003. *Cooperative partition model of nystatin interaction with phospholipid vesicles*. Biophys. J. 84:3061-3078.

Curran, A. R., and D. M. Engelman. 2003. *Sequence motifs, polar interactions and conformational changes in helical membrane proteins*. Curr Op. Struct. Biol. 13:412-417.

De Planque, M. R. R., and J. A. Killian. 2003. *Protein-lipid interactions studied with designed transmembrane peptides: role of hydrophobic matching and interfacial anchoring*. Mol. Membr. Biol. 20:271-284.

Didonè, M. 2001. *Trichogin analogs for photophysical studies in membranes*. Chemistry Degree Thesis, University of Padua, Italy.

Eccleston, J. F., J. P. Hutchinson, and H. D. White. 2000. *Stopped flow techniques*. In Protein Ligand Interactions: Structure and Spectroscopy. A Practical Approach Series. S. E. Harding and B. Z. Chowdhry, editors. Oxford University Press, Oxford, UK., 201-237

Epand, R. M., and H. J. Vogel. 1999a. *Diversity of antimicrobial peptides and their mechanisms of action*. Biochim. Biophys. Acta 1462:11-28.

Epand, R. F., Epand, R. M., Monaco, V., Stoia, S., Formaggio, F., Crisma, M., and C. Toniolo. 1999b. *The antimicrobial peptide trichogin and its interaction with phospholipid membranes*. Eur. J. Biochem. 266:1021-1028.

Epand, R. M., and Epand R.F. 2000. *Liposomes as models for antimicrobial peptides*. Methods Enzym. 372:124-133

Epand, R. F., Epand, R. M., Formaggio, F., Crisma, M., Wu, H., Leher, R. I., and C. Toniolo. 2001. *Analogs of the antimicrobial peptide trichogin having opposite membrane properties*. Eur. J. Biochem. 268:703-712.

Fattal, E., Nir, S., Parente, R. A., and F. Szoka Jr. 1994. *Pore-forming peptide induce rapid phospholipid flip-flop in membranes*. Biochemistry 33:6721-6731.

Foggi, P. Neuwahl, F. V. R., Moroni, L. and P.R. Salvi. 2003. *$S_1 \rightarrow S_n$ and $S_2 \rightarrow S_n$ absorption of azulene: femtosecond transient spectra and excited state calculations*. J. Phys. Chem. A 107:1689-1696.

Förster, Th. 1948. *Intermolecular energy migration and fluorescence*. Ann. Phys. 2:55-75.

Fung, B. K., and L. Stryer. 1978. *Surface density determination in membranes by fluorescence energy transfer*. Biochemistry 17:5241-5248.

Gazit, E., Boman, A., Boman, H. G. and Y. Shai. 1995. *Interaction of the mammalian antibacterial peptide cecropin P1 with phospholipid vesicles*. Biochemistry 34:11479-11488.

Gazit, E., Miller I. R.A., Biggin, P. C., Sansom, M.S.P. and Y. Shai. 1996. *Structure and orientation of the mammalian antibacterial peptide cecropin P1 within phospholipid vesicles*. J. Mol. Biol. 258:860-870.

Hancock, R. E., and D. Chapple. 1999. *Peptide Antibiotics*. Antimicrobial Agents and Chemotherapy 143:1317-1323

Haris P. I., and D. Chapman. 1995. *The conformational analysis of peptides using Fourier Transform IR spectroscopy*. Biopolymers. 37:251-263

Harroun, T. A., Heller, W. T., Weiss. T. M., Yang, L., and H. W. Huang. 1999. *Experimental evidence for hydrophobic matching and membrane-mediated interactions in lipid bilayers containing gramicidin*. Biophys J. 1999 76:937-945.

Huang, H.W. 1995. *Elasticity of lipid bilayer interacting with amphiphilic helical peptides*. J. Phys. II France, 5:1427-1431.

Huang, H. W. 2000. *Action of antimicrobial peptides: two-state model*. Biochemistry 39:8347-8352.

Hubel D. L. 1985. *Statistical model for stretched exponential relaxation in macroscopic systems*. Phys. Rev. B. 31:6070-6071.

IUPAC. 1988. *Reference materials for fluorescence measurements*. Pure and Applied Chem. 60:1107-1114.

Jackson, M., and H.H. Mantsch. 1995. *The use and misuse of FTIR spectroscopy in the determination of protein structure*. Crit. Rev. Biochem. Mol. Biol. 30:95-120.

Jones, G. R., and A. R. Cossins. 1990*. Physical methods of study*. In Liposomes: a Practical Approach. R. R.C. New, editor. Oxford University Press, Oxford. 183-220.

Juvvadi, P., Vunnam, S. and R.B. Merrifield. 1996. *Synthetic mellitin, its enantio, retro, and retroenantio isomers, and selected chimeric analogs: their antibacterial, hemolytic and lipid bilayer action*. J. Am. Chem. Soc. 118:8989-8997

Kaiser, R. D., and E. London. 1998. *Determination of the depth of BODIPY probes in model membranes by parallax analysis of fluorescence quenching*. Biochim. Biophys. Acta 1375:13-22

Karle, I., and P. Balaram. 1990. *Structural characteristics of a-helical peptide molecules containing Aib residues*. Biochemistry 29:6747-6755.

Killian, J.A. 1998. *Hydrophobic mismatch between proteins and lipids in membranes*. Biochim. Biophys. Acta 1376:401-416

Kleinkauf, H., and H. von Döhren. 1990. *Nonribosomial biosynthesis of peptide antibiotics*. Eur. J. Biochem. 192:1-15.

Knutson, J.R., Beechem J.M., and L. Brand. 1983. *Simultaneous analysis of multiple fluorescence decay curves: a global approach*. Chem Phys. Lett. 102:501-507.

König, W., and R. Geiger. 1970. *Eine neue Methode zur Synthese von Peptiden: Aktivierung der Carboxylgruppe mit Dicyclohexylcarbodiimid unter Zusatz von 1-Hydroxy-benzotriazolen*. Chem. Ber. 103: 788-798.

Kusba, J., Li, L., Gryczynsky, I., Piszczek, G., Johnson, M., and J. R. Lakowicz. 2002. *Lateral diffusion coefficients in membranes measured by resonance energy transfer and a new algorithm for diffusion in two dimensions*. Biophys. J. 82:1358-1372.

Ladokhin, A. S. 1997 *Distribution analysis of depth dependent fluorescence quenching in membranes: a practical guide*. Methods Enzym. 278:462-473.

Ladokhin, A. S., and S.H. White. 1999. *Folding of amphipathic helices on membranes: Energetics of helix formation by melittin*. J. Mol. Biol. 285:1363-1369

Ladokhin, A. S., Jayasinghe, S., and S. H. White. 2000. *How to measure and analyze tryptophan fluorescence in membranes properly, and why bother?* Anal. Biochem. 285:235-245.

Ladokhin, A. S., and S. H. White. 2001. *Alphas and taus of tryptophan fluorescence in membranes*. Biophys. J. 81:1825-1827.

Lagüe, P., Zuckermann, M. J. and B. Roux. 2000. *Lipid-mediated interactions between intrinsic membrane proteins: a theoretical study based on integral equations*. Biophys. J. 79:2867-2879.

Lakowicz, J.R. 1983. *Principles of fluorescence spectroscopy*. Plenum Press, New York.

Lee, D. C., Durrani, A. A., and D. Chapman. 1984. *A difference infrared spectroscopic study of gramicidin A, alamethicin and bacteriorhodopsin in perdeuterated dimyristoylphosphatidylcholine*. Biochim Biophys Acta. 769:49-56.

Lis, L. J., McAlister, M., Fuller, N.L., Rand, R. P., and V. A. Parsegian. 1982. *Measurement of the lateral compressibility of several phospholipid bilayers*. Biophys. J. 37:667-672.

Locardi, E., Mammi, S., Peggion, E., Monaco, V., Formaggio, F., Crisma, M., Toniolo, C., Bodo, B., Rebuffat, S., Kamphuis, J., and Q. B. Broxterman. 1998. *Conformation and membrane activity of an analogue of the peptaibol antibiotic trichogin GA IV with a lipophilic amino acid at the N-terminus*. J. Pep. Sci. 4:389-399.

Loidl, G., Musiol, H. J., Budisa, N., Huber, R., Poirot, S., Fourmy, D., and L. J. Moroder. 2000. *Synthesis of beta-(1-azulenyl)-L-alanine as a potential blue-colored fluorescent tryptophan analog and its use in peptide synthesis*. J. Pept Sci 6: 139–144.

London, E. and A. S. Ladokhin. 2002. *Measuring the depth of amino acid residues in membrane-inserted peptides by fluorescence quenching*. In Peptide-lipid interactions. S. Simon and T. J. McIntosh editors. Academic press, San Diego, 90-111

Loura, L.M.S., de Almeida, R.F.M., Coutinho, A. and M. Prieto. 2003. *Interaction of peptides with binary phospholipid membranes: application of fluorescence methodologies*. Chem. Phys. Lipids 122:77-96.

Ludtke, H. K. and H. W. Huang. 1996. *Mechanism of alamethicin insertion into lipid bilayers*. Biophys. J. 71:2669-2679

Manning, M. C., and R. W. Woody. 1991. *Theoretical CD studies of polypeptide helices: examination of important electronic and geometric factors*. Biopolymers 31:569-581.

Mao, D., and B. A. Wallace. 1984*. Differential light scattering and absorption flattening optical effects are minimal in the circular dichroism spectra of small unimellar vesicles*. Biochemistry 23:2667-2673.

Marx, U., Lassman, G., Holzütter H. G., Wüstner, D., Müller, P., Höhlig, A., Kubelt, J., and A. Herrmann. 2000. *Rapid flip-flop of phospholipids in endoplasmic reticulum membranes studied by a stopped-flow approach*. Biophys. J. 78:2628-2640.

Matsuzaki, K., Mitsunori, H., Funakoshi S., Fujii, N., and K. Miyajima. 1991. *Physicochemical determinants for the interactions of magainins 1 and 2 with acidic lipid bilayers*. Biochim. Biophys. Acta 1991: 162-170.

Matsuzaki, K., Murase, O., Fujii, N. and K., Miyajima. 1995a. *Translocation of a channel forming antimicrobial peptide, magainin 2, across lipid bilayers by forming a pore*. Biochemistry 34:6521-6526.

Matsuzaki, K., Murase, O. and K. Miyajima. 1995b. *Kinetics of pore formation by an antimicrobial peptide, magainin 2, in phospholipid bilayers*. Biochemistry 34:12553-12559.

Matsuzaki, K., Murase, O, Fujii, N., and K. Miyajima. 1996. *An antimicrobial peptide, magainin 2, induced rapid flip-flop of phospholipids coupled with pore formation and peptide translocation*. Biochemistry 35:11361-11368.

Matsuzaki, K., Nakamura, A., Murase, O., Sugishita, K., Nobutaka, F. and K. Miyajima. 1997. *Modulation of magainin 2-lipid bilayer interaction by peptide charge*. Biochemistry 36:2104-2111.

Matsuzaki, K. 1998. *Magainin as paradigm for the mode of action of pore forming polypeptides*. Biochim. Biophys. Acta 1376:391-400.

Matsuzaki, K. 2001. *Molecular mechanisms of membrane perturbation by antimicrobial peptides*. In Development of Novel Antimicrobial Agents: Emerging Strategies. K. Lohner, editor. Horizon Scientific Press, Wymondham. 167-181.

Mazeres, S., Schram, V., Tocanne, J. F., and A. Lopez. 1996. *7-nitrobenz-2-oxa-1,3-diazole-4-yl-labeled phospholipids in lipid membranes: differences in fluorescence behavior*. Biophys. J. 71:327-35.

McIntosh T.J., and P. W. Holloway. 1987. *Determination of the depth of bromine atoms in bilayers formed from bromolipid probes*. Biochemistry 26:1783-1788.

McIntyre, J. C., and R. G. Sleight. 1991. *Fluorescence assay for phospholipid membrane asymmetry*. Biochemistry 30:11819-11827.

Menger, F. M., and M. I. Angelova. 1998. *Giant vesicles: imitating the cytological processes of cell membranes*. Acc. Chem. Res. 31:789-797

Menestrina, G., Voges, K., Jung, G., and G. Boheim. 1986. *Voltage-dependent channel formation by rods of helical polypeptides*. J. Mol. Biol. 93:111-132

Miao, L., Nielsen, M., Thewalt, J., Ipsen, J. H., Bloom, M., Zuckermann, M. J. and O.J. Mouritsen. 2002. *From lanosterol to cholesterol: structural evolution and differential effects on lipid bilayer*. Biophys. J. 82:1429-1444.

Milov, A. D., Tsvetkov, Y. D., Formaggio, F., Crisma, M., Toniolo, C., and J. Raap. 2003. *Self-assembling and membrane modifying properties of a lipopeptaibol studied by CW-ESR and PELDOR spectroscopies*. J. Pept. Sci. 9:690-700.

Monaco, V., Locardi, E., Formaggio, F., Crisma, M., Mammi, S., Peggion, E., Toniolo, C., Rebuffat, S. and B. Bodo. 1998. *Solution conformational analysis of amphiphilic helical, synthetic analogs of the lipopeptaibol trichogin GA IV*. J. Pep. Res. 52:261-272.

Monaco, V., Formaggio, F., Crisma, M., Toniolo, C., Hanson, P., and G. L. Millhauser. 1999 . *Orientation and immersion depth of a helical lipopeptaibol in membranes using TOAC as an ESR probe*. Biopolymers 50: 239-253.

New, R.R.C.R. 1990. *Structure of liposomes*. In Liposomes: a Practical Approach. R. R.C. New, editor. Oxford University Press, Oxford. 1-32.

Papo N. and Y. Shai. 2003. *Exploring peptide-membrane interaction using surface plasmon resonance: differentiation between pore formation versus membrane disruption by lytic peptide*. Biochemistry 42:458-466.

Parasassi, T., De Stasio, G., Ravagnan, G., Rusch, R. M., and E. Gratton. 1991. *Quantitation of lipid phases in phospholipid vesicles by the generalized polarization of Laurdan fluorescence*. Biophys. J. 60:179-189

Parasassi, T., Krasnowska, E. K., Bagatolli, L. and E. Gratton. 1998. *Laurdan and Prodan as polarity-sensitive fluorescent membrane probe*. J. Fluorescence 8:365-373

Peggion, C., Formaggio, F., Crisma, M., Epand, R. F., Epand, R. M. and C. Toniolo. 2003. *Trichogin: a paradigm for lipopeptaibols*. J. Peptide Sci. 9:679-689.

Person, D., Toren, P. E. G., Herner, M., Lincoln, P., and B. Norden. 2003. *Application of a novel analysis to measure the binding of the membrane-translocating peptide penetratin to negatively charged liposomes*. Biochemistry 42:421-429.

Pispisa, B., L. Stella, M. Venanzi, A. Palleschi, F. Marchiori, A. Polese and C. Toniolo. 2000a. *A spectroscopic and molecular mechanics investigation on a series of Aib-based linear peptides and a peptide template, both containing tryptophan and a nitroxide derivatives as probes*. Biopolymers 53:169-181.

Pispisa, B., L. Stella, M. Venanzi, A. Palleschi, C. Viappiani, A. Polese, F. Formaggio, and C. Toniolo. 2000b. *Quenching mechanisms in bichromophoric, 3_{10}-helical Aib-based peptides, modulated by chain-length dependent topologies*. Macromolecules 33:906-915.

Pispisa, B., Mazzuca, C., Palleschi, A., Stella, L., Venanzi, M., Formaggio, F., Polese, A., and C. Toniolo. 2000c. *Structural features of linear (αMe)Val-based peptides in solution by photophysical and theoretical conformational studies*. Biopolymers 55:425-435.

Pispisa, B, Palleschi, A., Mazzuca, C., Stella, L., Valeri, A., Venanzi, M., Formaggio, F., Toniolo, C., and Q. B. Broxterman. 2002a. *The versatility of combining FRET measurements and molecular mechanics results for determining the structural features of ordered peptides in solution*. J. Fluoresc. 12:213-217.

Pispisa, B., Mazzuca, C., Palleschi, A., Stella, L., Venanzi, M, Formaggio, F. Toniolo, C., and Q. B. Broxterman. 2002b. *Structural features and*

conformational equilibria of 3_{10}-helical peptides in solution by spectrscopic and molecular mechanics studies. Biopolymers (Biospectroscopy) 67:247-250.

Pispisa, B., Mazzuca, C., Palleschi, A., Stella, L., Venanzi, M, Wakselman, M., Mazaleyrat, J.-P., Rainaldi, M., Formaggio, F., and C. Toniolo. 2003. *A combined spectroscopic and theoretical study of a series of conformationally restricted hexapeptides carrying a rigid binaphthyl-nitroxide donor-acceptor pair*. Chem. Eur. J. 9:2-11.

Polese, A., Formaggio, F., and C. Toniolo. 1996. *Circular dichroism spectrum of a peptide 3_{10}-helix*. J. Am. Chem. Soc. 118:2744-2745.

Pouny, Y. and Y. Shai. 1992. *Interaction of D-amino acid incorporated analogs of pardaxin with membranes*. Biochemistry 31:9482-9490

Pregel, M. J., Jullien, L., Canceill, J., Lacombe, L., and J. M. Lehn. 1995. *Channel-type molecular structures. Part 4. Transmembrane transport of alkali-metal ions by bouquet molecules*. J. Chem. Soc. Perkin Trans. 23:417-426.

Rebuffat, S., Goulard, C., Bodo, B., and M. Roquebert. 1999. *The peptaibol antibiotics from Trichoderma soil fungi: structural diversity and membrane properties*. Recent Res. Devel. Org. & Bioorg. Chem. 3: 65-91.

Roeske, R.W., and S. J. Kennedy. 1983. *Chemistry and biochemistry of amino acids, peptide and proteins*. In Weinsten, B. Ed.Dekker, New York. 7:205-265.

Rosoff M. 1996. *Vesicles*. Marcel-Dekker Inc., New York.

Sackmann, E. 1995. *Physics of vesicles*. In Handbook of Biological Physics. R. Lipowsy, and E. Sackmann editors. Elsevier Science B.V. 1:210-232.

Santos, N. C., Prieto, M., and M. A. R. B. Castanho. 2003. *Quantifying molecular partition into model system on biomembranes: an emphasis on optical spectroscopy methods*. Biochim. Biophys. Acta 1612:123-135.

Schümann, M., Dathe, M., Wieprecht, T., Beyermann, M., and M. Bienert. 1997. *The tendency of magainin to associate upon binding to phospholipid bilayers*. Biochemistry 36:4345-4351

Schwarz G., Gerke, H., Rizzo, V., and S. Stankowki. 1987. *Incorporation kinetics in a membrane, studied with the pore-forming peptide Alamethicin*. Biophys. J. 52:685-692.

Scrimin, P., Tecilla, P., Tonellato, U., Veronese, A., Crisma, M., Formaggio, F., and C. Toniolo. 2002. *Zinc(II) as an allosteric regulator of liposomal membrane permeability induced by synthetic template-assembled tripodal polypeptides*. Chem. Eur. J. 12:2753-2763.

Seddon, J.M., and R. H. Templer. 1995. *Polymorphism of lipid-water systems*. In handbook of biological physics. R. Lipowsy, and E. Sackman editors. Elsevier Science B.V. 1:101-134

Shai, Y. 2002. *Mode of action of membrane active antimicrobial peptides*. Biopolymers 66:236-248.

Sharpe, J. C., and E. London. 1999. *Diphtheria toxin forms pores of different sizes depending on its concentration in membranes: probable relationship to oligomerization*. J. Membr. Biol. 171:209-221.

Sitaram, N. and R. Nagaraj. 1999. *Interaction of antimicrobial peptides with biological activity and model membranes: structural and charge requirements for activity*. Biochim. Biophys. Acta 1462: 29-54.

Spach, G., Duchlohier, H., Molle, G., and G. M. Vallethon.1989. *Structure and supramolecular architecture of membrane channel forming peptide*. Biochemie 71:11-21

Stella, L. 2000. *Comparison between time-resolved fluorescence experiments and computer simulations*. In Spectroscopic Techniques in Biophysics. G. M. Giacometti, and G. Giacometti editors.

Stella, L., Venanzi, M., Carafa, M., Maccaroni, E., Straccamore, M. E., Zanotti, G., Palleschi, A. and B. Pispisa. 2002. *Structural features of model glycopeptides in solution and in membrane phase: a spectroscopic and molecular mechanics investigation*. Biopolymers 64:44-56.

Stewart, J. C. M. 1980. *Colorimetric determination of phospholipids with ammonium ferrothiocyanate*. Anal. Biochem. 104:10-14.

Strahilewitz, J., Mor, A., Nicolas, P., and Y. Shai. 1994. *Spectrum of antimicrobial activity and assembly of dermaseptin-b and its precursor form in phospholipid membranes*. Biochemistry. 33:10951-10960.

Szoka, F. Jr., and D. Papahadjopoulos. 1980. *Comparative properties and methods of preparation of lipid vesicles (liposomes)*. Ann. Rev. Bioeng. 9:468-508

Tamm, L.K. 2002. *Peptide-lipid interactions in supported monolayers and bilayers*. In Current topics in membranes. Elsevier Science 52:191-202.

Tejuca, M., Dalla Serra, M., Ferreras, M., Lanio, M. E., and G. Menestrina. 1996. *The mechanism of membrane permeabilization by Stikolysin I, a cytolysin isolated from the venom of the sea anemone Stichodactyla Heliantus*. Biochemistry 35:14947-14957

Tocanne, J. F., Dupon-Cezanne, L., and A. Lopez, 1994. *Lateral diffusion of lipids in model and natural membranes*. Prog. Lip. Res 33:203-207.

Toniolo, C., Peggion, C., Crisma, M., Formaggio, F., Shui, X., and D. S. Eggleston. 1994. *Structure determination of racemic trichogin GA IV using centrosymmetric crystals*. Nature Struct. Biol. 1:908-914.

Toniolo, C., Crisma, M., Formaggio, F., Peggion, C., Monaco, V., Goulard, C., Rebuffat, S., and B. Bodo. 1996. *Effect of N^{α}-acyl chain length on the membrane-modifying properties of synthetic analogs of the lipopeptaibol trichogin GA IV*. J. Am. Chem. Soc. 118:4952-4958.

Toniolo, C., Crisma, C., Formaggio, F., Peggion, C., Epand R. F., and R. M. Epand. 2001. *Lipopeptaibols, a novel family of membrane active, antimicrobial peptides*. Cell. Mol. Life Sci. 58:1179-1188.

Valcarcel, C. A., Dalla Serra, M., Potrich, C., Bernhart, I., Tejuca, M., Martinez, D., Pazos, F., Lanio, M. E. and G. Menestrina. 2001. *Effects of lipid composition on membrane permeabilization by sticholysin I and II, two cytolysins of the sea anemone Stichodactyla helianthus*. Biophys. J. 80:2761-2774.

Venanzi, M., Valeri, A., Palleschi, A., Stella, L., Moroder, L., Formaggio, F., Toniolo, C. and B. Pispisa. *Structural properties and photophysical behavior of conformationally constrained hexapeptides functionalized with a new fluorescent analog of tryptophan and a nitroxide radical quencher*. Biopolymers 75:128-139

Vogel, A., Scheidt, H. A., and D. Huster. 2003. *The distribution of lipid attached spin probes in bilayers: application to membrane protein topology*. Biophys. J. 85:1691-1701

W.H.O. 2002. *Antimicrobial resistance*. W.H.O. Fact Sheet 194. Available on-line at http://www.who.int/mediacentre/factsheets/fs194/en/

White S. H., Wimley, W.C., Ladokhin, A. S., and K. Hristova. 1998. *Protein folding in membranes: determining energetics of peptide-bilayer interactions*. Methods Enzymol. 295:62-87.

Wimley, W. C., and S. H. White. 2000. *Determining the membrane topology of peptides by fluorescence quenching*. Biochemistry 39:161-170.

Wolf, D. E., Winiski, A. P., Ting, A. E., Bocian, K. M., and R. E. Pagano. 1992. *Determination of the transbilayer distribution of fluorescent lipid analogues by nonradiative fluorescence resonance energy transfer*. Biochemistry. 31:2865-73.

Yang, L., Harroun, T. A., Weiss, T.M., Ding, L., and H. W. Huang. 2001*. Barrel stave or toroidal model? A case study on melittin pores*. Biophys. J. 81:1475-1485.

Zasloff, M. 2002. *Antimicrobial peptides of multicellular organisms*. Nature 415:389-395.

Zemel A., Fattal, D. R., and B. Avinoam. 2003. *Energetics and self-assembly of amphipathic peptide pores in lipid membrane*. Biophys. J. 84:2242-2255.

Zemel A., Avinoam, B., and S. May. 2004. *Membrane perturbation induced by interfacially adsorbed peptides*. Biophys. J. 86:3607-3619.

6

Table of contents